Bioactive Materials 33 (2024) 174–222

Contents lists available at ScienceDirect

Bioactive Materials

journal homepage: www.keaipublishing.com/en/journals/bioactive-materials

Review article

Tumor diagnosis using carbon-based quantum dots: Detection based on the hallmarks of cancer

Hang Wang [a,b,c,1], Siwei Yang [a,c,**,1], Liangfeng Chen [a,c], Yongqiang Li [a,c], Peng He [a,c], Gang Wang [d], Hui Dong [a,b,c], Peixiang Ma [e], Guqiao Ding [a,c,*]

[a] National Key Laboratory of Materials for Integrated Circuit, Shanghai Institute of Microsystem and Information Technology, Chinese Academy of Sciences, Shanghai, 200050, PR China
[b] CAS Center for Excellence in Superconducting Electronics (CENSE), Chinese Academy of Sciences, Shanghai, 200050, PR China
[c] Center of Materials Science and Optoelectronics Engineering, University of Chinese Academy of Sciences (UCAS), Beijing, 100049, PR China
[d] Department of Microelectronic Science and Engineering, School of Physical Science and Technology, Ningbo University, Ningbo, 315211, PR China
[e] Shanghai Key Laboratory of Orthopedic Implants, Department of Orthopedic Surgery, Shanghai Ninth People's Hospital, Shanghai Jiao Tong University School of Medicine, Shanghai, 200011, PR China

ARTICLE INFO

Keywords:
Tumor diagnosis
Carbon-based quantum dots
Hallmarks of cancer
Cell physiology
Structure design

ABSTRACT

Carbon-based quantum dots (CQDs) have been shown to have promising application value in tumor diagnosis. Their use, however, is severely hindered by the complicated nature of the nanostructures in the CQDs. Furthermore, it seems impossible to formulate the mechanisms involved using the inadequate theoretical frameworks that are currently available for CQDs. In this review, we re-consider the structure-property relationships of CQDs and summarize the current state of development of CQDs-based tumor diagnosis based on biological theories that are fully developed. The advantages and deficiencies of recent research on CQDs-based tumor diagnosis are thus explained in terms of the manifestation of nine essential changes in cell physiology. This review makes significant progress in addressing related problems encountered with other nanomaterials.

1. Introduction

Carbon-based quantum dots (CQDs), including carbon dots (CDs), graphene quantum dots (GQDs), and carbonized polymer dots (PDs), have aroused the interest of researchers around the world [1]. Nowadays, the rapid development of modern research techniques has brought CQD to the forefront of attention. Compared to more traditional markers (fluorescent dyes, fluorescent proteins, and II-IV quantum dots), CQDs have some highly desirable properties, e.g., remarkable stability, biocompatibility, controllable photoluminescence (PL) property, outstanding catalytic performance, and easily modified chemical structure [2–7]. Thus, CQDs have shown promising application value in the field of nanomedicine (especially tumor diagnosis and therapy) [8–10]. As a result, different tumor-diagnosis strategies (e.g., immunofluorescence methods [11], fluorescence imaging [8,12], and electrochemical sensing) and therapy strategies (e.g., nano-dr ug formulation [13–15], photodynamic therapy [16–18], immunotherapy [19,20], photothermal therapy [21], and sonodynamic therapy [22,23]) have been developed based on CQDs. These research progresses not only greatly enhance our knowledge and understanding of carbon nanostructures but also provide new strategies for diagnosing and treating tumors.

Despite spectacular recent progresses, there are still many burning questions surrounding the use of CQDs in tumor diagnosis and therapy. Thus, CQDs have not reached their full potential in this particular field of application. One of the most severe challenges is to clarify the interfacial interaction mechanism of CQDs [24–26]. In this respect, numerous research papers and reviews have been published on the

Peer review under responsibility of KeAi Communications Co., Ltd.
* Corresponding author. National Key Laboratory of Materials for Integrated Circuit, Shanghai Institute of Microsystem and Information Technology, Chinese Academy of Sciences, Shanghai, 200050, PR China.
** Corresponding author. National Key Laboratory of Materials for Integrated Circuit, Shanghai Institute of Microsystem and Information Technology, Chinese Academy of Sciences, Shanghai, 200050, PR China.
E-mail addresses: yangsiwei@mail.sim.ac.cn (S. Yang), gqding@mail.sim.ac.cn (G. Ding).
[1] These authors contributed equally to this work.

https://doi.org/10.1016/j.bioactmat.2023.10.004
Received 28 June 2023; Received in revised form 15 September 2023; Accepted 5 October 2023

mechanisms that may be directly involved [27–29]. However, further development is severely hindered by the complicated nature of the carbon nanostructures in the CQDs. It thus seems impossible to formulate the likely mechanisms responsible using the inadequate theoretical frameworks currently available. Thus, the research based on CQDs with specific chemical structures just provides a limited amount of information on the CQDs.

In contrast, the complexity of the illness may now be explained in the laboratory and clinic as a result of the development of cancer research into a mature and rational science [30–32]. As a result, cancer has become understandable in terms of a small number of underlying principles. Thus, from a standpoint of application, a summarization of the recent research on the use of CQDs in tumor diagnosis and therapy which is based on fully developed biological theories is of great significance. In this review, we summarize the current state of development of CQDs-based tumor diagnosis methods based on the hallmarks associated with cancer. Consequently, the manifestation of nine crucial alterations in cell physiology (self-sufficiency in growth signals, evading apoptosis, insensitivity to anti-growth signals, sustained angiogenesis, tissue invasion and metastasis, limitless replicative potential, genomic mutations & instability, energy metabolism changing, and immune destruction escape) can be used to explain both the advantages and deficiencies of the recent research in CQDs-based tumor diagnosis.

2. Development of CQDs

Developments in human society and science have often been closely associated with advances in the application of carbon materials such as diamond, coal, and graphite [33–35]. In the past few decades, nanomaterials have started to emerge as a potential replacement for many traditional materials due to their distinctive properties. Carbon nanomaterials are among the most extensively studied applied and discussed synthetic nanomaterials [36–42]. Essentially, such materials first started to attract attention in 1985 with the discovery of C_{60} by Kroto et al. [43] This was rapidly followed by subsequent research on carbon nanotubes (CNTs) (since 1991) [44], graphene (since 2004) [45], and C_3N (since 2017) [46]. Fig. 1 gives a more detailed illustration of the discoveries made in the field which have heralded great revolutions in basic research and applications in fields such as nanoelectronics, nanocatalysis, energy, and biomedicine.

In 2004, Xu et al. [47] accidently discovered 'zero'-dimensional carbon nanostructures during an experiment aimed at separating and purifying single-walled carbon nanotubes. Since their discovery, CQDs have triggered subsequent studies aimed at exploiting their fluorescent properties and a new class of viable fluorescent nanomaterials was thus created. CQDs, including spherical CDs and GQDs, are an innovation class of PL materials with distinctive qualities. Currently, CQDs with definite chemical structures and controllable morphology are being pursued, including GQDs [48], chiral CDs, PDs, crystalline g-C_3N_4 dots, and crystalline C_3N dots.

2.1. Classification and definition of CQDs

For the further development of CQDs, a precise definition of what constitutes a CQD is a vital prerequisite and of paramount significance. Inevitably, CQDs need to be distinguished from other carbon nanostructures in order to be accurately classified and defined. According to Nekoueian et al., CQDs are a subclass of zero-dimensional carbon-based nanomaterials with discrete quantized energy levels and variable densities of state [49]. Contrary to other carbon nanostructures, the characteristics of CQDs are substantially governed by quantum mechanical forces and other features including band gap and band edge location, which are constant in bulk carbon become size dependent [49]. More specifically, when size of the CQD decreases, the band structure of the density of states splits into separate sets of energy levels. Further decrease in size (to molecular or atomic dimensions) results in additional constraint of the excitons (electron-hole pairs) and the energy bandgap structure resembles a molecular electrical structure [50].

Unfortunately, as argued by Yang et al., the complex chemical structure makes the definition and classification of CQDs remains controversial [24]. However, they can be distinguished by their degree of carbonization (integrity of the sp^2 carbon skeleton) (Fig. 2). In this way, CQDs can be divided into four main categories: (i) highly-crystallized CQDs (HC-CQDs), such as g-C_3N_4 dots and C_3N dots [56], (ii) well-crystallized CQDs with some defects owning to a high content of crystalline sp^2 carbon nanostructures [49,57], (iii) CDs whose surfaces are filled with more sp^3 carbon nanostructures and functional groups [49], and (iv) PDs that contain cross-linked or aggregated

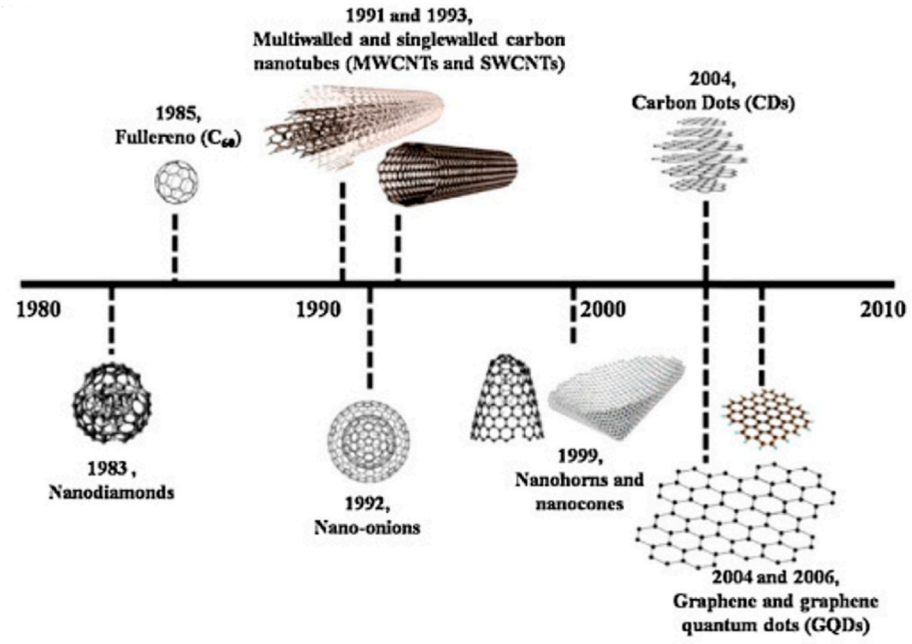

Fig. 1. Road map of the discovery of various carbon nanomaterials.

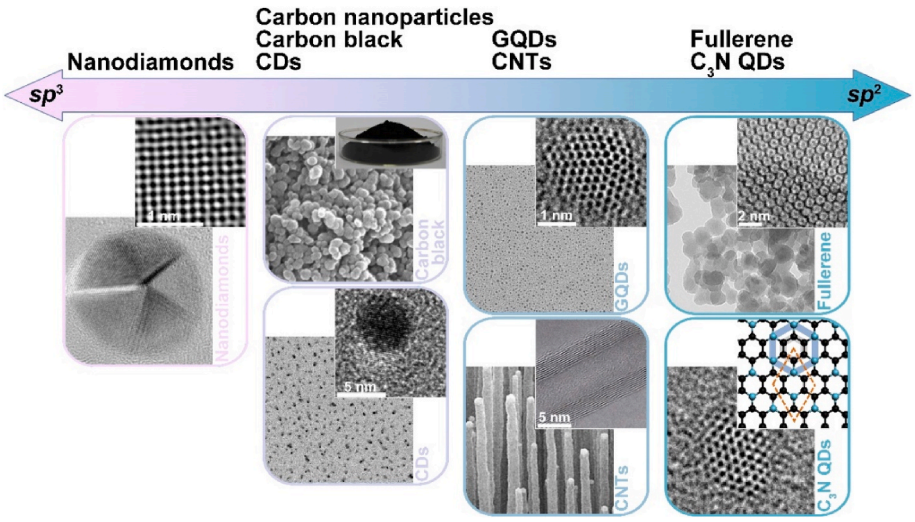

Fig. 2. Visualizing carbon-based nanomaterials: transmission electron microscopy (TEM) and high-resolution TEM (HR-TEM) images of nanodiamonds [51]. Copyright 2014, National Academy of Sciences. Scanning electron microscopy (SEM) image of carbon black [52]. Copyright 2014, Royal Soc. Chemistry. TEM and HR-TEM images of CDs. TEM and HR-TEM images of GQDs [53]. Copyright 2015, Wiley-VCH Verlag GmbH. SEM and HR-TEM images of CNTs [54]. Copyright 2001, Elsevier Science Ltd. TEM and HR-TEM images of C_{60} [55]. Copyright 2015, Pergamon-Elsevier Science Ltd. HR-TEM image of C_3N quantum dots [46]. Copyright 2017, Wiley-VCH Verlag GmbH.

polymers prepared from linear monomers or polymers which aggregate at a carbon core [58]. However, there is a diverse range of opinions on how CQDs should be classified.

Also, some researchers (for example, Liu et al. [57] and Sun et al. [59]) tend to equate CDs with CQDs. From this point of view, Park et al. stated that all nanosized fluorescent carbon materials derived from various carbon materials such as fullerenes, graphite, carbon nanotubes, and graphene with at least one dimension under 10 nm can categorized as CDs or CQDs [60]. Thus, GQDs, PDs, and HC-CQDs can be considered to be subsets of CQDs. However, when defining CQDs that are prepared by a 'bottom-up' approach, e.g., GQDs cut from two-dimensional graphene, the structure of the GQDs is significantly different from that traditionally recognized for CDs (which are generally taken to be spherical) [49]. Obviously, from this perspective, simplifying CDs as CQDs may not be sufficiently convincing. A similar problem also arises when classifying PDs.

At the same time, Yang et al. [1] suggest that GQDs, carbon nanodots (CNDs), and PDs should all be regarded as independent subsets of CDs due to their different levels of crystallinity and quantum confinement effects (Fig. 3a). This approach does allow their physical and chemical properties (e.g., luminescent emission characteristics) to be more readily distinguished which is, after all, one of the main focuses of CQDs research. However, up to now, there are still no definite and rigorous boundaries between CNDs, GQDs, and PDs, as well as CQDs, in this perspective. Although the current classification methods have unclear boundaries between materials, they can still be used to form feasible classification strategies. In this review we tentatively classify the CQDs based on the classification method of Yang et al. [1]: CQDs (equivalent to the definition of CDs), including carbon dots (equivalent to the definition of CNDs), GQDs, and PDs.

Besides taxonomic controversies, the definitions of HC-CQDs, GQDs, CDs and PDs are also divergent. HC-CQDs are the latest addition to the nanocarbon family. Because of their specific and highly crystallized structures, the chemical structures of HC-CQDs (such as g-C_3N_4 and C_3N) are generally easy to define and characterize using transmission electron microscopy (TEM) and elemental analysis. More specifically, g-C_3N_4 and crystalline C_3N dots are zero-dimensional fragments of g-C_3N_4 and C_3N, respectively. However, this definition presents another problem, namely, how small do these quantum dot (QD) materials need to be to show quantum confinement effects? Yang et al. [46] prepared a series of C_3N quantum dots of different sizes on a sheet of C_3N and showed that there is an upper limit to the size of C_3N fragments (15 nm) exhibiting quantum size effects (Fig. 3b). As a result, C_3N dots can be defined as fragments of C_3N whose transverse dimensions are less than 15 nm.

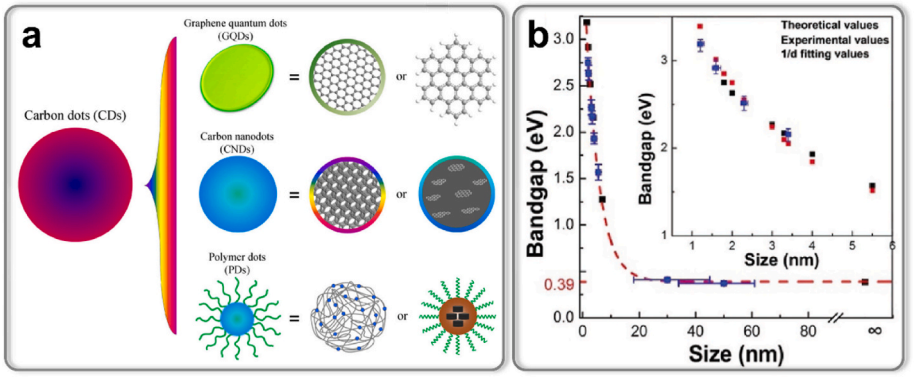

Fig. 3. (a) Illustration of three different kinds of carbon dots: GQDs, carbon nanodots (CNDs), and PDs [1]. Copyright 2015, Tsinghua Univ. Press. (b) Plots showing the dependence of bandgap energy on size of the C_3N fragments (blue datapoints are experimental values; black ones are theoretical). The inset shows a magnified plot of the data near the origin of the main plot [46]. Copyright 2017, Wiley-VCH GmbH.

Compared to other CQDs, the definition of HC-CQDs is, at present, the one that is most clearly specified. Nevertheless, the precise definition of the size of HC-CQDs is still in need of further clarification due to the potential for errors to arise due to surface/edge groups and lattice defects.

In 2010, Li et al. synthesized soluble GQDs of large and uniform size for the first time *via* a stepwise chemical procedure in solution [48]. In general, the quantum size effects in graphene are known to be a key factor affecting the bandgap which increases as the graphene fragments decrease in size [61]. In the opinion of Yan et al. [62] GQDs are zero-dimensional graphene materials with lateral dimensions typically less than 10 nm and an atomically thin graphitic plane (typically 1 or 2 layers, less than 2 nm thick). GQDs are often prepared starting from graphene-based precursors or graphene-like polycyclic aromatic hydrocarbons. As a result, GQDs usually possess graphene lattices which have a crystalline structure like that in a sheet of 1–2 layers of graphene. The main body of a GQDs is thus comprised of conjugated sp^2 carbon atoms, although some other elements (e.g., oxygen, nitrogen, and sulfur) may be encountered on its edge.

CDs are probably the most researched type of CQDs. They are fluorescent, carbon-based particles that are spherical in shape. More formally, they are usually defined as quasi-spherical carbon nanoparticles (NPs) with carbon cores less than 10 nm in size and surfaces adorned with functional groups containing (usually) oxygen or nitrogen. Furthermore, they mainly consist of sp^2-sp^3-hybridized carbon atoms or sp^2 domains embedded in amorphous carbon [62]. CDs typically have diameters that are >3 nm and generate relatively wide X-ray diffraction peaks due to the amorphous carbon present. Additionally, in contrast to GQDs, crystalline lattices are not observed when completely amorphous CDs are imaged *via* high-resolution transmission electron microscopy (HR-TEM). Moreover, while the electronic bandgap structure in GQDs is heavily influenced by quantum confinement effects [62], the bandgap structure in CDs is dictated by surface energy traps. Hoang et al. [63] have also suggested that surface functional groups and inner structure make CDs and GQDs differentiated, GQDs with a large conjugated domain and regular structure can be treated as a special kind of carbon nanodots (CNDs).

In 2012, Sun et al. showed that water-soluble, nitrogen-doped, carbon-rich, photoluminescent polymer nanodots can be generated by hydrothermally treating grass [64], thus generating a new kind of luminescent carbon material: PDs. In general, cross-linked or aggregated polymer derived from linear polymers or monomers are known as PDs [65]. They have a hybrid structure which mainly consists of organic polymer chains and a small carbon core possibly containing a small amount of inorganic material [66]. PDs have a lower degree of carbonization compared with CDs and their crystalline carbon cores are usually unnoticeable [67]. From the point of view of their method of preparation, PD formation mainly depends upon the polymerization and carbonization of small precursor molecules. This is very similar to the 'bottom-up' approach used to make CDs. As a result, the boundary between PDs and CDs is rather blurred and whether or not PDs can be viewed independently from CDs is a controversial subject. Some scientists (such as Song et al. [66]) think that PDs should be regarded as being different from CDs due to their unique characteristics, e.g., high oxygen content, superior aqueous solubility, and exceptional quantum yields. Others (like Shao et al. [67]) believe that PDs are just special kinds of CDs with low carbonization. Also, it may not be very logical to separate PDs from CDs as they have very similar chemical and fluorescence properties.

2.2. Properties of CQDs

CQDs have received a significant amount of attention as PL materials as their optical properties compete well with those of traditional fluorescent materials (i.e., dyes and semiconductor QDs). Also, they typically have magnetic and catalytic capabilities, which make them excellent candidates for use in fields including magnetic resonance imaging (MRI) [68] and electrochemical sensing, etc. Moreover, due to their nanocarbon structures, CQDs usually have other advantages when it comes to preparation and biological application. We list some advantages below.

2.2.1. Convenient functional modifications

CQDs invariably have various functional groups on their surfaces, e.g., hydroxyl, epoxy/ether, carbonyl, and carboxylic acid groups, etc. (Fig. 4) [69]. Moreover, doping and modifying their surfaces with heteroatoms can also be employed to 'tune' their chemical structures and hence properties. It has been demonstrated that heteroatoms such as nitrogen, boron, and sulfur, may be readily integrated (or co-doped) into CQDs by using heteroatom-containing precursors (Fig. 4) [70–72]. Unfortunately, given the intricate nature of the associated reaction mechanisms, the precise chemical structures of the doped CQDs produced always remain unclear.

In contrast, surface functionalization is more controllable as it is based on organic reactions whose reaction mechanisms are well-established. Moreover, various approaches can be used to achieve modification of the CQD surface. Methods have thus been developed that involve the use of surface chemistry or strong intermolecular interactions (e.g., covalent bonding, coordination bonding, π-π interactions, etc.) to regulate the band gap of the CQD and thus improve PL emission.

In addition, CQDs modified with $–NH_2$, –COOH, –CHO, and $–N(CH_3)_2$ groups have been demonstrated to exhibit low toxicity at concentrations up to 200 μg mL^{-1}, however CQDs modified with –OH groups have exhibited some cytotoxicity at concentrations around 100 μg mL^{-1} [29,73]. The burgeoning subject of CQDs modification has received much interest in recent years and a variety of chemical techniques have been successfully employed to functionalize the CQDs periphery (using both covalent and noncovalent means) [74,75].

2.2.2. Tunable PL properties

A key characteristic of CQDs is the propensity to display quantum confinement effects when the CQDs is smaller than its exciton Bohr radius [76]. These effects affect the separations between the energy levels in the CQDs. Therefore the spacing between the discrete energy levels is significantly affected by both the size and structure of the CQDs. That is, their luminescent characteristics strongly depend on their size and the level of doping and functionalization employed [77]. As a result, while investigate PL processes in CQDs, researchers tend to use the molecular orbital band model that is typically employed to describe the features of fluorescent organic dyes.

According to molecular orbital theory, in general, the smaller the particle, the bluer the shift in emission frequency will be (i.e., the luminescence has greater energy). So far, researchers have successfully managed to modulate the wavelength of the luminescence emitted by CQDs from 380 to 700 nm (Fig. 5a) [78]. The quantum yield has also been increased, it was initially less than 0.1 but it now extends up to 0.9 [79]. Thus, CQDs can readily meet the application requirements needed for using in fluorescent labeling. Tremendous achievements (e.g., solid state PL and phosphorescence) have also been made in other aspects of CQDs-based optical research (Fig. 5b, c, and Table 1).

2.2.3. Catalytic activity and photodynamic/sonodynamic activity

CQDs can also exhibit outstanding catalytic activity since the abundance of functional groups on their surfaces and in their lattices. For example, Kang et al. demonstrated that CDs-gC_3N_4 nanocomposites can be used as a photocatalyst to split water molecules using solar radiation and achieved impressive conversion efficiencies (Fig. 6a) [104]. More recently, Huang et al. demonstrated that CDs can be used as a photocatalyst to polymerize amino acids into polypeptides and proteins (Fig. 6b) [105]. They even managed to obtain proteins with tertiary structures, namely, an artificial insulin with biological functionality.

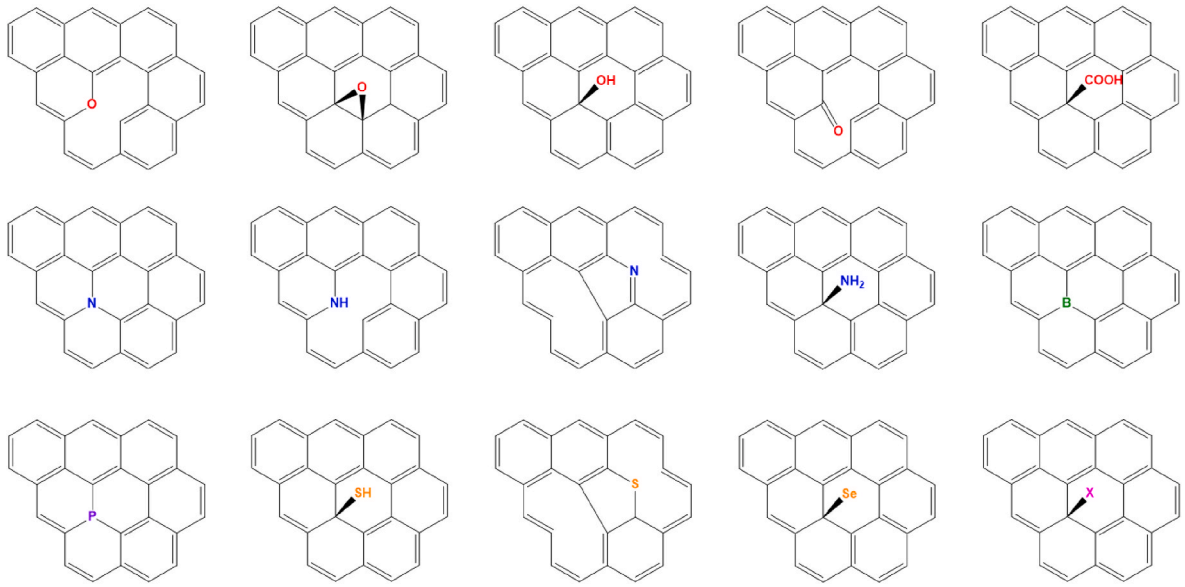

Fig. 4. Typical functional groups encountered in CQDs.

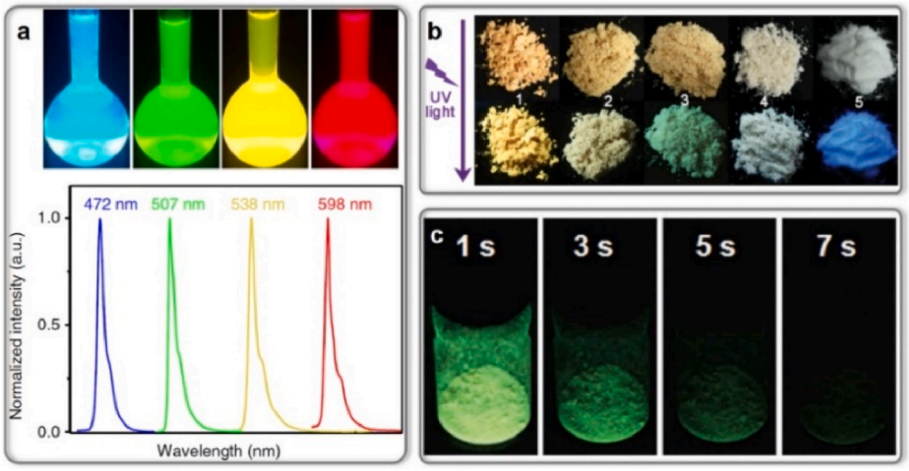

Fig. 5. (a) Fluorescent emission from GQDs excited using UV light at 365 nm (top) and corresponding normalized PL spectra (bottom) [80]. Copyright 2018, Springer Nature. (b) Photographs of CD powders in daylight (top) and under UV light at 365 nm (bottom) [81]. Copyright 2015, Wiley-VCH GmbH. (c) Photographs of a room-temperature phosphorescent CDs powder captured at different times after switching off the exciting radiation (UV at 365 nm) [82]. Copyright 2018, Wiley-VCH GmbH.

Owing to their outstanding catalytic activity, some CQDs also have inherent anticancer properties. They have thus found application in photodynamic therapy (PDT) and sonodynamic therapy (SDT) [49, 106–109]. The CQDs used in PDT mainly act as photosensitizers to produce reactive oxygen species (ROS) when illuminated. Previous research state that the special structures (heterogeneous atoms and defects) is the catalytic centers in photodynamic acoustic processes [110]. This is consistent with results of photocatalytic mechanism study based on CQDs. Indeed, some reports have shown the $^1O_2$ quantum yield of GQDs is ~1.3 under 1280 nm, which is approximately twice as high as that of all of the state-of-the-art PDT agents [111]. Yang et al. also demonstrated the rate constant for $^1O_2$ of N doped GQDs is 1.677 min^{-1} which is much higher than that of traditional sonosensitizers (porphyrin: 0.540 min^{-1}, porphyrin Mn: 0.415 min^{-1}, porphyrin Zn: 0.505 min^{-1}, TiO_2: 0.693 min^{-1}) [110].

The light used in PDT may be strategically tailored to solely irradiate the tumor lesion and spare healthy tissues. Such selectivity means that PDT is much less toxic to the host than conventional treatments like chemotherapy and radiotherapy [112,113]. The effectiveness of PDT, of course, depends on the ability of the light to penetrate the host to reach the target cells.

In contrast, SDT, which is a relatively novel method of non-invasively eliminating tumors, has much greater penetration depths in tissues. Furthermore, it improves patient compliance while having fewer negative effects. SDT uses ultrasound to activate a sonosensitizer and thus produce cytotoxic ROS. As a result, they force vacuoles in solution to collapse, permanently harming cancer cells. Clearly, CQDs with intrinsic phototheranostic and acoustic theranostic properties have considerable potential for application in the treatment of tumors [114]. Moreover, CQDs with good catalytic activity may also find application as electrocatalysts for use in the electrochemical detection of tumor markers.

2.2.4. *Magnetic properties*

Doping with heteroatoms is another way of providing CQDs with new properties [116]. For example, doping CQDs with lanthanides can

Table 1
Change in the PL performance of CQDs with time.

Aspect	Type	λ_{ex} (nm)	λ_{em} (nm)	Quantum yield (%)	Publication year	Ref.
Development of CQDs emitting short-wavelength light	CDs	340	450	NA	2010	[83]
	CDs	310	450	5.5	2011	[84]
	CDs	350	400	25	2012	[85]
	GQDs	346	425	33.6	2013	[86]
	CQDs	300	382	NA	2014	[87]
	CDs	300	375	11	2015	[88]
	CQDs	290	324	NA	2016	[89]
	CDs	360	255	6.17	2017	[90]
Development of CQDs emitting long-wavelength light	GQDs	670	780	2	2010	[91]
	CDs	460	520	2.72	2011	[92]
	CDs	480	542	2.2	2012	[79]
	GQDs	370	815	NA	2013	[93]
	PDs	570	760	1	2014	[94]
	CDs	360	880	NA	2015	[95]
	CQDs	432	1068	<0.5	2016	[94]
	PDs	*ca.* 470	*ca.* 800	8	2017	[96]
Quantum yield of the CQDs	CNPs	365	550	40	2010	[97]
	CQDs	440	510	80	2011	[98]
	GQDs	350	457	35	2012	[99]
	GQDs	360	435	78	2013	[100]
	CDs	360	437	83	2014	[101]
	g-C_3N_4	350	NA	90.2	2015	[85]
	GQDs	360	450	96	2016	[102]
	GQDs	356	426	99.8	2017	[103]

NA: not mentioned.

lead to species capable of emitting near infrared (NIR) luminescence or exhibiting magnetic resonance effects. Wu et al. [117] prepared manganese-doped CDs which produce intense luminescence and has a high sensitivity for ion detection. Manganese-doped CDs containing paramagnetic ions also display a good magnetic resonance response that allows them to serve as positive contrast agents (CAs) in MRI [117]. Furthermore, Li et al. demonstrated that the modulation of the local superacid microenvironment surrounding magnetic GQDs can accelerate the rate of proton exchange and effectively enhance the longitudinal magnetic relaxivity [115]. The relaxivity of the magnetic GQDs is thereby increased significantly (by 20-30-fold) throughout an extensive range of static magnetic field strengths compared to certain commercially available MRI CAs (Fig. 6c–6e).

2.2.5. *Chemical stability, photostability and biocompatibility*

Traditional organic fluorophores are not conducive to long-term imaging because of photobleaching. Semiconductor quantum dots have been extensively employed to address this issue. However, being much larger than biomolecules, semiconductor QDs may change the dynamics (functions) of the intended target and also attach with multiple targets to form artificial clusters. They can also be toxic as heavy metal ions can leach out from them. In contrast, CQDs are ideal for molecular imaging in cells. This is because they possess several key merits: good photostability and biocompatibility, very small size, facile functionalization, tunable PL emission, good dispersibility, as well as chemical stability [2].

Due to the stability of sp^2-sp^3 carbon nanostructure of CQDs, the photostability of CQDs is significantly better than that of traditional organic fluorophores. Indeed, the fluorescence intensity of CQDs slightly decreases after long-term UV-irradiation. This makes the long-time fluorescent image possible. On the other hand, the biocompatibility of a material is dependent on the specific application it is used for. However, the general definition of biocompatibility is the capacity of the material to carry out its intended function without trigger undesired biological responses [118]. Despite the fact that many carbon-based nanoparticles exhibit toxicity due to aggregation, CQDs display excellent solubility in water. As they are entirely composed of carbon, they also serve as a harmless substitute for metal-based nanoparticles as they eliminate the concern that toxic metallic residues may accumulate in body [29].

CQDs have thus shown strong application potential in various biological applications due to their low toxicity, e.g., in bioimaging, as biosensors, and in distinguishing specific cell, as markers. The cytotoxicity of GQDs, which are a specific kind of CQDs, was examined in human breast cancer cells and found to be essentially harmless at

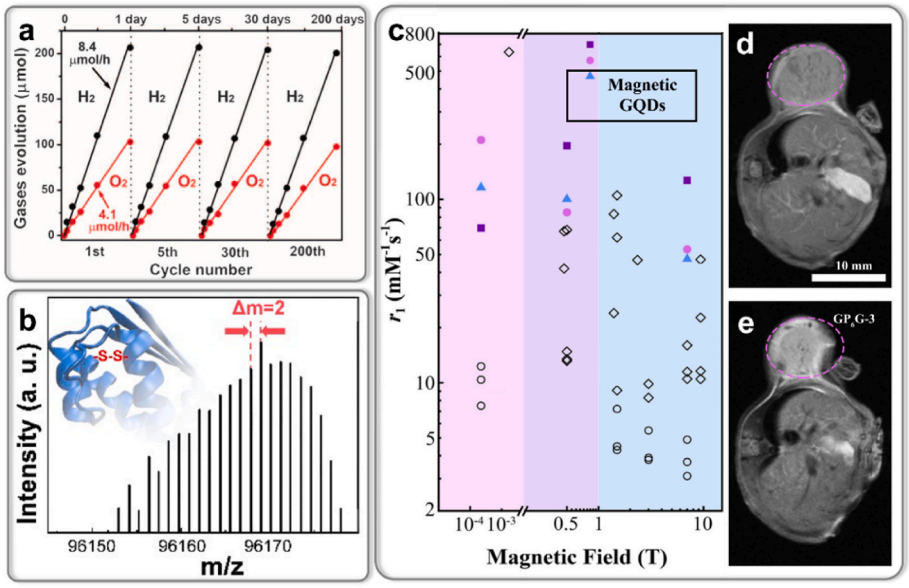

Fig. 6. (a) Rate of production of H_2 and O_2 from water irradiated with visible light and catalyzed using a CDs-gC_3N_4 composite [104]. Copyright 2015, American Association for the Advancement of Science. (b) Matrix-assisted laser desorption/ionization time-of-flight mass spectrum of the product obtained from the photocatalytic condensation of glutathione after reacting for 28 days [105]. Copyright 2019, American Chemical Society. (c) Comparison of the relaxivities of magnetic GQDs, commercially available MRI contrast agents (CAs), and other reported MRI CAs. (d) A pre-injection *in vivo* MRI image of a nude mouse with a tumor (circled). (e) Corresponding MRI image captured 30 min after the injection of magnetic GQDs. A 7.0 T animal MRI scanner was used to image the mouse after a subcutaneous injection [115]. Copyright 2020, Elsevier Science Ltd.

concentrations below 50 μg mL^{-1} [119]. Zhu et al. also discovered that GQDs do not cause cell toxicity lower than 400 μg mL^{-1} [120].

Because of their structural diversity, CQDs can be employed to tune the catalytic activity of enzymes, permeability of cell membranes, and expression of genes [19,121–124]. Besides their use in fluorescence on/off applications, CQDs-based sensing systems can also be designed to take advantage of peak shifts and lifetime changes and be used for ratiometric sensing and bi-modular detection. In particular, high-performance CQDs-based lab-on-chip devices are highly desirable for use in some very important sensing/detection applications, e.g., the early diagnosis of diseases, radiation prevention, and public safety [125,126].

2.3. Application of CQDs to biological fields

There has been a great deal of published reviews about CQDs recently, which tend to highlight various aspects of CQDs, such as their preparation techniques, structures characteristics, optical properties, and applications [127]. The number of CQDs-related publications has thus increased rapidly in recent years (Fig. 7a). Of particular note is that CQDs are gradually replacing semiconductor QDs (e.g., CdTe [128,129] and copper indium sulfide [130]) which have been employed in a multiple fields for some years (especially in biology).

Interestingly, the focus of CQDs research has varied somewhat over the decades. The main topics covered have included: the development of various synthetic techniques (2010–19) [93,131–138], structural modifications (2017–19) [61], modifying emission wavelengths (2013–17) [78,139–141], and enhancing quantum yield (2014–19) [142,143].

Various types of syntheses have been developed, encompass typical bottom-up [139,144,145] and top-down [146] approaches. The synthesis techniques thus developed made it feasible to synthesize CQDs on a large scale as well as produced them rapidly, efficiently, and eco-friendly. Modifying the structures of the CQDs produced in a controllable manner is one of the most fundamental methods of improving their performance in specific applications [61,147]. As a result, large amount of effort has been made in this direction in the past few years. The techniques employed include edge modification, lattice doping, and modifying the functional groups on the surfaces of the CQDs [148].

CQDs have been reported with a wide range of emission wavelengths (λ_{em}). Collectively, the entire range from deep ultraviolet to NIR (380–700 nm) can thus be covered [78]. This indicates that they are now easily applicable in a variety of applications, such as photo/electron catalysis [104], photoelectric conversion [149,150], biological imaging [151–154], disease diagnosis [155], and treatment [156,157].

Initially, because of their unique luminescent properties, CQDs only tended to be utilized as fluorescent probes for supplying fluorescence images and mediate drug delivery in combination with anticancer drugs to treat tumors [14,158,159]. For example, in order to combine the optical properties of CQDs with the therapeutic value of anticancer agents, Sun et al. successfully bonded oxidized oxaliplatin onto the surface of CQDs [160]. The *in vitro* and *in vivo* studies showed that the fluorescence from the CQDs can be used to successfully monitor and track the distribution of the oxidized oxaliplatin and, consequently, adjust the medication's injection timing and dosage.

The use of CQDs as drug carriers has achieved positive results in the diagnosis and treatment of tumor. However, certain significant issues remain, such as drug leakage and the complexity of synthetic routes. Therefore, in recent years, finding CQDs with intrinsic therapeutic properties, as well as excellent optical properties, has been extensively explored. In the biological area, this has led to the rise of inherent PDT, PTT, and multimodal or stimulus-responsive phototherapeutic characteristics in tumor therapy [109]. Since it was first proposed by Hsu et al. in 2013 [161], CQDs are also extensively employed in phototherapy and clinical treatment of superficial cancers e.g., skin cancer. With this technique, photosensitizers are concentrated inside the tumor tissue, and then radiation is used to cause the creation of ROS and subsequently cause apoptosis (programmed cell death) [159].

Overall, CQDs have attracted a considerable amount of attention in recent years (especially in tumor diagnosis and treatment) due to their exceptional nanostructures, advantageous electronic, mechanical, optical, thermal properties and their safety and biocompatibility.

3. Overview of tumor diagnosis with CQDs

The word 'cancer' refers to a broad range of illnesses that can manifest in virtually any organ or bodily tissue when aberrant cells begin to grow out of control. They may also cross their initial boundaries to invade surrounding bodily regions and thereby spread to other organs.

The World Health Organization has estimated that there were nearly 20 million new patients suffering from cancer in 2020 (https://gco.iarc.fr/today/online-analysis-table, International Agency for Research on Cancer). Cancer can, of course, lead to the death of the host patient. In fact, they are the second most common cause of death in humans, globally accounting for the death of an estimated 9.6 million people in 2018 (i.e., one in six of all deaths) [162]. Fig. 7b gives a plot of the estimated age-standardized incidence rates of some high-risk cancers in 2020. As can be seen, breast, prostate, and lung cancers are the most prevalent types of cancer encountered in humans. As a result, these are the cancers that receive the most attention from researchers [163].

Although lifestyle modification, regular medical care, chemoprevention, and immunotherapy have proved beneficial for cancer prevention [164], tumor-related illness continues to grow globally. Naturally, this is placing a tremendous amount of physical, emotional, and financial strain on individuals, families, communities, and health systems. Defeating tumor-related illness is therefore of great significance in improving the quality of our lives and prolonging our life-spans. To achieve these goals, it is necessary to find better ways of diagnosing and treating tumors.

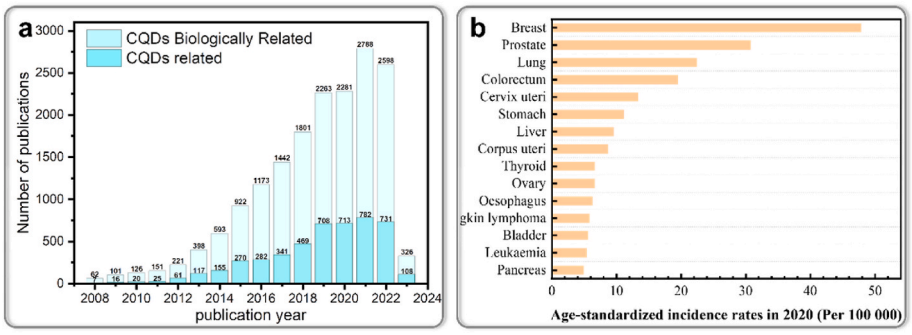

Fig. 7. (a) The number of articles published on CQDs since 2008 highlighted those that are related to biological applications. The decline in the number of articles in 2022 could be caused by the COVID-19. (Results from Web of Science, Jan. 2022.) (b) Estimated age-standardized incidence rates of some high-risk cancers in 2020.

3.1. Development of tumor diagnostic technologies

A precondition for tumor therapy is the existence of effective ways of diagnosing the occurrence of tumors. In particular, if tumor can be identified in its early stages of development, there is a greater probability that it will respond to treatment more effectively, making the treatment less expensive and greatly improving the survival rate of the patient [165].The aim of early diagnostic techniques is not only to identify symptomatic cancer patients but also those who have not yet developed any symptoms. Such patients can then be promptly referred for further diagnosis and appropriate treatment.

Currently, the diagnosis of tumor-related illness has great importance in patient screening. As a result, the demand for highly sensitive and accurate techniques for tumor diagnosis has increased year-on-year. Clinically, the diagnosis of tumor can be divided into two main types: (i) tumor tissue imaging and pathological diagnosis, and (ii) tumor-related biomarker detection. Typical techniques used to image tumor tissue include endoscopy, ultrasound (US) imaging, X-ray imaging, fluorescence imaging, MRI, and positron emission tomography (PET). Techniques used in tumor-related biomarker detection include antigen detection, antibody detection, nucleic acid detection, circulating tumor cell detection, extracellular vesicle detection, and microenvironment monitoring.

The use of CQDs in tumor diagnosis has advanced rapidly in the last two decades. They have shown great potential for use in imaging tumor tissues and detecting tumor-related biomarkers and microenvironments.

3.1.1. Imaging tumor tissues using CQDs

Tissue imaging is the most common approach used to clinically diagnose tumors. Images can be captured in various ways but endoscopy, US diagnosis, X-ray computed tomography (CT), MRI, and PET are the most commonly used clinical techniques. Each technique can be used to provide specific information about the tissues imaged, and the general aim is to directly visualize and identify any abnormal tissues that may be present. This information is then used by medical professionals to determine the best therapeutic steps to take to treat the patient. Table 2 summarizes the key features of some of the imaging techniques that are frequently used.

The CQDs used in imaging tumor tissues generally serve as either part of the imaging media or are directly imaged. The use of CAs has become routine in contemporary medical imaging as they can provide more evidence that can be used for clinical diagnosis and also reduce imaging time. The use of carbon nano-structural properties of CQDs to obtain MRI CAs with high magnetic relaxation rates gained significant attention [16,166–168]. Correspondingly, CQDs have also been explored for some applications in X-Ray imaging as CAs [116,169–171]. For the completeness of the review logic, we present a brief overview of the current research status of CQDs in X-Ray imaging. In fact, the research around CQDs in the field of CT is still comparatively scarce. Therefore, the specific advantages and application prospects of CQDs in this field still need to be further explored by researchers. In this section, we review the CQDs-based CAs that have been developed for use in X-ray imaging and MRI.

Table 2
Comparison of various imaging techniques.

Technique	Imaging time	Penetration depth	Resolution	Invasiveness	Radiation
Endoscopy	Real-time	Surface	Camera dependent	✓	None
US	Real-time	Shallow	Limited	None	None
CT	Few minutes	Deep	High	None	✓
MRI	Tens of minutes	Unlimited	Field dependent	None	None
PET	Few minutes	Deep	1–2 mm	None	✓

3.1.1.1. CQDs-based CAs used in X-ray imaging. When X-rays are used to image the body, hard tissues like bone and cartilage may be clearly distinguished from adjacent soft tissues. However, the contrast between various soft tissues is typically negligible or even nonexistent. Hence, contrast agents are required to improve the contrast in such images and thus reveal details about the soft tissues present [172]. X-ray CAs are often employed in X-ray imaging procedures including radiography, computed tomography, and fluoroscopy to give transitory contrast enhancement. Elements with high atomic numbers (Z) tend to absorb X-rays more strongly than those with low Z values (due to the photoelectron effect). Thus, the use of CAs with supeior X-ray attenuation (high Hounsfield unit, HU) enhances the X-ray images quality and makes it simpler to identify regions of interest. Current agents usually have poor X-ray attenuation and so better CAs need to be developed for use in X-ray imaging.

It is also worth noting that noble gases are another general class of contrast media, especially in certain applications such as X-ray CT imaging. Mesbahi et al. found a way to combine GQDs with bismuth oxide ($Z_{Bi} = 83$) to use as a CA and found it to be 1.7 times as effective a CA as Urografin® [173]. Gold nanoclusters coated with GQDs, which played the role of reducing agent, stabilizer, and drug carrier, have also been synthesized that can be used in CT imaging ($Z_{Au} = 79$) and also treat tumors therapeutically [174].

3.1.1.2. CQDs-based CAs used in MRI. CAs are used in MRI to improve the contrast of images and hence diagnostic accuracy. They are routinely used in about 40 % of all MRI scans, which represents about 40 million administrations of CAs worldwide per year [175,176].

Complexes containing superparamagnetic gadolinium ions (Gd^{3+}) are generally used as CAs in MRI. According to the Solomon-Bloembergen-Morgan hypothesis, these ions contribute to the relaxing of proton spins by producing a fluctuating magnetic field through electronic spin relaxation and molecular motion [177,178]. They thus lead to shorter longitudinal relaxation times (T_1) of the protons and faster imaging (high throughput), making the images less sensitive to artifacts caused by motion (i.e., the image has better quality). Since the use of Magnevist® (Gd-DTPA) was first approved in 1988, the growth of contrast-enhanced MRI has shown extraordinary development and nearly 50 tons of gadolinium are administered annually [175,177]. However, the longitudinal relaxivities (r_1, usually expressed in units of $mM^{-1}\,s^{-1}$) of commercially-available Gd^{3+}-based CAs are low, which means that high doses of toxic Gd^{3+} compounds need to be administered before conducting the MRI scan. Moreover, in 2006, these agents were associated with nephrogenic systemic fibrosis, a catastrophic and potential fatal sickness [179].

In the past decade, the feasibility of using GQD-based CAs in MRI was demonstrated by several workers who developed agents with r_1 values ranging from 9.87 to 15.995 $mM^{-1}\,s^{-1}$ [180–182]. Building on these results, Ding et al. showed that by modifying the superacid microenvironment surrounding the GQDs, ultra-high r_1 values can be attained (corresponding to 210.9 $mM^{-1}\,s^{-1}$ at 114 μT) [183]. The localized superacid microenvironment strongly enhances the rate of proton exchange and hence increases image contrast. The authors also showed that suitably modifying the surface of the QDs (with folic acid ligands) enhanced the ability of the CAs to target tumors. They were thus suitable for use in MRI-fluorescence dual-mode *in vivo* tumor imaging with an uptake rate in tumorous cells of over 98.3 % [183].

3.1.2. Tumor-related biomarker detection using CQDs

The fact that CQDs can be used to detect and quantify different analytes points to another (non-invasive) way in which they can be used to diagnose the presence of tumors. In the current context, the analytes

in question may be present (for example) in samples of fluid obtained from the body. Furthermore, the analytes we wish to detect might be antigens, antibodies, nucleic acids, circulating tumor cells, extracellular vesicles (EVs), or any other biomarker that may point to the presence of a tumor in the host. Specific examples are given below.

3.1.2.1. Antigen detection. Tumor-related carbohydrate antigens are molecular markers that are overexpressed on the surfaces of tumor cells. They contain glycan structures and produced by the combined activity of glycotransferases and glycosidases which are abnormally expressed in tumor cells [184]. Such antigens can be classified as glycoprotein antigens and glycolipid antigens. Carcino-embryonic antigens are one of the most widely used tumor markers on cell surfaces and can be used to identify a series of tumors and evaluate curative effects, as well as prognosing some tumors [185,186].

3.1.2.2. Antibody detection. Antibodies are a special nature class of immune-system associated glycoproteins known as immunoglobulins. They are produced by differentiated B-cells as part of the immune response to the presence of an immunogen [187]. Antibodies are vital to survival and play an irreplaceable role in the immune systems of higher animals. A typical mammalian antibody unit is a heterodimer composed of two identical long heavy chains (about 450–600 amino acid residues) and two identical short light chains (around 220 residues) [188]. The heavy chains, which differ from animal to animal, are substantial polypeptide subunits. The four chains are joined together to create a 'Y'-shaped molecule [187].

The concept of using antibodies to selectively target tumors was first proposed by Ehrlich over a century ago [189]. Ever since tumor-related autologous antibodies were first observed [190], the suggestion that they could serve in a diagnostic strategy is using minimal invasive procedures as an early disease sign. However, because some specific antibodies form tumor may possibly elicit response against a huge variety of antigens, therefore it cannot be successfully employed for tumor screening and early diagnosis [191]. Another strategy is to incorporate several types of antibody responses into a diagnostic algorithm [191]. Increased sensitivity should be achievable with such a method without significantly complicating the diagnostic process. Moreover, the antibodies can be used to effectively treat patients with tumors [192–194].

3.1.2.3. Nucleic acid detection. MicroRNAs (miRNAs) are a class of non-coding RNA species that are very short (about 21 nucleotides) and have critical functions across a variety of biological processes, including development, differentiation, apoptosis, and proliferation [195–197]. Compared with long non-coding RNA molecules (which have tens or hundreds of thousands of bases) [198], miRNAs are relatively easy and convenient to identify because the RNA can be rapidly cloned [199,200].

It has been proposed that miRNAs contribute to oncogenesis because they can function either as tumor suppressors or oncogenes [201–203]. It has been shown, for example, that miRNA alterations are involved in the initiation and progression of human cancer [199]. MiRNA is expressed with an extraordinary level of diversity across different cancers, and so a small number of miRNAs can furnish a large amount of diagnostic information [204]. In fact, unlike messenger RNA (mRNA) expression, a modest number of miRNA molecules (*ca.* 200 in total) might be sufficient to classify all of the tumors found in humans [204].

Circulating cell-free DNA (cfDNA) was first reported in 1948 [205] and has been found to circulate in the blood and other body fluids including urine [206], cerebrospinal fluid [207], pleural fluid [208], and saliva [209]. An increase in cfDNA concentration was detected in the blood of cancer patients in 1977 [210], suggesting that cfDNAs could potentially be used as messengers heralding the occurrence of tumors. Furthermore, the cfDNA concentration is higher in the blood of patients with benign diseases compared to that in healthy individuals, but lower than that in cancer patients [211,212]. Additionally, it has been shown that cfDNA expression is higher in patients with metastatic cancer and those with large-sized tumors, and its concentration is further increased in the advanced stages of cancer development.

It has also been found that the concentration is further and that cfDNA expression is higher in patients with metastatic cancer and those with large-sized tumors [213]. However, no significant differences were found in cfDNA concentrations in the blood of patients with different oncological diseases [214]. Thus, the use of cfDNA concentration as a specific marker for a specific type of cancer does not seem to be a realistic proposition [214]. More recently, however, the fragmentation patterns of cfDNA across the genome have been found to have good prospects for application in tumor screening [215].

Circulating tumor DNAs (ctDNAs), which were first reported in 1989 [216], are mutant DNA fragments that are shorter than cfDNAs [217] and also circulate in the plasm. As the name implies, they originate from tumor cells [218] and, when present, account for a mere 0.01 % of the total circulating DNA [219]. The ctDNAs are highly specific markers for tumors and have therefore been explored as potential prognostic and/or predictive markers for tumor diagnosis [220,221].

3.1.2.4. Detection of circulating tumor cells. First described in 1869, circulating tumor cells (CTCs) are malignant cells that have migrated into the circulation system and derive from either the primary tumor itself or its metastases [222]. CTCs have been adopted as a class of clinical biomarkers in molecular pathology [223] and their occurrence in patients is a useful source of information that can be used in early-diagnosis investigations [224], prognosis [225], and relapse identification [226]. CTCs occur at low concentrations in the peripheral blood, ranging between 1 and 10 cells per 10 mL in most cancer patients, which makes their detection rather challenging [227]. The enrichment and detection of CTCs is thus a significant field of investigation.

3.1.2.5. Detection of membrane vesicles. Direct interaction between tumor cells and their environment is essentially required for cancers to progress. Therefore, an efficient means of information exchange must exist to facilitate this cell-cell communication. Membrane vesicles (EVs) are heterogeneous, membrane-bound, phospholipid vesicles that are actively secreted by mammalian cells [228]. They can mediate long-range intercellular communication *via* the delivery of genetic material from one cell to another and therefore constitute potential tumor-related biomarkers [229]. EVs contain a treasure trove of cellular cargo (informative biomarkers like nucleic acids that can allude to the presence of certain diseases [230,231]). They are relatively small, 50–200 nm, which makes them smaller than cells but larger than proteins [232]. EVs can be classified into three groups: exosomes, microvesicles, and apoptotic bodies [233].

Exosomes are derived from the inward invagination of the endosomal membrane pathway [234], and the protein topology in exosomes has the same orientation as in the plasma membranes of cells [235]. Microvesicles are produced by the outward blebbing of the plasma membrane [236] and can also be formed *via* a process that parallels viruses budding from cells. The plasm membrane bilayer has an asymmetrical distribution of phospholipids [237]. Unlike the occurrence of exosomes and microvesicles, apoptotic bodies are generated from the programmed apoptosis of both normal and tumorous cells [238].

Different techniques (electrochemical sensing, PL sensing and imaging, electrical sensing, etc.) have been developed for detecting tumor-related biomarkers that take advantage of the outstanding properties of CQDs, e.g., their PL properties, modifiability, catalytic activity, and electroactivity (Fig. 8). More specifically, electrochemical sensing, PL sensing, and electrical sensing are widely used in the detection of antigens, antibodies, nucleic acids, EVs, and microenvironment. Moreover, due to their outstanding PL properties, CQDs have remarkable application value in PL imaging of tumor cells.

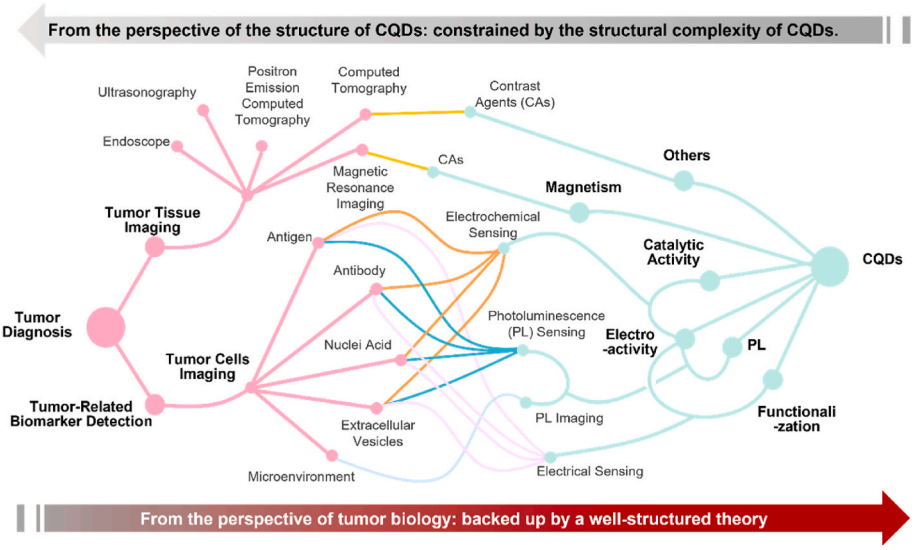

Fig. 8. Schematic diagram illustrating how CQDs-based techniques and basic properties of CQDs can be employed to detect tumor-related biomarkers.

3.2. Challenges in tumor diagnosis with CQDs

Reviews often summarize progress in research on CQDs-based tumor diagnosis from the point of view of CQDs structure or specific diagnosis technique [49,62,239]. However, as described in Section 1, the classification, definition, and structural definition of CQDs is still controversial and open. This makes it impossible to formulate their action mechanisms using the current (inadequate) theoretical frameworks available for CQDs (the direction indicated by the upper arrow in Fig. 8). Undoubtedly, advances in synthesis/characterization techniques, throughput screening technology, and machine-learning strategies will result in there being many great opportunities being discovered for CQDs. However, there is still an urgent need to summarize recent progress in research in terms of a well-developed framework.

Tumors themselves, however, have been systematically studied using established molecular biological techniques for many years. As a result, a fully developed biological theoretical framework for tumors has been developed. In the next part of this review, we summarize the current development of CQDs-based tumor diagnosis from the point of view of the hallmarks of cancer (the direction indicated by the bottom arrow in Fig. 8). Based on the manifestation of nine essential alterations in cell physiology (self-sufficiency in growth signals, evasion of apoptosis, insensitivity to anti-growth signals, sustained angiogenesis, tissue invasion and metastasis, limitless replicative potential, genomic mutations & instability, energy metabolism changing, and immune destruction escape), both the individual advantages and deficiencies in recent CQDs-based tumor-diagnosis research are found to be self-explanatory.

4. Sustaining proliferative signaling

One of the most striking differences between tumor tissues and normal tissues is the ability of the former to sustain proliferative signaling. It is well known that the production and release of growth-promoting signals is carefully controlled in normal tissues. When a normal cell receives a growth-promoting signal, the signal enters into the cell and leads to a cycle of cell growth and division, guaranteeing the cells remain in a state of homeostasis.

On the other hand, in tumor cells, these growth-promoting signals are deregulated. This behavior dominates the survival and energy metabolism of tumor cells. Typically, intracellular tyrosine kinases generate the abovementioned signals that are conveyed by growth factors that bind to receptors on the cell's surface. The mitogenic signaling pathway in cancer cells is well understood and can acquire the ability to maintain proliferative signaling in many ways [240–243].

In general, tumor cells can use three common molecular strategies to sustain proliferative signaling that involve: (i) altering extracellular signaling, (ii) altering extracellular sensors that change the signal, and (iii) altering the cellular circuits that convert signals into action. We discuss these strategies in more detail below. The main mechanisms responsible for sustained proliferation are illustrated in Fig. 9. As might be expected, some tumor diagnostic techniques have already been developed based on the main markers involved in these strategies.

4.1. Altering extracellular signaling

Tumor cells can achieve cell proliferation by generating autocrine growth factors. Normal mitogenic growth factors (GFs) are polypeptides produced by specialized cells and can produce signals to stimulate growth. GFs can enforce proliferation (and other cellular functions) by binding to specific highly compatible receptors in the cell membrane. Tumor cells, however, generate GFs, such as platelet-derived growth factor (PDGF) and transforming growth factor α (TGFα), which react with the expression of cognate receptors, causing the cells to enter active cell cycles and enhancing their ability to proliferate independently. The main markers of this molecular strategy are shown in Fig. 10a.

Microtubules are unique tubular organelles that are common in eukaryotic cells and form an important part of their cytoskeletons. They are crucial to cell mitosis and chromosome segregation. Thus, the effective detection of α-tubulin is helpful for diagnosing tumors. Chiu et al. [244] created a cross-linking approach that provides functional groups for biomolecular conjugation while also covalently attaching functional molecules to the polymer dots. They prepared anti-α-tubulin modified PFBT–NH–PIMA PD-streptavidin and used the PDs to label the subcellular microtubules in HeLa cells. As shown in Fig. 10b, the individual tubular structures are well-resolved and can be clearly seen. This paper describes a technique for creating stable and uniformly functionalized PDs, which is significant for enhancing labeling effectiveness and sensitivity in cellular tests.

4.2. Extracellular sensors that change the signal

Here the tumor cells overexpress or transform the GF receptor proteins thereby intensifying the delivery of GF. After binding with the GF, the GF receptors on the cell surface can activate the intracellular signaling system to deliver the growth stimulation signal into the cell

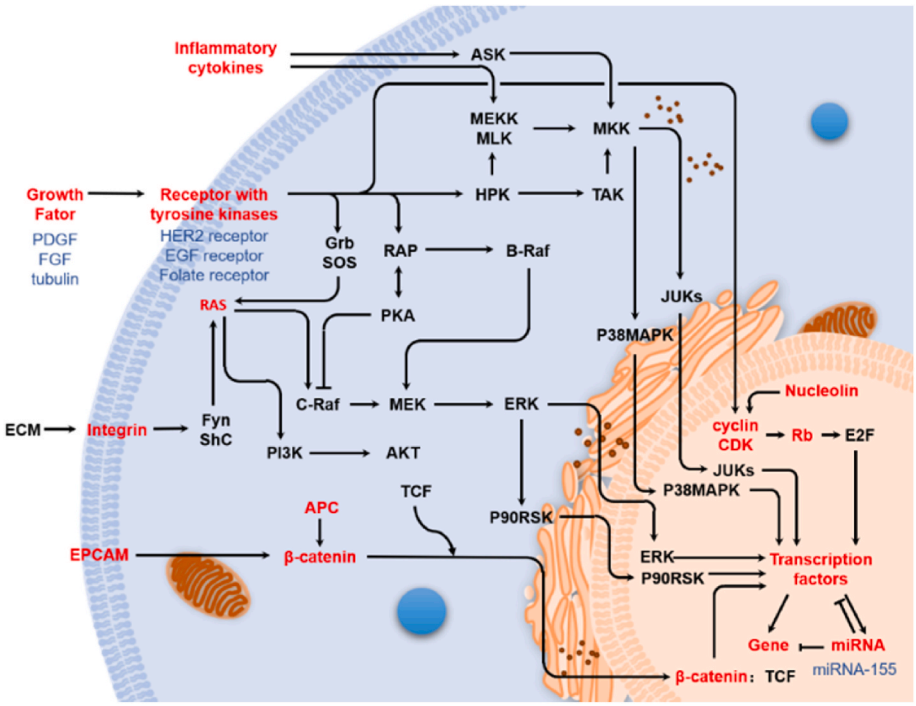

Fig. 9. The intracellular signaling networks that dominate the sustained proliferation of tumor cells. Some genes that are acknowledged to be associated with carcinomas are marked in red. This depiction emphasizes the primary functions of the biomarkers as their participation in tumorigenesis is often multifarious.

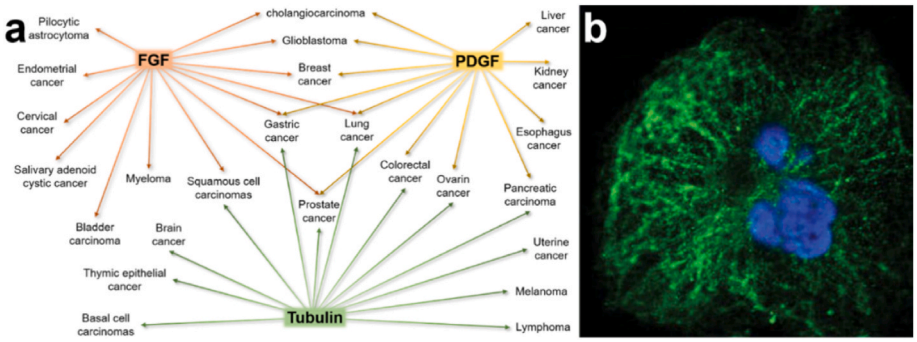

Fig. 10. (a) Cancer cell lines that are responsive to fibroblast GF (FGF), PDGF, and tubulin. (b) PD-streptavidin-crosslinked HeLa cell microtubules in a confocal fluorescence microscopy image [244]. Copyright 2012, Wiley-VCH GmbH.

and produce the corresponding biological effects. GF receptors usually carry tyrosine kinase activity within their cytoplasmic domain and are overexpressed in many tumors.

Overexpression of GF receptors may cause tumor cells to overreact to GF levels that would not normally trigger proliferation. In addition, the overexpression of GF receptors can induce ligand-independent signal transduction. The main markers of this molecular strategy are shown in Fig. 11a. In recent work, it has been shown that AS1411, HER2, epithelial cell adhesion molecules (EpCAMs), and folic acid (FA) receptors can be used as markers to detect tumor cells that use this proliferation strategy. In these works, CQDs were modified and used as PL or electrical probes in order to achieve tumor diagnosis and treatment. With the aim of destroying tumors by inhibiting tumor proliferation, for example, Wang et al. [245] developed a theranostic agent made of AS1411-GQD conjugates capable of actively targeting tumor cells (Fig. 11b). The aptamer AS1411 induces micropinocytosis in the tumor cells which allows the AS1411-GQD conjugates to quickly enter them. The AS1411-GQD conjugates thus showed high specificity with respect to tumor cells (including A549, HeLa, MCF-7, HepG2, COS-7, and HEK293). Moreover, the AS1411-GQD conjugates further promoted micropinocytosis by inducing EGFR, Akt, p38, and Rac1 activity, eventually leading to non-apoptotic cell death [247].

Noh et al. fabricated polyarginine co-modified 'dots-on-spheres' structures (neu-Parg@gDoS) in which conjugated PDs are immobilized on the surface of Si spheres [246]. It is known that the transmembrane tyrosine kinase receptor HER2, which exhibits partial homology, regulates cell growth and survival in a typical manner [248–250]. In Ref. 246, Noh et al. used their neu-Parg@gDoS dots-on-spheres to target HER2 receptors and achieved good levels of specificity and targetability. They were used to target and PL-label HER2 overexpressed by tumor cells such as SKBR-3 breast cancer cells (Fig. 11c). In contrast, the neu-Parg@gDoS species showed no targeting and PL-labeling ability towards cells with low HER2 expression (e.g., MDA-MB-231 cells, as shown in Fig. 11c).

EpCAM is one of the most well-studied tumor-associated antigens and has been found to be overexpressed in most types of cancer (e.g., colorectal, breast, pancreatic, and liver cancer) [251–256]. It accelerates the cell cycle and induces cell proliferation which leads to tumorigenesis [257–260]. Therefore, EpCAM is an important biomarker and has long been used in tumor diagnosis/prognosis [261–266].

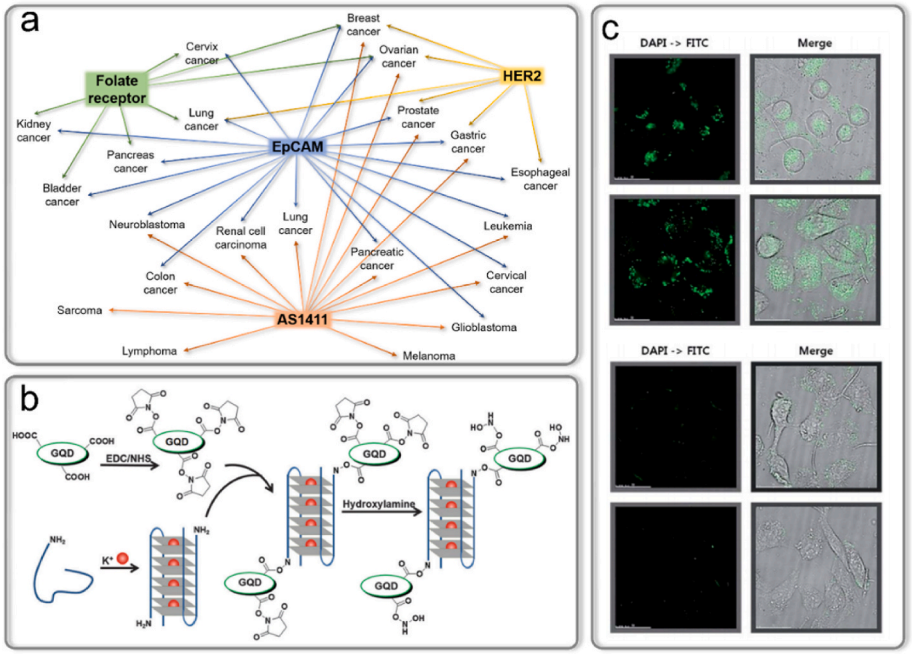

Fig. 11. (a) Cancer cell lines that are responsive to folate receptor, HER2, epithelial cell adhesion molecules (EpCAM), and AS1411. (b) Schematic diagram showing the conjugation of GQDs with AS1411 [245]. Copyright 2015, the Royal Society of Chemistry. (c) Confocal laser scanning microscopy images of SKBR-3 breast cancer cells and MDA-MB-231 cells after incubation with neu-Parg@gDoS for 2 and 6 h [246]. Copyright 2014, the Royal Society of Chemistry.

Yang et al. [262] devised a 'turn-on' fluorescence sensing platform based on MoS_2 nanosheets modified with GQDs, polyethylene glycol (PEG), and EpCAM aptamer that can be used to detect EpCAM. The PL signal from the GQDs is quenched by the MoS_2 nanosheet *via* fluorescence resonance energy transfer (FRET, see Fig. 12a). In the presence of EpCAM, the stronger affinity that exists between aptamer and EpCAM leads to the GQDs being detached from the MoS_2, restoring the PL signal from the GQDs. The concentration of the EpCAM could

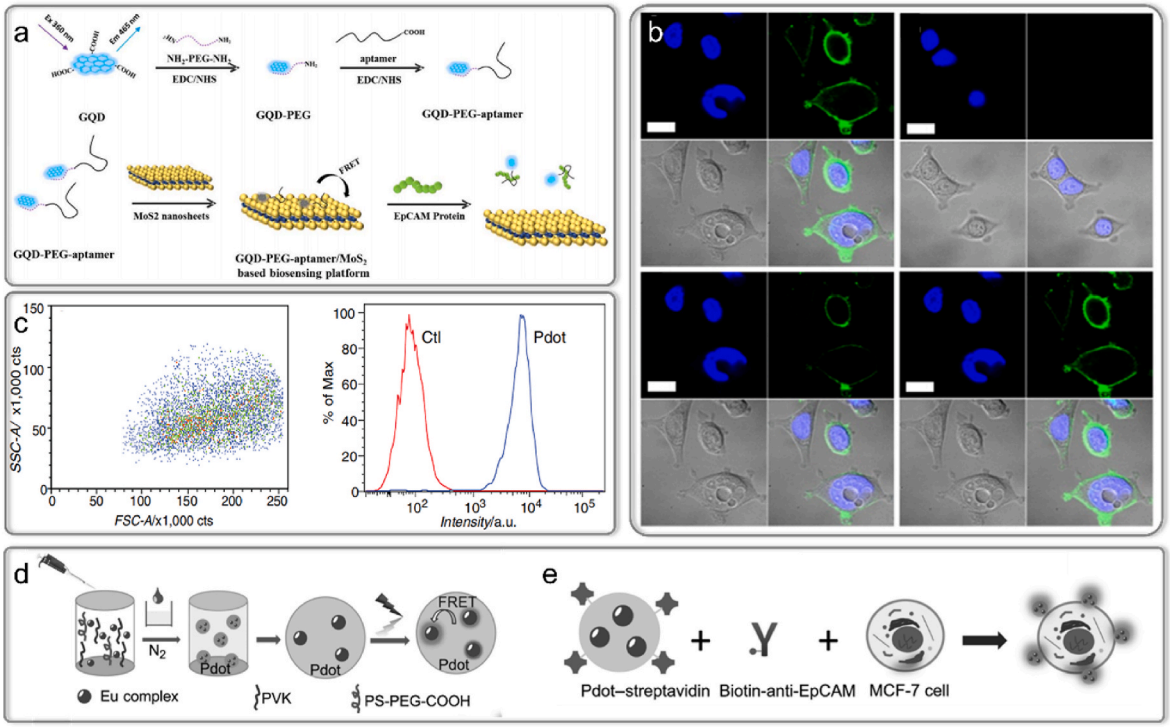

Fig. 12. (a) Fabrication of the GQD-PEG-aptamer/MoS_2 sensing platform and mechanism involved in EpCAM detection [262]. Copyright 2017, Elsevier. (b) Confocal fluorescence images of PFBT-SP-streptavidin-labeled MCF-7 cells. The nuclear counterstain (Hoechst 34580) and PFBT-SP-streptavidin exhibit green and blue fluorescence, respectively [267]. Copyright 2012, American Chemical Society. (c) Flow cytometry measurements made using cross-linked PFBT–NH–PIMA PD-streptavidin [244]. Copyright 2012, Wiley-VCH GmbH. (d) Procedure used to prepare Eu complex/PVK PDs. (e) Labeling cells using Eu complex/PVK PD-streptavidin bioconjugates [268]. Copyright 2013, Wiley-VCH GmbH.

then be measured spectrophotometrically. The limit of detection (LOD) of the method was determined to be 450 pM and the linear range of detection corresponded to 3–54 nM. Chan et al. [267] conjugated streptavidin onto the surfaces of PDs using biotin-streptavidin interactions and thus created photoswitchable PDs (PFBT-SP-streptavidin conjugates). They were then used to specifically target Michigan cancer foundation-7 (MCF-7) cells, the PD-streptavidin probes effectively labeling the EpCAM receptors on the surfaces of the MCF-7 cells (Fig. 12b). Yu et al. [244] also developed green-emitting cross-linked PDs which were subsequently used to carry out flow cytometry measurements (Fig. 12c). Chiu et al. [268] developed a time-gated tumor--imaging technique based on Eu complex/semiconducting polymer poly (9-vinylcarbazole) (PVK) PDs (Eu complex/PVK PDs) (Fig. 12d, e). The Eu complex/PVK PDs have a high quantum yield (0.315) and long fluorescence lifetime (509 μs). Eu complex/PD-streptavidin conjugates were subsequently used to successfully label EpCAM receptors on the surfaces of cells. As a result of the PDs' prolonged luminescence lifetime, its fluorescence can be readily separated (time-gated) from that of other sources, which enhances particle discrimination and the signal-to-noise ratio of ensuing images. Recent diagnostic techniques based on EpCAM detection using CQDs are summarized in Table 3.

Unlike the macromolecular markers already discussed (AS1411, HER2, and EpCAM), FA is a small molecule with simple chemical structure (Fig. 13). The molecule contains both basic (-NH_2, –NH–) and acidic functional groups (-OH, –COOH) which means it can be readily used to modify CQDs. Some recent approaches used (including surface modification and polymerization-carbonization) are illustrated in Fig. 13 and Table 4.

FA can be reduced to tetrahydrofolate, which is a one-carbon coenzyme involved in one-carbon metabolism and de novo synthesis of purines and thymine. When folate receptors (FRs) are expressed at a high level, the de novo synthesis of nucleotides is accelerated, leading to accelerated division of tumor cells which accelerates the occurrence and development of tumors. Many experiments involving FRs and CQDs have been carried in order to diagnose tumors [269–295].

In 2012, Song et al. [274] proposed a new method for modifying green fluorescent CDs with FA. (Fig. 14a). The FA-modified CDs were then used to target tumor cells *via* their FR. In this way, they could easily distinguish between tumorous and normal cells in a mixture of NIH-3T3 and HeLa cells. Zhang et al. [270] heated FA with tris(hydroxymethyl) aminomethane to prepare FR-targeting GQDs (FR-GQDs). PL spectrophotometry and confocal imaging could then be used with the FR-GQDs to distinguish between tumor and normal cells (Fig. 14b and c). In addition, the amino groups play a significant role in producing the high quantum yield and stability of the FR-GQDs.

Ding et al. [299] synthesized GQD nanozymes ('GQDzymes') and developed exosome-like nanozyme vesicles for use in H_2O_2-responsive photoacoustic imaging of nasopharyngeal carcinomas *in vivo* (Fig. 14d). They also obtained fluorescence images to test for tumor targeting and utilized confocal laser scanning microscopy to analyze the distribution of nanozyme vesicles within the cells. Liu et al. [284] designed a label-free photoelectrochemical cytosensor based on the occurrence of resonance energy transfer between CDs and gold nanoparticles. The tumor cells attach to the electrode surface due to the affinity between the overexpressed FRs on cancer cells and FA, which handicaps electron donation and lowers the photoelectrochemical response. (Fig. 14e and f).

4.3. Altering the cellular circuits that convert signals into action

Growth-promoting signals are normally activated in cells by receptors responding to ligands outside the cells. Some tumor cells, however, can obviate the need for this ligand-mediated activation process. They do this by altering extracellular matrix receptors (integrins) so that they deliver growth-promoting signals. Integrins are bifunctional heterodimeric transmembrane receptors that connect the cell to the extracellular matrix (ECM) in a physical way. When successfully bound to the ECM, the integrin receptor can transduce signals into the cytoplasm thereby influencing the cell's behavior. It can, for example, cause the cell to enter an active cell cycle. Both activated GF receptors and integrins are involved in activating the SOS-Ras-Raf-MAP kinase pathway. The Ras proteins transform their structures to implement the release of mitotic signals into the cell without the constant activation of their normal upstream regulators.

MiRNAs are short, single-stranded RNA molecules [300–307] whose dysregulated expression is associated with various tumors: the miRNAs associated with some of the most common tumors are listed in Fig. 15. MiRNAs can have an impact on various tumor signals, and each regulate hundreds of target genes, hence accommodating multiple links between different aspects of tumor behavior, e.g., growth, differentiation, apoptosis, etc. (Table 5). By concurrently targeting many genes that prevent mutations, miRNA-155 and miRNA-21 increase the mutation rate while lowering the effectiveness of DNA protection systems by targeting cell-cycle regulators, therefore, they may make it possible to

Table 3
Recent tumor diagnostic techniques based on detecting EpCAM using CQDs.

Materials	Method	λ_{ex} (nm)	λ_{em} (nm)	LOD	Linearity range	Sample	Cell line	Ref.
GQD-PEG-aptamer/MoS_2	PL spectrophotometry; Confocal fluorescence imaging	365	468	450 pM	3–54 nM	EpCAM aqueous solution	MCF-7	[262]
PFBT-SP-streptavidin conjugates		450	540	NA	NA	NA	MCF-7 HeLa	[267]
Eu-complex-grafted PSMA PDs		<350	615	2.4 nM	0–0.5 μM	EpCAM aqueous solution	MCF-7	[261]
SA-dot		350	672	NA	NA	NA	MCF-7	[263]
PFDPFBT-PS-PEG-COOH PDs		425	530	NA	NA	NA	MCF-7	[264]
PFS1 PD	Flow cytometry measurement; Confocal fluorescence imaging	380	693	NA	NA	NA	MCF-7	[266]
PFS2 PD		380	711					
PD16		400	610	NA	NA	EpCAM aqueous solution	MCF-7	[296]
PD33		400	600					
PD59		400	600					
PF-BT-DBT PDs		450 695 775	640 720 780	NA	NA	NA	MCF-7 HeLa	[297]
PFBT–NH–PIMA PDs		450	540	NA	NA	NA	MCF-7	[244]
CL-BODIPY 565 PDs		450–460	565	NA	NA	NA	MCF-7	[298]
Eu complex/PVK PDs	Time-gated fluorescence microscope imaging	342	612	NA	NA	NA	MCF-7	[268]

NA: not mentioned.

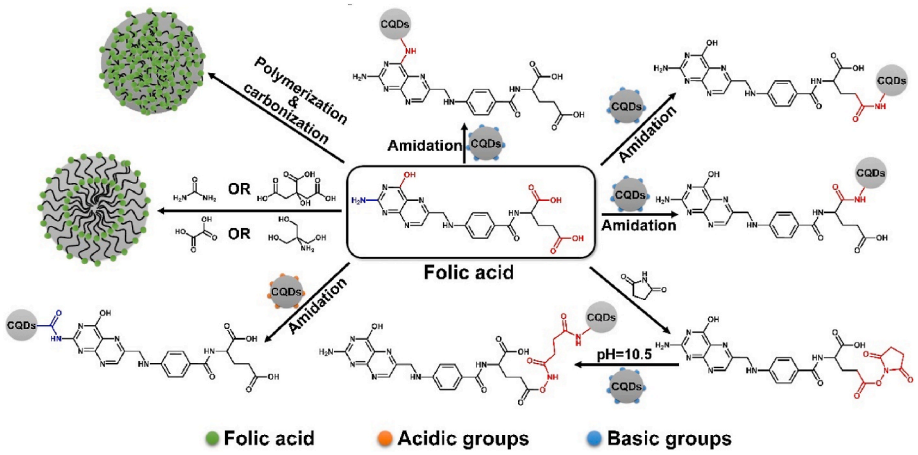

Fig. 13. Different ways folic acid can be used to modify CQDs.

Table 4
Preparation method, morphology, optical properties, and tumor-targeting ability of CQDs modified using FA.

Method	Reaction Conditions	Size (nm)	λ_{ex} (nm)	λ_{em} (nm)	φ	τ (ns)	Cell line	Targeting rate (%)	Ref.
Polymerization of FA	180 °C, 2 h[a]	9	360	454	0.23	3.1	U87	NA	[269]
	aqueous NaOH solution, 90 °C, 1.5 h[c]	3.5	365	450	0.09	NA	HeLa	*ca.* 98	[283]
							SKOV3	*ca.* 98	
							HePG2	NA	
							MCF-7	NA	
	240 °C, 6 h[a]	5.4	320	400	0.945	15.4	HeLa	NA	[292]
Polymerization of FA and other precursors	Tris(hydroxymethyl)amino methane, 220 °C, 6 h[a]	1.95	320	395	0.77	NA	MCF-7	NA	[270]
							MDA-MB-231		
							SKOV3		
	Sodium citrate, 300 °C, 0.5 min[b]	1.8	365	465	0.28	12.5	HeLa	NA	[271]
							H9C2		
	Polyethyleneimine (MW:1800), 180 °C, 6 h[a]	5.8	370	452	0.42	7.68	HeLa	42.63	[288]
	Maleic acid, 180 °C, 2.5 h[a]	5.2	372	472	NA	NA	HepG2	NA	[280]
	Urea, 500 W, 8 min[d]	3.2	380	460	0.25	NA	GES-1	90	[290]
							HeLa	90	
Combined with amino groups in CQDs	C_3N QDs, 80 °C, 24 h[a]	4.6	368	540	0.91	NA	OCM-1	93.4	[19]
	Polyethyleneimine dots, 25 °C, 2 h[c]	30	400	475	0.026	4.07	KB	NA	[275]
	Polyethyleneimine modified CDs, 60 °C, 3 h[c]	2.5	300	385	NA	NA	HeLa	NA	[287]
							HepG2	NA	
	N-GQDs, 25 °C, 2 h[c]	5	370	440	NA	NA	MCF-7	NA	[278]
	$CHCl_3$, 60 °C, 2.5 h[c]	19	488	528	0.07	NA	HeLa	NA	[281]
							A459		
							MDA-MB-231		
Combined with amino groups in CQDs	SiO_2@CDs, citric acid, 25 °C, 15 min[c]	2.8	360	430	NA	NA	HeLa	NA	[285]
	80 °C, 12 h[a]	7.5	431	542	0.56	NA	MDA-MB-231	98.8	[22]
							SGC7901	99.2	
							SKOV3	96.4	
							SGC996	97.5	
							HCC827	98.5	
							PC3	96.7	
							8305C	94.6	
							WM-115	98.8	
							MCF-7	22.8	
	GQDs, 25 °C, 12 h[c]	2.3	488	590	NA	NA	HeLa	NA	[286]

NA: not mentioned.
[a] solvothermal treatment.
[b] Direct heating of solid mixture.
[c] With reflux.
[d] Microwave treatment.

choose the gene changes needed for the emergence and development of tumors [308–311].

Hu et al. [312] developed an electrochemical biosensor to detect miRNA-155. They activated the carboxyl groups of GQDs using N-(3-(dimethylaminopropyl)-N′-ethyl carbodiimide hydrochloride (EDC) and NHS adsorbed onto a gold electrode incorporating the target DNA. Horseradish peroxidase (HRP) was then noncovalently bound to the GQDs to immobilize it. The GQD-bound HRP could effectively

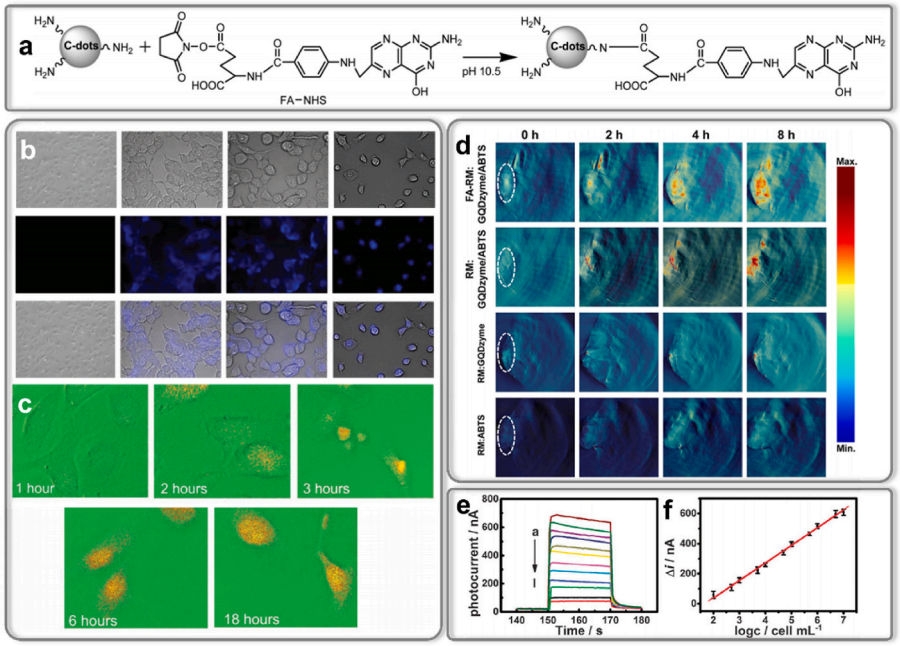

Fig. 14. (a) Conjugation of FA-NHS to CDs passivated with 4,7,10-trioxa-1,13-tridecanediamine [274]. Copyright 2012, the Royal Society of Chemistry. (b) Images of bone marrow-derived stem cells, MCF-7, MDA-MB-231, and SKOV3 cells. (c) Confocal images of transmission images (green channel) and fluorescence signal (yellow channel) in SKOV3 cells [270]. Copyright 2018, Wiley-VCH GmbH. (d) *In vivo* H_2O_2-responsive photoacoustic images illustrating the diagnosis of nasopharyngeal carcinoma [299]. Copyright 2019, American Chemical Society. (e) Photoelectrochemical response curves obtained using a cytosensor based on CDs and gold nanoparticles. (f) Linear calibration curve based on the data in (e) [284]. Copyright 2015, the Royal Society of Chemistry.

catalyze the H_2O_2-mediated oxidation of 3,3′,5,5′-tetramethylbenzidine (TMB) leading to an increase in the electrochemical current signal (Fig. 16a). The biosensor was found to be capable of detecting miRNA-155 with high sensitivity (concentrations from 1 fM to 100 pM) with a detection limit of 0.14 fM. Cao et al. [313] synthesized molecular beacons (MBs) containing fluorescent GQDs to discriminate between normal cells and cancer cells (*via* the interaction of the MBs with miRNA-155). Their multifunctional theranostic agent (GQD-PEG-P) exhibited a photothermal conversion efficiency of 28.58 % and high quantum yield with respect to singlet oxygen generation (up to 1.08). It is therefore suitable for use in PTT and PDT (Fig. 16b). A drug delivery system created by Yang et al. [314], in which CDs connect to stem-loop MBs that have been doped with the chemotherapy medication doxorubicin (Dox). The MB interacts with overexpressed miRNA-21 in cancer cells facilitating fluorescence recovery (thus aiding imaging) and release of chemotherapeutic drugs (Fig. 16c).

Nucleolin has a variety of biological functions. It promotes the growth of blood vessels [316–318], is involved in the inflammatory response [319–321], and plays a dominant role in disrupting the signal that inhibits proliferation and promotes cell division [316,322,323]. It thus helps to regulate ribosome biosynthesis and maturation and regulate cell proliferation, growth, embryogenesis, cytokinesis, chromatin replication, and nucleolar generation [324,325]. Nucleolin is overexpressed on the surface of cancer cells or tumor cell-related endothelial cells and it can shuttle between the cell surface and cytoplasm [317,324,326], making it an appropriate target for conjugation [316,322,327]. Many papers have employed AS1411 (a 26-mer oligonucleotide) as an MB for nucleolin [328,329].

Zheng et al. [315] selected AS1411 to use as a receptor. They first fabricated fluorescent mesoporous silica nanoparticles (FMSNs) to act as nanocarriers. AS1411 and ATP aptamer were assembled on their surfaces and GQDs adsorbed onto them *via* π-π stacking interactions. The GQDs act to cap the pores of the FMSNs as well as quench their emission of fluorescence (*via* fluorescence resonance energy transfer, FRET). The FRET-quenched nanocarriers were subsequently internalized into cells through the dual recognition of nucleolin and ATP. Inside the cell, the Dox is desorbed from the GQDs and mesopores and the FMSNs regain their ability to fluoresce, thus signaling that the drug has been successfully delivered (Fig. 16d). Motaghi et al. [330] incubated cancer and control cells in CD-AS1411 aptamer solution and detected the targeted cancer cells spectrofluorimetric ally. In the presence of tumor cells, the intensity of the fluorescence from the CDs is enhanced. In contrast, no significant change in the signal was detected in human foreskin fibroblast control cells.

5. Evading growth suppressors

Normal cells secrete growth suppressors to sustain the stability of cells and tissues. However, tumor cells have found ways of evading these growth suppressors. The cell cycle employs three checkpoints (G_1, G_2, and M) to ensure the cycle is properly regulated (Fig. 17). If a fatal mistake is discovered at a checkpoint, there are two possible denouements: (i) the cell enters a quiescent or resting phase (G_0) of mitosis and will not resume splitting until activated by a subsequent growth signal, (ii) the cell enters the anaphase of mitosis, depriving it of the ability to proliferate. Tumor cells dodge the effect of growth suppressors by mainly disrupting two pathways to acquire the ability to proliferate indefinitely. These are the retinoblastoma protein (pRb) and p53 pathways, which are the main pathways regulating the cell cycle.

5.1. Disruption of the Rb pathway

Growth suppression is required to ensure that cells do not grow uncontrollably. The retinoblastoma protein is one of the quintessential tumor suppressors and infiltrates virtually all the anti-growth pathways.

GF bond to growth-factor receptors to stimulate cells to move from the G_0 phase to continue with their growth cycle. They further boot the expression of immediate early genes (IEGs) such as *fos*, *jun*, and *myc*. Cyclin-dependent kinases (CDKs) and cyclin (and other molecules) are activated when stimulated by IEGs to generate CDK-cyclin complexes with kinase activity. These complexes promote the phosphorylation of pRb which deactivates it and allows the cell to divide. Growth

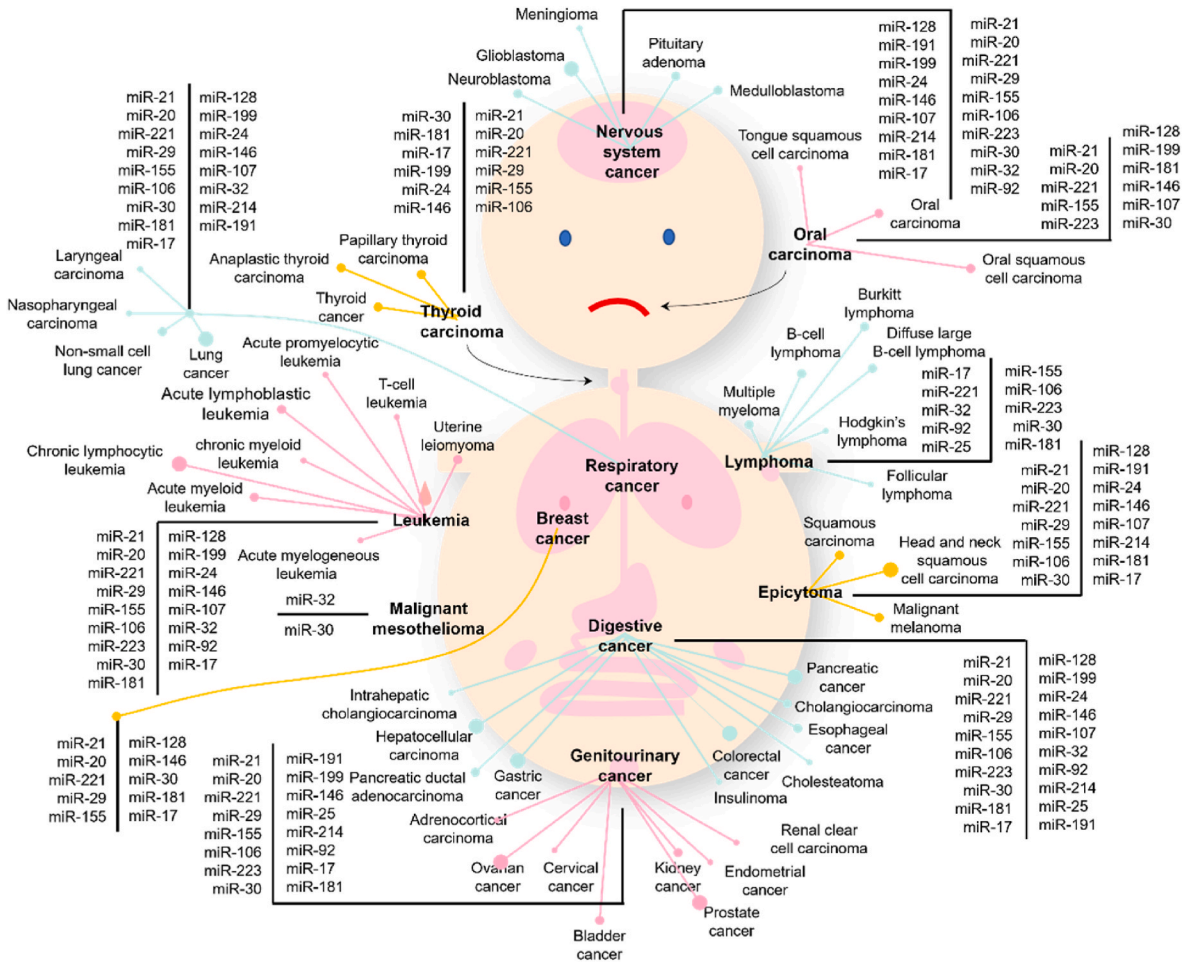

Fig. 15. Map of common tumors showing the miRNAs that are aberrantly expressed. The size of the circle on an arrow is an indication of the amount of miRNA expressed.

Table 5
Impact of different miRNAs in common tumors.

MiRNA	Effect					
	Proliferation	Metastasis	Inflammation	Apoptosis	Differentiation	Angiogenesis
miRNA-21	✓	✓				
miRNA-155	✓		✓	✓		
miRNA-17	✓	✓		✓		
miRNA-191	✓				✓	
miRNA-29	✓	✓		✓	✓	
miRNA-223	✓	✓		✓		
miRNA-128	✓	✓		✓	✓	✓
miRNA-199	✓	✓		✓	✓	
miRNA-24	✓				✓	
miRNA-146	✓	✓	✓	✓	✓	
miRNA-181	✓		✓		✓	
miRNA-20	✓	✓				
miRNA-107	✓		✓		✓	
miRNA-32	✓	✓	✓	✓	✓	
miRNA-92	✓	✓		✓		
miRNA-214	✓			✓	✓	✓
miRNA-30		✓			✓	✓
miRNA-25	✓	✓	✓	✓		✓
miRNA-221	✓	✓		✓		
miRNA-106	✓	✓		✓		

suppressor pRb binds to E2F transcription factor which prevents the E2F from regulating the cell cycle and therefore prevents growth. Kinase complexes such as CDK4/6-cyclinD and CDK2-cyclinA/E phosphorylate pRb allowing it to dissociate from E2F so that growth is restored. CDK inhibitors (CKIs) can bind with cyclin and therefore compete with CDKs or CDK-cyclin complexes, reducing the catalytic activity of the CDKs. CKIs can be divided into two main groups: those that inhibit CDK4 (INK4) and restrain the activation of CDK4/6-cyclinD, and kinase

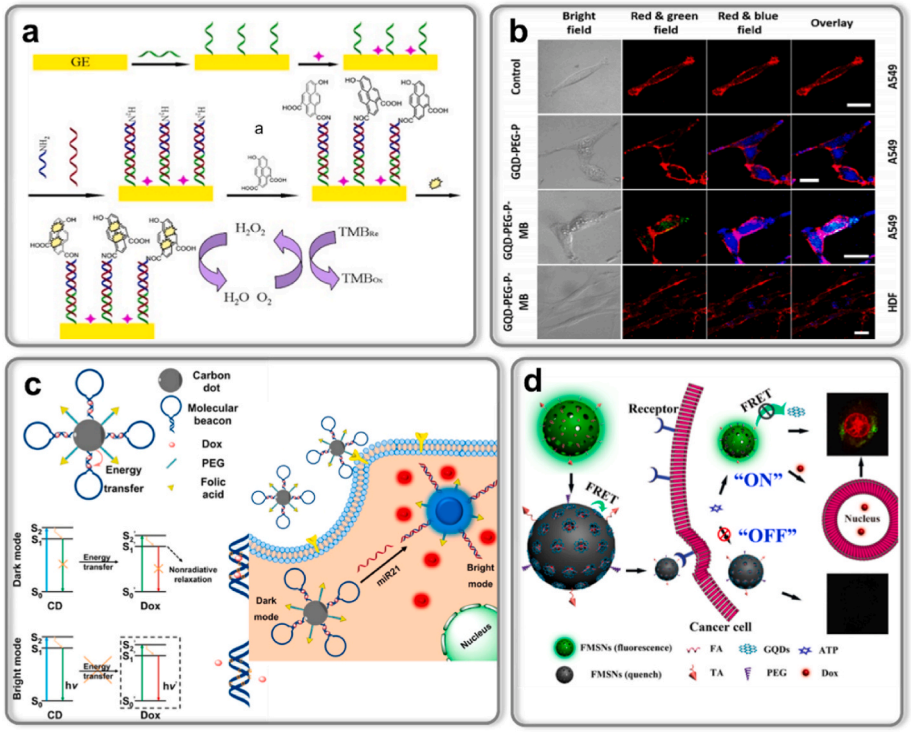

Fig. 16. (a) Principles underlying the detection of miRNA-155 using a GQD-based electrochemical biosensor [312]. Copyright 2015, Elsevier Advanced Technology. (b) Confocal microscope images of A549 cells transfected with GQD-PEG-P [313]. Copyright 2017, American Chemical Society. (c) Diagram illustrating the endogenous miRNA-triggered Dox release mechanism [314]. Copyright 2017, American Chemical Society. (d) Preparation and application of ATP-responsive FRET nanocarriers [315]. Copyright 2015, American Chemical Society.

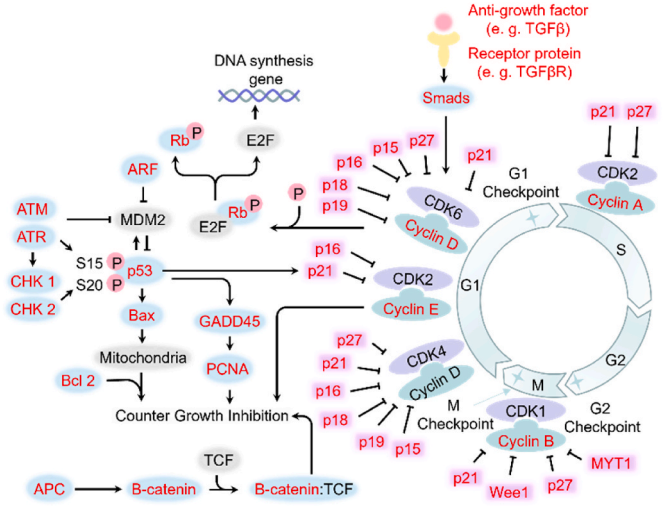

Fig. 17. Cell cycle regulatory pathways and ways of evading growth suppressors. Only the two main pathways, pRb and p53, are illustrated for the sake of simplicity. The key regulatory molecules, CDK and cyclin, are labeled in their high frequency time. INK 4 involves p15, p16, p18, p19 and KIP involves p21, p27, p57 (not shown here as it is only expressed in specific cells or tissues). Red highlights are placed on a few of the genes that are known to have functional changes.

inhibition proteins (KIPs) that inhibit CDK2-cyclinA/E. Thus, the disruption of cyclins and deactivation of CDKs are common tools tumor cells use to evade growth suppressors.

To take advantage of this pathway, Bajpai et al. [331] fabricated nitrogen/phosphorus co-doped CDs (NPCDs) using a single-step thermal treatment. The NPCDs, as-synthesized, exhibited a high quantum yield (*ca.* 9 %) and resulted in dose-dependent cell cycle arrest, as indicated by the reduction in CDK-2, -4, and -6 protein levels and increase in p21 level (Fig. 18).

TGFβ also plays an important part in the pRb pathway. It obstructs pRb phosphorylation, prevents pRb inactivation, and thus inhibits proliferation. As a circumvention strategy, TGFβ may be down-regulated in tumors. Thus, many studies have shown that tumors may down-regulate or lose responsiveness to relevant antigrowth factor receptors to evade growth suppressors. Tumor cells can also mutate the TGFβ receptor directly. In the pRb pathway, TGFβ expresses the *c-myc* gene, which can regulate the processes in the G_1 phase. Myc/Max/Mad network structure is an important structure for regulating cell growth in which Max plays a linking role. The Mad-Max complex has an opposite effect to the Myc-Max complex: the Mad-Max complex inhibits the role of Myc target gene transcription in terminal differentiation, cell growth, and antagonizes Myc-induced carcinogenesis. However, tumor cells withstand this tenor by overexpressing the *c-myc* gene which shifts the balance back to Myc-Max and thus promotes proliferation. The Smad4 protein transmits signals between ligand activated TGFβ receptors and downstream targets and is commonly found to be mutated in human cancers.

The overexpression of TGFβ may prove significant in tumor diagnosis, although there are no reports of CQDs being used in such a role. However, several authors have utilized CDs to affect TGFβ-related pathways to achieve favorable therapeutic effects on diseases. For example, Wang et al. [332] prepared CDs to induce the epithelial-mesenchymal transition (EMT) process which further activated the TGFβ/p-38 mitogen-activated kinase/Snail signaling pathway and finally promoted wounds to heal with fewer scars (Fig. 19a). Lu et al. [333] fabricated an injectable collagen-genipin-CD nanoparticle (CGN) hydrogel for use in PDT aimed at enhancing chondrogenesis (Fig. 19b). By controlling the TGF/SMAD and mTOR signaling pathways, respectively, the increased stiffness and ROS production synergistically supported chondrogenic development. Meng et al. [334]

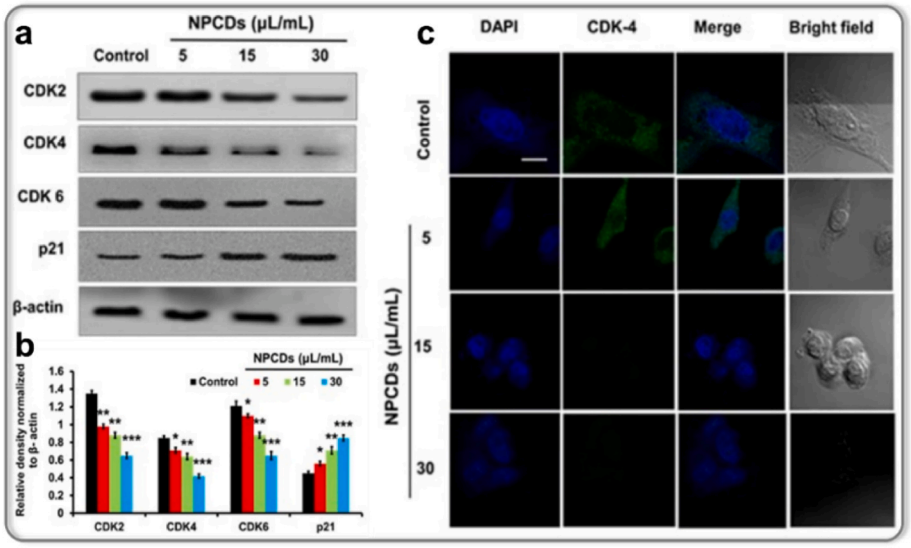

Fig. 18. Effect of nitrogen/phosphorous co-doped CDs on cell cycle arrest. (a) Western blot analysis of various cell cycle arrest markers. (b) ImageJ analysis of B16F10 melanoma cancer cells after treatment with NPCDs. (c) Confocal microscope images illustrating the immunocytochemistry of cell cycle arrest marker CDK-4 after treatment with NPCDs [331]. Copyright 2020, Ivyspring International Publisher.

developed a way of introducing therapeutic agents (SOX9 and TGFβ) to human bone marrow-derived mesenchymal stromal cells (hMSCs) *via* CD-modified recombinant adeno-associated virus (rAAV) vectors. The administration of the therapeutic agents led to the effective over-expression of each independent transgene, thus resulting in increased cell proliferation and cartilage matrix deposition (Fig. 19c). In summary, there appear to be various ways that tumors may contrive to take advantage of the pRb pathway to avoid growth suppression.

5.2. Mutation and dysfunction of the p53 pathway

The p53 protein is another quintessential tumor suppressor. The controlling effects of p53 can be divided into two fields: regulating concentration and changing activity. As an example of the first aspect, Mouse double minute 2 (MDM2), as a ubiquitin ligase, can connect to p53 to assist the ubiquitin in degrading p53 when it encounters the p53. A dynamic equilibrium is thus constructed between p53 and MDM2 that keeps the concentration of p53 low. However, this equilibrium is destroyed when the DNA is damaged (and the concentrations of ATM, ATR, and ARK begin to pile up) and by hyperproliferation signals. The suppression of MDM2 causes the concentration of p53 to increase dramatically. On the other hand, ATM and ATR can phosphorylate p53, directly or indirectly, increasing the ability of other species to bond to the target DNA of p53. At the same time, the affinity between phosphorylated p53 and MDM2 declines sharply and facilitates a decrease in ubiquitination degradation. In addition to acute DNA damage and hyperproliferation signals, there are a series of other factors that also regulate p53, e.g., hypoxia, nutrient deprivation, and telomere attrition.

Aimed at controlling the abnormal expression of ARF in tumors, Xie et al. [335] revealed for the first time that using CDs to target the nuclear MET (nMET) axis can be a creative way to combat cancer drug resistance, particularly prostate cancer. (Fig. 20a-20d). Xie et al. also demonstrated that their tea-derived CDs are able to interact with ARF in nuclei and may consequently cause YAP to localize outside of the nucleus [336]. They revealed a novel crosstalk involving ARF/β-catenin dysregulated YAP in the hippo signaling pathway. The ability to use nanomaterials to stimulate ARF-mediated signaling to inhibit nuclear YAP may constitute an innovative avenue for treating cancer (Fig. 20e,

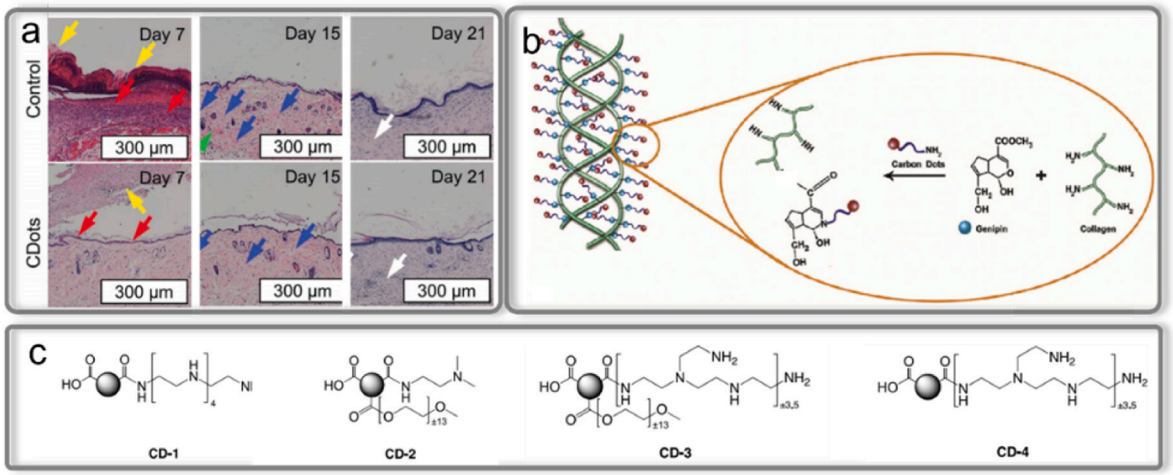

Fig. 19. (a). Images of using CDs to heal wounds *in vivo* [332]. Copyright 2020, Wiley-VCH GmbH. (b) The preparation procedure and implementation of CGN nanocomposite hydrogels [333]. Copyright 2019, Elsevier Sci. Ltd. (c) Structures of various CDs employed in Ref. 334 [334]. Copyright 2020, Multidisciplinary Digital Publishing Institute.

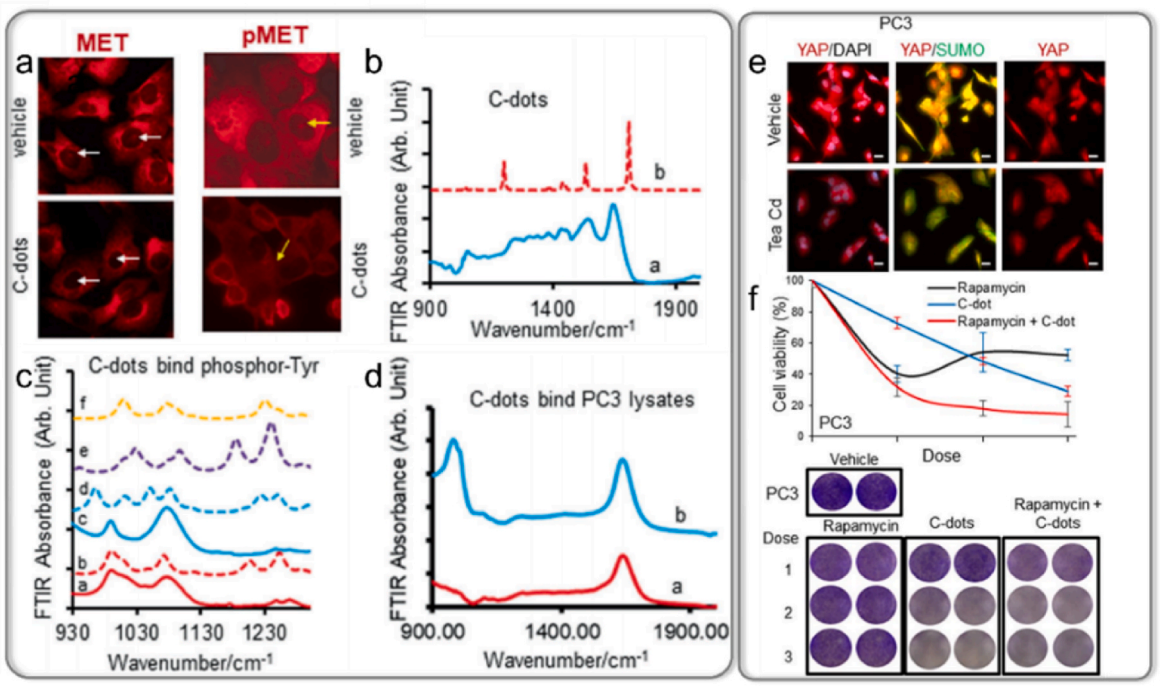

Fig. 20. nMET phosphorylation is sustained by ARF and abolished by CDs. (a) CDs abolish nMET and phosphorylated nMET levels in PC3 cells. (b) FT-IR spectra of CDs. (c) FT-IR spectra of phosphorylated tyrosine before and after addition of CDs. (d) FT-IR spectra of total protein extracted from PC3 cells [335]. Copyright 2018, Springer Nature Limited. (e) Treatment of cancer cells with tea-derived CDs increases co-localization of SUMO and non-nuclear YAP in PC3 cells. (f) Treatment of cancer cells with CDs sensitizes PC3 cells to rapamycin [336]. Copyright 2017, Nature Portfolio.

f).

p53 plays a role in regulating the cell cycle where it can arrest growth at the G_1 checkpoint if the cell is perceived to be abnormal. At best, it can directly affect over 129 genes in three ways: (i) It can induce the genetic transcription of p21 which suppresses CDK2-cyclinE and CDK4/6-cyclinD activity. (ii) It can accelerate the synthesis of GADD45 which combines with PCNA and shuts down the synthesis of DNA. (iii) It can promote the generation of Bax (an apoptosis-related protein) which together with B-cell lymphoma 2 (Bcl-2) activates cell apoptosis.

Many studies aimed at using CQDs to treat tumors indicate that the overexpression of p53 may reactivate the competence of the p53 pathway and therefore promote the death of the tumor [337–339]. Unfortunately, the p53 pathway can become mutated in tumor cells as they attempt to evade growth suppression. A mutated p53 pathway losses the ability to properly regulate the cell towards repair or death. On the contrary, it will tend to expedite tumorigenesis. Thus, several researchers have attempted to diagnose tumors by focusing on p53 as the target DNA (Table 6).

Wang et al. [340] developed a resonance light scattering (RLS) method for selectively detecting mutant p53 (Fig. 21a). Their method uses a GQD-based catalytic hairpin assembly amplification strategy and was found to be linear over two ranges (1.0 pM - 1.5 nM and 1.5–50.0 nM); the LOD was 0.8 pM. Su et al. [341] prepared nitrogen-doped GQDs (NGQDs) and used them to develop a dual-signal ratiometric fluorescence probe NGQDs/P1 DNA/berberine. The dual fluorescence peaks at 440 nm and 537 nm derive from the NGQDs and berberine, respectively

Table 6
Recent CQDs-based tumor diagnostic techniques for detecting p53.

Materials	Method	λ_{ex} (nm)	λ_{em} (nm)	QY	LOD	Linear range	Sample	Cell line	Ref.
NGQDs/P1 DNA/berberine	PL spectrophotometry; Confocal fluorescence imaging.	360	440	26.7 %	0.06 nM	0.2–30.0 nM	Human serum	MCF-7	[341]
CQDs-SiNP		340	425	NA	2.7 pg L^{-1}	0.01–50 ng/mL	Human serum	MCF-7 HeLa	[343]
GQDs-H1 GQDs-H2	Resonance light scattering.	360	460	NA	0.8 pM 0.8 pM	1.0 pM - 1.5 nM 1.5–50.0 nM	P53 solution	NA	[340]
Au/GQDs/P-Cys/GNP-Streptavidin- HRP/BSA/Ab/BSA/p53	Electrochemical immunosensing.	NA	NA	NA	0.065 fM	0.000592–1.296 pM 0.000197–0.016 pM 0.00533–11.66 pM	Human plasma Standard p53 Standard p53	MCF-7, HCT, PC3 NA NA	[342]
AuNPs-ssDNA/GQDs		260, 314	430	15.5 %	13 nM	25–4000 nM	P53 solution	NA	[344]
HM-SGQDs		NA	NA	NA	66 fM	100 fM - 100 nM	P53 solution	NA	[345]
Au@CDs		NA	NA	NA	0.34 fM	1 fM - 10 pM	P53 solution	NA	[346]

NA: not mentioned.

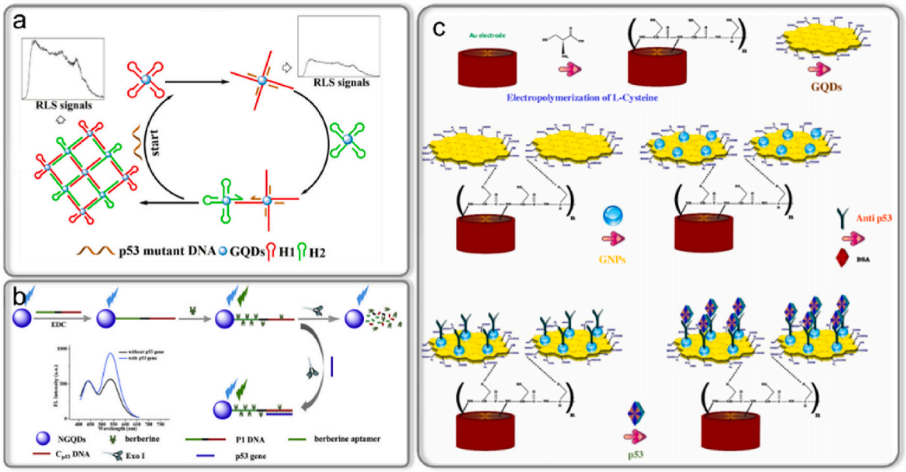

Fig. 21. (a) The fundamental of resonance light scattering of graphene quantum dots for the identification of mutant DNA with CHA-assisted target recycling amplification [340]. Copyright 2019, Elsevier Science SA. (b) Schematic illustration of the label-free electrochemical immunosensor used to detect p53 [341]. Copyright 2018, Elsevier. (c) Using a dual-frequency fluorescent probe (NGQDs/P1 DNA/berberine) to analyze p53 gene content [342]. Copyright 2019, Elsevier.

(Fig. 21b). Using this strategy, they obtained a detection range of 0.2–30.0 nM with an LOD of 0.06 nM. Hasanzadeh et al. [342] developed an electrochemical method for detecting p53 based on an Au/GQD/p-cys/GNP-streptavidin-HRP/BSA/Ab/BSA/p53 working electrode (Fig. 21c). The technique was found to be linear over the concentration range 0.000197–0.016 pM (using square wave voltammetry (SWV)) and 0.195–50 pM (using differential pulse voltammetry (DPV)) using standard p53 samples. Using unprocessed human plasma, it was linear over the range 0.000592–1.296 pM (using the DPV technique) with an LOD of 0.065 fM.

An intricate crosstalk can be discerned between the pRb and p53 pathways as they share some of the same molecules. In other words, evading growth suppressors is an obligatory step for tumors and is articulated in two pathways. Some of the genes known to be functionally converted are highlighted in red in Fig. 17. These genes are convenient starting points for establishing GQD-based diagnosis and therapeutic methods. In particular, as they form the hubs of the two most renowned pathways, checking or treating pRb and p53 is a valuable approach as these species are linked to most tumorigenic processes. However, unlike directly restraining the oncogenes involved, treatment involving 'gene security' can be much more formidable. In the context of p53, for example, the idea of treating and obliterating cancer cells by restoring the ability of p53 to promote apoptosis is quite a challenge.

6. Resisting cell death

The most notable feature of tumor cells, their ability to rapidly increase in number, requires both an excessive rate of cell proliferation and the prevention of cell apoptosis. Apoptosis is triggered by the detection of signals that indicate something abnormal is occurring (for example, signatures indicative of DNA injury, disrupted signal balances that point to cancer activity, deficiency of survival factors and oxygen, and so on). Once triggered, various apoptosis-related procedures are executed. Apoptosis ultimately leads to the disruption of cellular membranes, disintegration of the cytoplasmic and nuclear skeletons, extrusion of cytosol, degradation of chromosomes, and destruction of the nucleus. Such measures are aimed at keeping the number of normal cells constant while eliminating any mutated cells with active oncogenes.

It is thus clear that tumor cells need to resist apoptosis in order to maintain their growth. There are many ways this can be accomplished. For example, they may increase the expression of anti-apoptotic factors, down-regulate pro-apoptotic factors, or disrupt the external ligands that induce the activation of death pathways. Of course, as we have seen, any deficiency of pro-apoptotic factors in tumor cells is likely to be associated with the p53 tumor suppressor gene. That is, the functional inactivation of p53 is ubiquitous in tumor cells.

6.1. Mitochondrial endogenous apoptotic pathway

Mitochondria are usually thought of as energy providers that help cells to develop and grow. However, they also have a hidden talent: they can issue tactical commands that lead to cell apoptosis. Once disturbance signals are recognized by the mitochondria (indicating, for example, the occurrence of DNA damage, presence of ceramide or oxidant, or other change that may have an adverse effect on the mitochondria), apoptosis-related procedures are aroused that change the permeability of the mitochondrial membrane.

The outer membranes of mitochondria feature Bcl-2 proteins, some that promote apoptosis (Bax, Bak, Bid, Bim) and others that inhibit apoptosis (Bcl-2, Bcl-XL, Bcl-W). When a death signal arrives, the Bcl-2 family of proteins on the outer mitochondrial membrane release cytochrome *c* (cyt *c*) from the mitochondrial stroma into the cytoplasm. The incorporation of cyt *c* and apoptotic protease activating factor-1 leads to a conformational change. A heptamer called apoptosome is formed which combines with caspase-9 to form a proenzyme which leads to the catalytic activation of caspase-9, multiplying its activity by 100–1000 times. The fully active caspase-9 further activates caspase-3 and caspase-7.

Occasionally, a caspase may be accidently activated by an interfering signal. Fortunately, there is a protection mechanism in which an inhibitor of apoptosis proteins (IAP) competitively binds to caspase-9 or caspase-3 and thus contains their activity. When a death signal is transmitted to a mitochondrion, cyt *c* is simultaneously liberated with second mitochondria-derived activator of caspases (Smac). The cyt *c* leads to the formation of apoptotic bodies and is positively associated with death progress. On the other hand, Smac binds to IAPs and thereby increases the resistance to apoptosis.

In addition to the functionally mutated proteins shown in red in Fig. 22, the expression of IAPs in the mitochondrial induced endogenous apoptotic pathway can disrupt the therapeutic treatment of tumors. The overexpression of IAPs may therefore be one of the reasons that chemotherapy is not as effective as it should be. As a result, a battery of anticancer drugs has been developed that oppose the function of IAPs and have come a long way. Furthermore, activating caspase-9 is a crucial aim in chemotherapy, radiation therapy, and other therapies.

Survivin is an IAP that is highly expressed in many tumor cells lines (Fig. 23a). By preventing the activities of caspase-3 and caspase-7, it

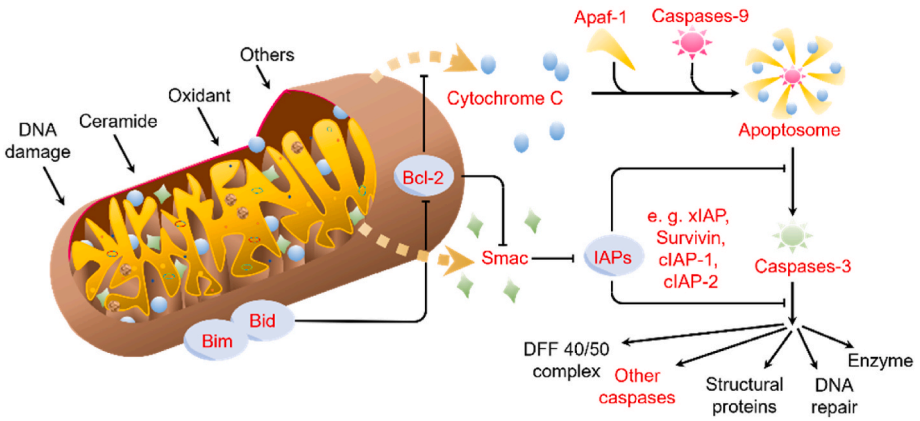

Fig. 22. Mitochondria as the core of the endogenous apoptosis pathway.

stimulates cellular mitosis and prevents cancer-related cellular death [348,349]. Dong et al. [347] reported an imaging and gene therapy technique based on the delivery of multiple genetic probes (Fig. 23b). The GQDs employed were functionalized by grafting PEG and polylactic acid onto them. They were then combined with MBs to target to miRNA-21. The MBs separate from the GQDs due to their high affinity towards miRNA-21, allowing the GQDs to emit red fluorescence (thus facilitating imaging). For therapeutic purposes, the GQDs were integrated with a probe to inhibit miRNA-21 as well as a survivin antisense oligodeoxynucleotide. The delivery of the inhibitors was again revealed by the emission of red fluorescence. The decrease in both miRNA-21 and survivin synergistically induced an increase in caspase-3 and caspase-7 activity, leading to better growth inhibition and enhanced cancer cell apoptosis.

There are other endogenous apoptotic pathways that derive from other organelles, e.g., the Golgi apparatus, endoplasmic reticulum, and lysosomes. They will participate in programmed cell death but the mechanisms responsible have not been clearly expounded.

6.2. Death receptors inducing exogenous apoptotic pathways

Upstream sensors appraise the growth environment of the cell and determine what cellular processes need to be triggered. They are composed of cell surface receptors that can combine with various survival and death factors. Exogenous apoptotic pathways are triggered in exactly this way originating from an encounter between a death ligand and a death receptor. When a death ligand is encountered, receptor trimerization facilitates the formation of the death-inducing signaling complex (DISC) inside the cell membrane. With the help of DISC, DNA cleavage can further activate the effector caspases (Fig. 24).

Intracellular protease caspases are the terminal effectors of apoptosis. Caspase-8 and caspase-9 are two apoptosis-activating components that are triggered by apoptosis receptors and cyt *c*, respectively. The effectors selectively demolish the subcellular fraction, organelle, and genome and further activate more caspases to execute apoptosis. The regulatory and effector factors are controlled by the Bcl-2 family of proteins which act as apoptotic triggers to deliver signals.

6.3. Survival signals inducing the PI3K-Akt pathway

Tumor cells can also resist death by modifying the PI3K-Akt pathway that is dominated by the transmission of survival signals. The pathway involves IGF-1/2 and interleukin 3 (IL-3), for example, that are involved in apoptotic remission in human tumors (Fig. 25). PI3K is commonly mutated in tumors and can therefore be used as a target for diagnosis and therapy.

As an upstream sensor, IL-13 can activate the PI3K-Akt/PKB pathway which transmits anti-apoptotic signals and participates in apoptosis remission. Hence, it has been postulated that the decoy receptor IL-13Rα2 which is overexpressed in cancer cells [350] and binds IL-13 with high-affinity can be used as a tumor marker (Fig. 26a) [351]. Serafín et al. [352] subsequently developed an integrated electrochemical immunosensor for the determination of IL-13Rα2. By grafting p-aminobenzoic acid (p-ABA) onto electrodes that had been screen-printed with streptavidin and activating them with EDC/Sulfo-NHS, biotinylated recapture antibody (BCAb) was immobilized. A hybrid nanomaterial composed of multiwalled carbon nanotubes (MWCNTs) and GQDs was utilized as nanocarriers to transport detector antibodies and HRP molecules (Fig. 26b). The detection process yielded a linear calibration plot over the range 2.7–100 ng/mL IL-13Rα2 with an LOD of 0.8 ng/mL. The sensor was subsequently used to successfully analyze raw cellular lysates and extracts from paraffin-embedded tissues from patients with colorectal cancer.

On the other hand, there is a caspase-independent anti-death pathway in tumor cells where apoptosis inducing factor (AIF) and endonuclease G are involved in. AIF is normally located behind the outer

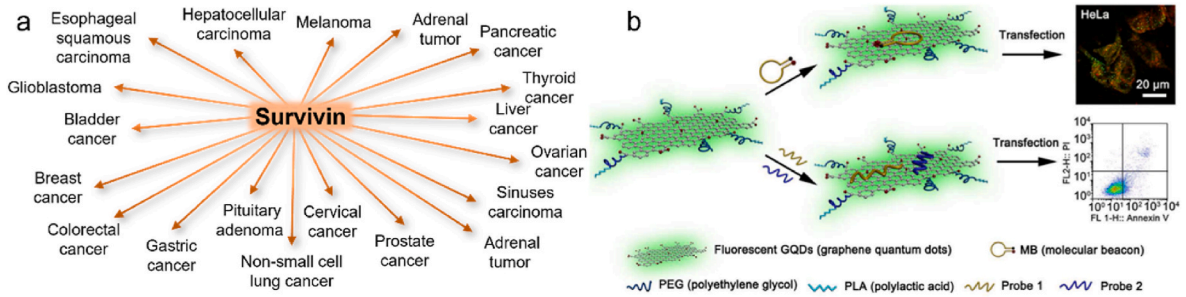

Fig. 23. (a) Cancer cell lines with overexpressed levels of survivin. (b) Use of functionalized GQDs to image HeLa cells and deliver gene-targeting agents. Probe 1 is a miRNA-21 inhibitor probe and probe 2 is survivin antisense oligodeoxynucleotide [347]. Copyright 2015, American Chemical Society.

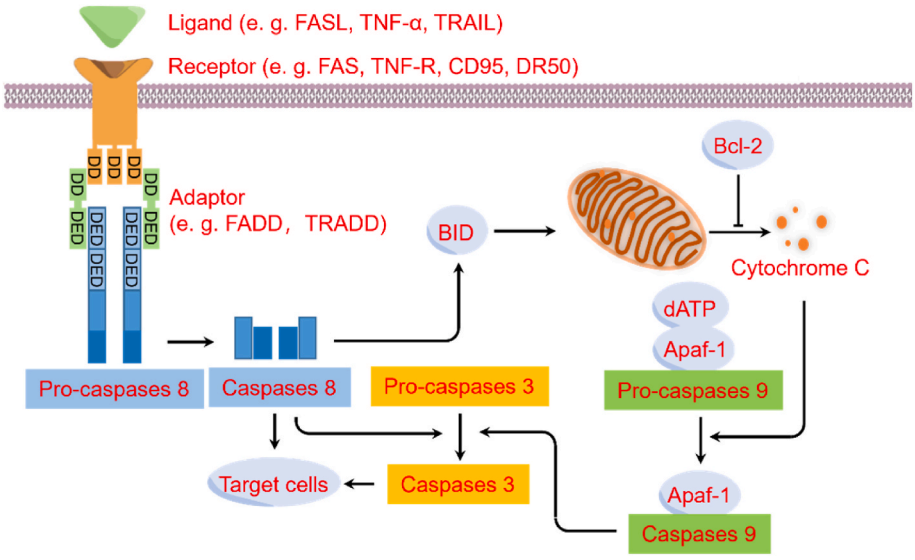

Fig. 24. Concurrent extracellular (*via* caspase-8) and intracellular (*via* caspase-9) induction of apoptosis.

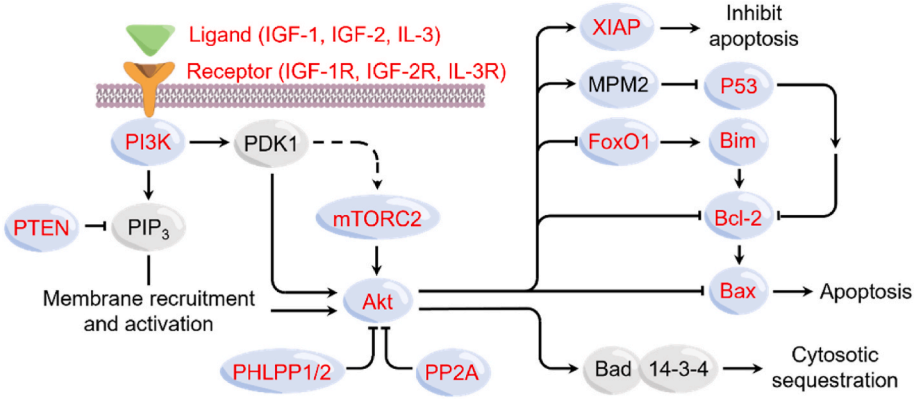

Fig. 25. Sketch map illustrating the PI3K-Akt pathway. The pathway plays an important role in regulating the cell cycle and is therefore involved in tumorigenesis in multiple ways.

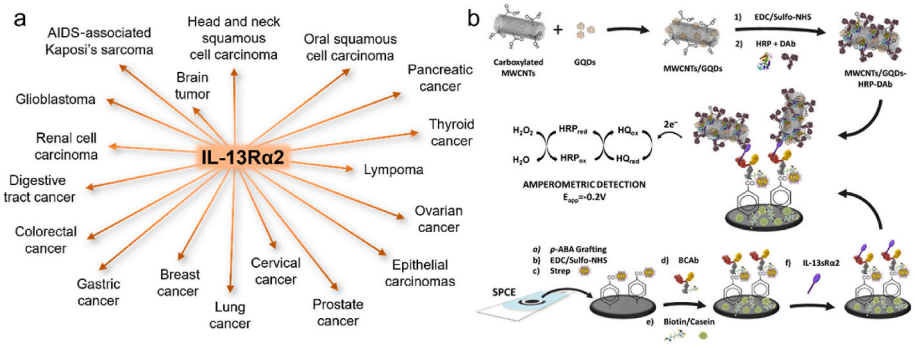

Fig. 26. (a) Cancer cell lines with overexpressed levels of IL-13Rα2. (b) Procedures required in construction of an amperometric immunosensor for detecting IL-13sRα2. BCAb is immobilized onto strep/*p*-ABA/SPCE and used in conjunction with MWCNTs/GQDs-HRP-DAb nanocarriers [352]. Copyright 2019, Elsevier science SA.

mitochondrial membrane but gains access to the cell nucleus after it is released into the cytoplasm (which can happen, for example, if the mitochondrion becomes damaged). It can then cause the DNA to agglutinate and fragment further. The DNA fragments produced consist of 50,000 base pairs rather than the 200 base pairs typically encountered in fragments produced by apoptosis. Endonuclease G is emancipated from mitochondria when they are stimulated by death signals. When it enters the cell nucleus, the endonuclease G cuts the DNA up into fragments in nucleosome units. Apart from the two cases outlined above, there are other genes that can also induce cell apoptosis without involving caspases. However, no CQDs-related studies have been conducted in this area.

7. The capability of infinite replication

In principle, a deregulated proliferation program should be sufficient to allow the generation of a vast population of cells, that is, the formation of a macroscopic tumor. However, the ability to replicate indefinitely is another prerequisite for forming harmful tumors. Once a cell population has doubled a certain number of times, it stops growing and enters a period of senescence. Senescence in cultured human fibroblasts can be avoided by blocking the tumor suppressor proteins pRb and p53. If this can be achieved, the cells will keep growing for additional generations until they reach a second state: crisis. Even here, a small number of mutated cells can sometimes break through this second barrier to division and can double without limit. When this occurs, such cells are said to be 'immortal' [353].

There is evidence that telomeres, which guard the ends of chromosomes, are crucial in enabling unrestricted proliferation [354,355]. Moreover, unlimited proliferation seems to be assured by two main mechanisms: (i) up-regulation of telomere expression (which modifications telomeric DNA ends with hexanucleotide repeats), and (ii) activation of the alternative lengthening of telomeres (ALT) mechanism (which maintains telomeres *via* a recombination-based inter-chromosomal exchange of sequence information). We discuss each of these mechanisms in turn.

7.1. Up-regulation of telomere expression

Telomeres are nucleoprotein structures composed of 10–15 kb of tandem hexanucleotide arrays of TTAGGG repeats that shield the ends of linear chromosomes [356,357]. During non-immortalized cell propagation, telomeres are progressively shortened and eventually lose their ability to protect the end of the chromosomal DNA from end-to-end fusion. Such fusion generates unstable dicentric chromosomes whose resolution leads the karyotype to become disorganized and endangers the survival of cells. Thus, telomerase is employed in order to prolong the life of telomeres.

Telomerase is a specialized DNA polymerase that adwds telomere repeat segments to the ends of telomeric DNA. As shown in Fig. 27, telomerase is a ribonucleoprotein composed of multiple proteins and an RNA molecule. The RNA acts as a template for DNA polymerase activity and features a sequence of nucleotides complementary to that in the telomere (TTAGGG). The telomerase utilizes its template to synthesize DNA using reverse transcription. Once the template is completed, the telomerase is released and is free to rebind again (with the three nucleotides at the end). The telomere can thus be extended by repeating this process several times. In contrast to the nearly complete absence of telomerase in non-immortalized cells, the great majority of numerous spontaneously immortalized cells, especially human cancer cells, express telomerase at levels that are functionally meaningful. By prolongling telomeric DNA, telomerase can prevent the progressive telomere degradation that would otherwise take place in its absence.

In 2017, Huang et al. [358] created a label-free nanosensor based on amino-functionalized GQDs (af-GQDs) coupling catalytic

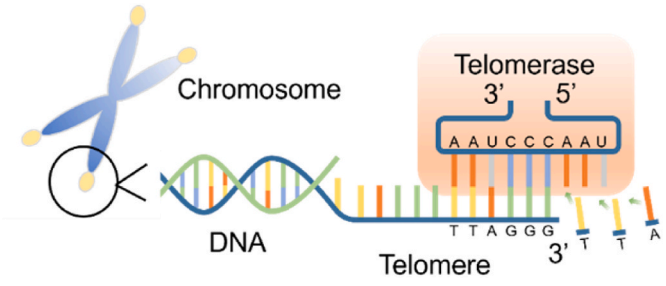

Fig. 27. Schematic diagram showing telomerase adding a basic repeat segment to a telomere.

G-quadruplex/hemin DNAzyme for the determination of human telomere DNA (Fig. 28). The af-GQDs are used as a reference fluorophore (at 440 nm) and 2,3-diaminophenazine was chosen to form the specific response signal (at 553 nm). The nanosensor was linear in the range 0.2–50 pM and its LOD with respect to human telomere DNA recognition was found to be 25 fM. Four-stranded helical G-quadruplex structures are adopted by telomere DNA that are abundant in guanine nucleic acid sequences. They are held together by Hoogsteen hydrogen bonding and require the presence of a monovalent metal ion [359]. The formation of G-quadruplex structures in human telomere DNA can effectively reduce the activity of telomerase which subsequently inhibits the proliferation of most cancer cells.

7.2. Activation of the ALT mechanism

The ALT mechanism is another way in which the functions and lengths of telomeres can be sustained. Mutations in the ATRX/DAXX/H3.3 complex have been discovered by high throughput genome sequencing of cells and malignancies exhibiting the ALT phenotype. ATRX (Fig. 29a) is a member of the Snf2 family of chromatin remodeling proteins which, in cooperation with the histone chaperone DAXX, permits the incorporation of histone variant H3.3 into telomeric and pericentromeric chromatin [360].

Two models exist for the ALT mechanism [361]. In the first one, telomere lengthening on one sister chromatid occurs at the expense of the other due to inconsistent telomere sister chromatid exchange (T-SCE) (Fig. 29b). This model must take into account the non-random segregation of sister chromatids in order to be effective as a daughter cell will only have an enhanced mean telomere length and hence an improved potential for proliferation if it inherits primarily chromatids with long telomeres. To be effective, this model must account for the non-random segregation of sister chromatids, as a daughter cell will only have an enhanced mean telomere length and hence an improved potential for proliferation if it inherits primary chromatids with long telomeres. In the other mechanism (Fig. 29c), a longer telomere on an alternate chromosome is invaded by a 3′ overhang from a short telomere on that chromosome. Following the resolution of the heteroduplex, the extension process produces the substrate for the synthesis of the second strand through lagging mechanisms. As an alternative, the invasion/extension reaction may result in the creation of a true fork on the target telomere, with concurrent leading and lagging replication continuing to the end of the chromosome, like break-induced replication.

Although the ALT maintenance mechanism is encountered in numerous cancers, its occurrence is minimal or completely absent in most somatic cells, suggesting that it may be used as a cancer biomarker. For the development of broad-spectrum anti-cancer treatments, telomerase itself is a very alluring target, and over the past 20 years, numerous methods for preventing telomerase activity have been proposed [362]. On the other hand, the creation of ALT-specific inhibitors is extremely difficult, since ALT cells do not exhibit exclusively enzymatic activity [363]. Nevertheless, according to several studies, telomere-targeting drugs such G-quadruplex ligands can stop the growth of both telomerase and ALT cancer cells [364–367]. The occurrence of ALT presents difficulties for the development of anticancer treatments intended to hinder telomere maintenance and adds some complication to suggested applications of telomere-related markers in cancer diagnosis and prognosis.

8. Sustained aberrant angiogenesis

The adequate supply of oxygen and nutrients is essential for cell function and survival. As a result, the majority of cells must be located within 100 μm of a capillary blood vessel. Once tissue has been generated, the angiogenesis process is transitory and strictly controlled. In order to progress to a larger size, incipient neoplasia must therefore

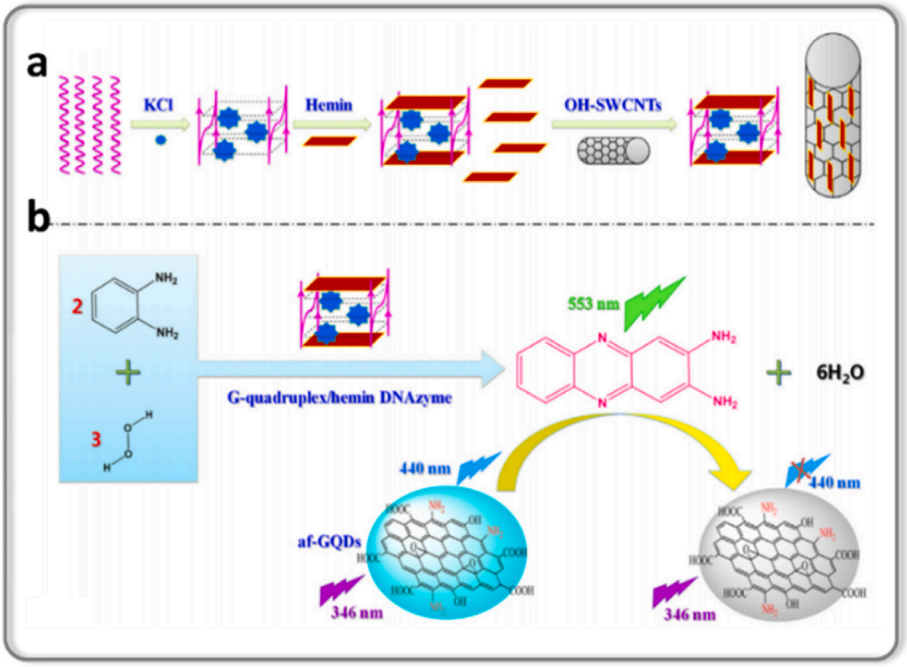

Fig. 28. (a) Synthesis and purification of G-quadruplex/hemin DNAzyme. (b) Diagram of the measurement of human telomere DNA using a ratiometric fluorescent nanosensor based on an af-GQD [358]. Copyright 2017, Elsevier Science SA.

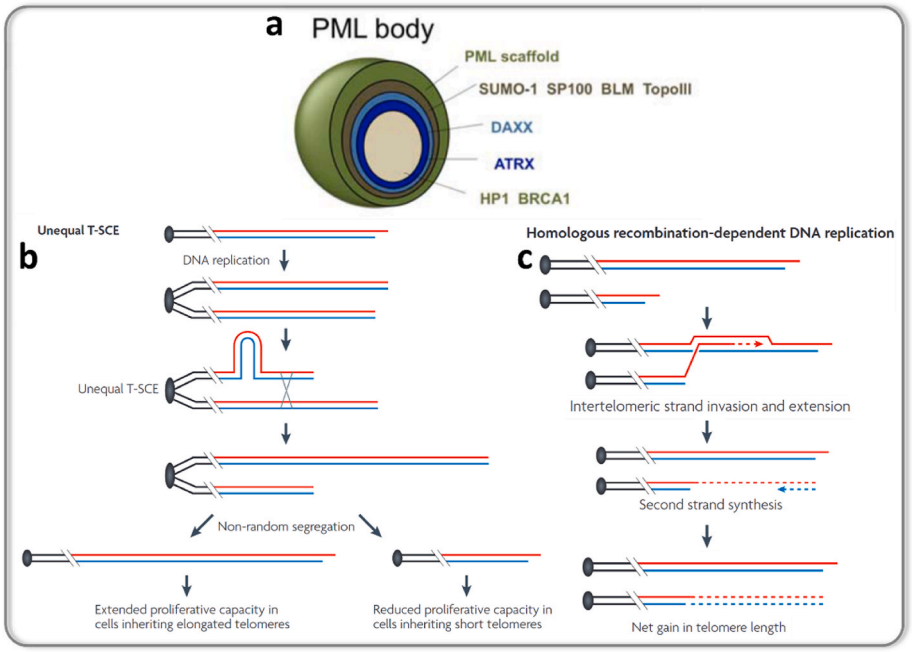

Fig. 29. (a) The scaffold protein promyelocytic le'ukemia (PML) defines the outside boundaries of PML bodies, while a large number of other proteins are crammed into the center in onion-like concentric rings [360]. Copyright 2013, Frontiers in Bioscience Inc. (b, c) Two models for the ALT mechanism [361]. Copyright 2010, Nature Research.

develop new blood vessels if a macroscopic tumor is to be successfully formed.

For purpose of achieve neovascularization, tumors release cytokines and growth factors to activate normally quiescent cells around them so they become dysregulated (Fig. 30). The altered tumor vasculature is leaky and tortuous which results in the exposure of the basal lamina at different sites. Activated endothelial cells and platelets produce greater quantities of PDGF, which attracts and stimulates perivascular cells. The recruitment of tumor-associated fibroblasts, which abnormally deposit ECM proteins and produce stimulants, further fuels the remodeling process. The ECM is broken down and remodeled by matrix metalloproteinases (MMPs), which also reveal previously concealed epitopes which function as endogenous angiogenesis inhibitors. Beyond that, inflammatory cells wound attracted to this perceived wound where they liberate substances that can stimulate or inhibit the angiogenic response.

For tumor development and metastasis, angiogenesis is crucial. Therefore, a possible strategy for preventing cancer progression is to decrease tumor-associated angiogenesis. As described above, the

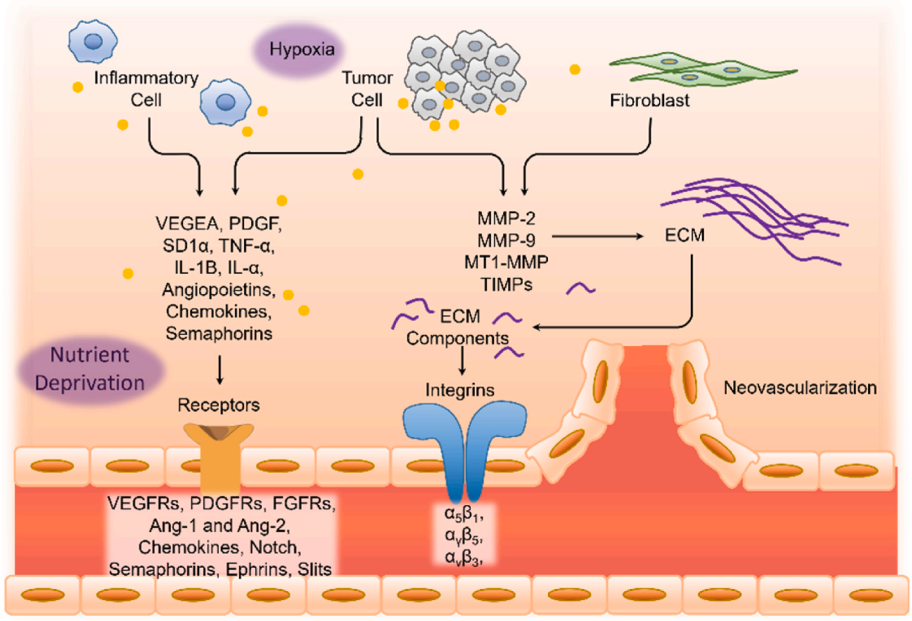

Fig. 30. Schematic diagram showing how unrestrained angiogenesis is governed inside the tumor microenvironment.

'angiogenesis switch' is mainly governed by signaling members, integrins, and ECM remodeling. Therefore, a large number of experiments have proposed strategies that target the key factors involved in neovascularization. Among these, several have employed CDs to assist diagnosis and treatment.

8.1. *Signaling factors and their receptors alter angiogenesis activators*

Vascular sprouting requires certain cell types to migrate, elongate, or retract in order to local cues. Each signaling family in angiogenic growth factors involved in guidance is comprised of multiple ligands that are recognized by one or more receptors. A cell expressing a certain ligand can bind to a receptor expressed by a neighboring cell and drive signaling *via* a paracrine mechanism. On the other hand, if the same cell expresses both ligand and receptor it can activate signaling in an autocrine manner. Thus, an interlaced angiogenic response is produced in response to the various guidance molecules and their receptors on multiple types of cells. These multiple guiding factors regulate tip cell sprouting, perivascular cell coverage, recruitment of progenitor cells, and attraction of macrophages. Tumors may therefore exhibit different sensitivities to different anti-vascular therapies. These therapies can, of course, target either the key upstream factors regulate these pathways or their common downstream mediators.

Vascular endothelial growth factor (VEGF) is one of the most powerful inducers of angiogenesis [369]. VEGF is up-regulated during hypoxia and orchestrates the formation of blood vessels mainly *via* activation of VEGF receptor-2 (VEGFR-2) which is expressed by endothelial cells [370]. Some recent works have proved that VEGF can be detected using CDs [371–373]. For example, a novel 'signal-off' photoelectrochemical (PEC) aptasensor based on an aptamer-bridged DNA network structure was developed for the detection of $VEGF_{165}$ by Da et al. [368] In this case, g-C_3N_4 nanosheets were used as a photoactive material (Fig. 31). A linear relationship was obtained between the PEC signal and logarithm of the VEGF165 concentration over the range from 100 fM to 10 nM. The LOD was found to be 30 fM.

Yan et al. [374] synthesized viscosity-dependent CDs (V-CDs) with anti-VEGF characteristics for detecting and promoting apoptosis in cancerous cells. The fluorescence from the V-CDs changes (from blue to green) as the viscosity of their environment changes (as this affects the freedom with which rotation occurs around an intramolecular single bond). By incorporating Taxol as well, the authors were able to simultaneously visualize and treat cancerous cells (Fig. 32a and b).

Another fluorescent aptasensor for detecting $VEGF_{165}$ was constructed by Cui et al. [375] Their device employs a porphyrin-based covalent organic framework (p-COF) and CDs and was used for the 'off-on' imaging of MCF-7 breast cancer cells. The CDs employed were obtained by the controlled thermal pyrolysis of citric acid and urea. They were subsequently used as donors to label $VEGF_{165}$-targeting aptamers (Fig. 32c–32e). Adsorption of the CDs onto the p-COF framework (*via* π-π stacking, hydrogen bonding, and Van der Waals interactions) causes their fluorescent emissions to be quenched due to the

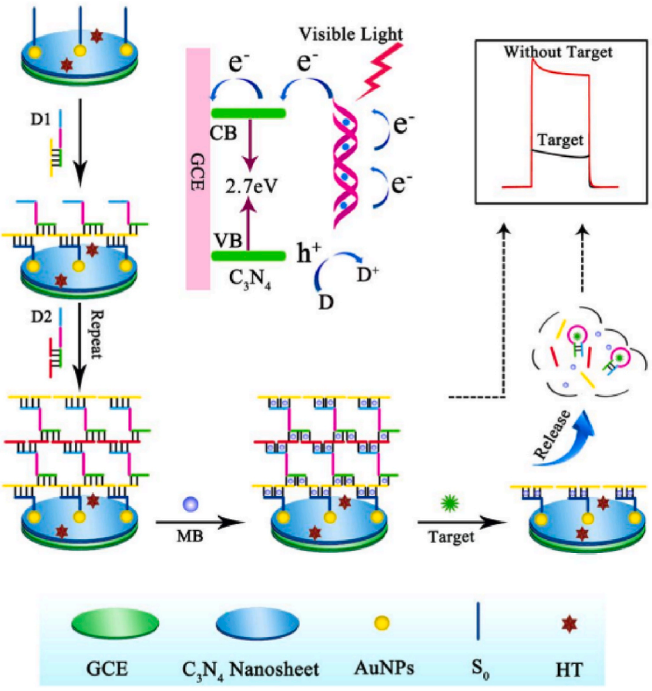

Fig. 31. The assembly and mechanism of the PEC aptasensor [368]. Copyright 2018, Elsevier Advanced Technology.

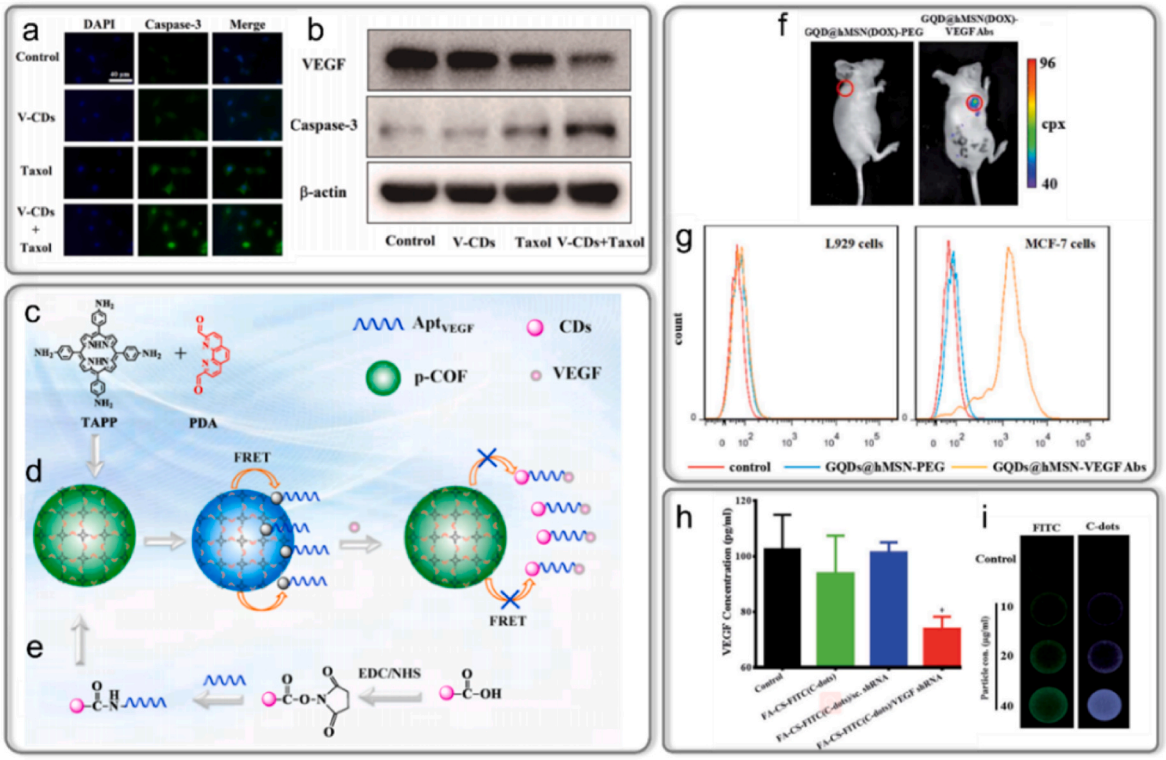

Fig. 32. (a) Representative fluorescence images illustrating enhanced caspase-3 expression by synergistic treatment with V-CDs and Taxol. (b) Western blot results for the control, V-CDs, Taxol, and V-CDs + Taxol [374]. Copyright 2021, Elsevier Science SA. (c–e) The synthesis method and working pringciple of CDs based $VEGFs_{165}$ biosensor [375]. Copyright 2017, Elsevier. (f) Fluorescence images of mice after intravenous injection with GQDs@hMSN(Dox)-PEG and GQDs@hMSN (Dox)-VEGF Abs. (g) Flow cytometry analysis of GQDs@hMSN-PEG and GQDs@hMSN-VEGF Abs in MCF-7 and L929 cells [376]. Copyright 2019, the Royal Society of Chemistry. (h) Decrease in VEGF expression 48 h after treatment with nanocomplexes. (i) Representative *in vitro* fluorescence images produced by activating FITC (left) and CDs (right) [377]. Copyright 2016, the Royal Society of Chemistry.

occurrence of FRET (the 'off' state). In the presence of $VEGF_{165}$, however, the aptamers bind to the $VEGF_{165}$ causing the CDs to move away from the p-COF, preventing FRET from occurring, and restoring the emission of fluorescence (the 'on' state). The biosensor was found to have a detection limit of 20.9 fg/mL and a wide range of linearity (1.0 pg/mL to 100 ng/mL).

Dong et al. [376] recently synthesized hollow mesoporous silica nanoparticles (hMSNs) with GQDs encapsulated inside (GQDs@hMSN) for use in drug delivery. In particular, GQDs@hMSN-PEG species functionalized with VEGF antibodies (Abs) were used for targeting VEGF in breast tumors. These can be further loaded with Dox to cure the detected tumors. Confocal fluorescence microscopy and *ex vivo* fluorescence signals in mice were used to show that the drug could be selectively delivered to the cancer cells requiring treatment (Fig. 32f, g). Yang et al. [377] designed multifunctional chitosan hybrid nanoparticles FA–CS–FITC(Dox/CDs)/VEGF shRNA for use in cancer therapy and dual fluorescence imaging. Transfected HeLa cells exhibited greatly reduced VEGF expression, inhibited cell proliferation, and increased cell apoptosis, which contributed to synergistic antitumor efficacy. Furthermore, superb dual fluorescence cellular images can be produced using only modest amounts of the nanocomplexes (Fig. 32h, i).

There are 23 members of the mammalian fibroblast growth factor (FGF) family, 18 of which interact with high affinity with the tyrosine kinase receptors FGFR1, FGFR2, FGFR3, and FGFR4 [378]. FGFs are secreted glycoproteins that are sequestered in the ECM. Hwang et al. [379] designed a kinase-inhibitor-modified QD probe to study the reaction between FGFRs and potential inhibitors. More specifically, turbo-green fluorescent protein-FGFR3s were overexpressed in HeLa cells to explore the colocalization of FGFR3 and AZD4547 using the QD probe.

It has been demonstrated that IL-6 signaling is crucial for tumor development and metastatic spread in a variety of tumor types. Patients with various malignancies and patients with recurrent tumors have been found to carry high circulating levels of IL-6. Tiron et al. [380] have developed CDs prepared from *N*-hydroxyphthalimide (CDs-NHF) for use as antitumoral agents. Doping these CDs with Gd^{3+}, Fe^{3+}, or Mn^{2+} preserves their antitumoral properties and allows them to be imaged *via* magnetic resonance. The *in vitro* investigations showed that the level of IL-6 mRNA in cancer cells treated with Mn-doped CDs-NHF was significantly lower than that in the control cells (which were treated with Gadovist, a gadolinium-based contrast agent). Luta et al. [381] found a significant impairment in the IL-6 level in all of their groups treated with CDs-NHF thus confirming the antitumoral properties of these CDs.

Özcan et al. [382] reported a new molecularly imprinted biosensor based on GQDs/functionalized MWCNTs that can be used to detect IL-6 protein. An IL-6-imprinted electrode was prepared on the GQDs/f-MWCNTs in the presence of 100.0 mM pyrrole and 25.0 mM IL-6. For analytical purposes, the biosensor was found to have a linearity range of 0.01–2.0 pg/mL and LOD of 0.0030 pg/mL in plasma samples (Fig. 33a, 33b).In order to target receptors, Wang et al. [383] prepared polymer-coated CDs combined with peptide fragments of IL-6 (pCDPI) and used them for imaging and drug delivery. The *in vitro* and *in vivo* results demonstrate that the pCDPI can overcome the blood-brain barrier and penetrate deep inside orthotopic gliomas in mice. They can then be monitored in real-time *via* their fluorescent emission. At the same time, they can be used to deliver a therapeutic drug (e.g., Dox) thus inhibiting IL-6-induced cell proliferation (Fig. 33c-33e).

8.2. ECM remodeling and its inhibitors

The tumor stroma must undergo continuous remodeling in order to support angiogenesis. MMPs that proteolytically degrade ECM

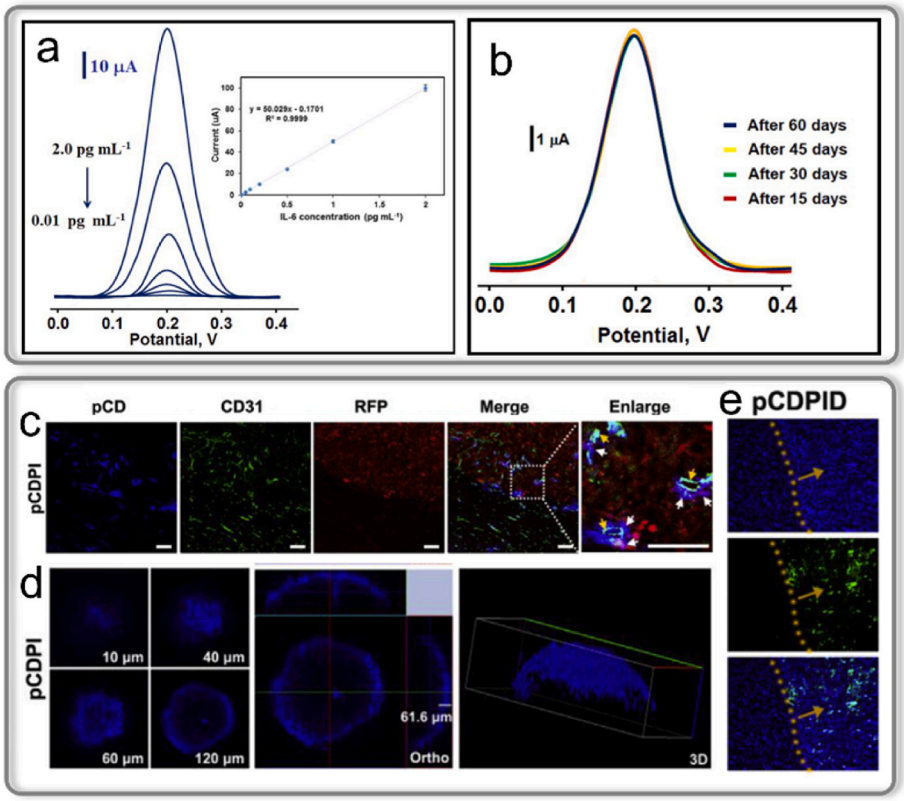

Fig. 33. (a) Effect of concentration on the DPV signal. Inset: calibration curve obtained using different concentrations of IL-6. (b) Reproducibility of measurements recorded over several days using one imprinted electrode [382]. Copyright 2008, Electrochemical Soc. Inc. (c) pCDPI-injected brain slices in immunofluorescence pictures from glioma-bearing mice. (d) U87 glioma spheroids' fluorescent distribution after incubation with pCDPI for 4 h. (e) Tumor apoptosis in glioma-bearing mice treated with pCDPID [383]. Copyright 2017, Elsevier Sci. Ltd.

components are essential to this process. MMPs (such as MMP-2, MMP-9, and MT1-MMP) participate in the angiogenic process by transforming the basement membrane to permit sprouting, releasing matrix-bound angiogenic factors, and cleaving matrix proteins into antiangiogenic fragments [384,385].

The expression of MMPs by the tumor cells will therefore aid them in remodeling the ECM and releasing ECM- and membrane-bound growth factors hence boosting tumor growth, metastasis, and tumor-associated angiogenesis. Chen et al. [386] demonstrated that a CQDs/Cu_2O composite can be used to selectively inhibit SKOV3 ovarian cancer cells by targeting MMPs, angiogenic cytokines, and the cytoskeleton. The IC_{50} value of CQDs/Cu_2O with respect to SKOV3 cells is 0.85 μg mL^{-1}. The composite's performance is also superior to that of other commercially available anticancer drugs (the IC_{50} values of oxaliplatin and artesunate are approximately 75 and 114 times larger than that of the composite, respectively). The CQDs/Cu_2O composite selectively mediates the death of SKOV3 cells by mainly decreasing the expression of MMP-2, MMP-9, F-actin, and VEGFR2. (Fig. 34a and b).

Li et al. [387] constructed a graphene oxide-peptide-PD (GO-Pep-PD) nanocomplex for detecting MMP-9. The nanocomplex is in a 'off' state in the absence of MMP-9 but is switched 'on' in the presence of MMP-9, resulting in the emission of a fluorescent signal that is linearly associated with the MMP-9 concentration. The LOD of the technique was found to be 3.75 ng/mL, which is lower than most approaches. The nanocomplex was subsequently used to successfully detect MMP-9 in clinical serum samples from patients with prostate cancer (Fig. 34c).

9. Activate tumor invasion and metastasis

The original tumor mass will eventually give rise to pioneer cells that spread out and infiltrate surrounding tissues during the development of

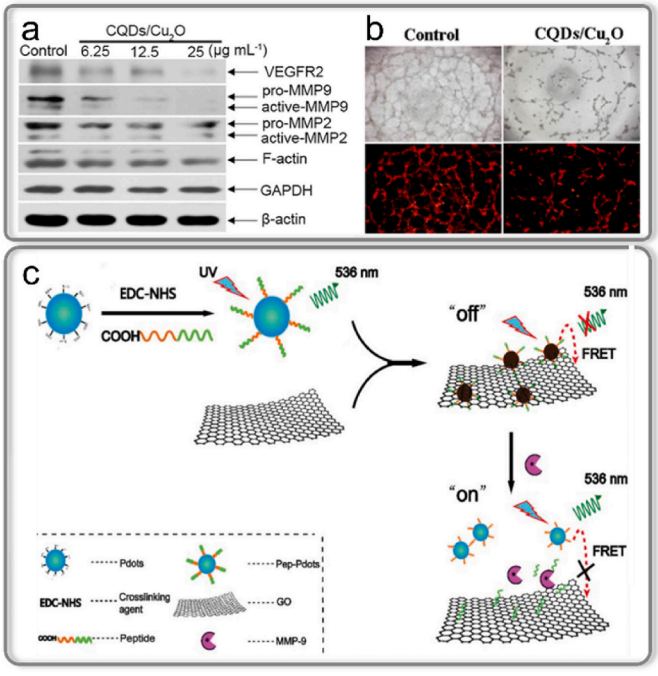

Fig. 34. (a) Western blot results for SKOV3 cells incubated with CQDs/Cu_2O. (b) Fluorescence microscope images showing that CQDs/Cu_2O inhibits blood vessel formation in human umbilical cord vein endothelial cells [386]. Copyright 2021, BMC. (c) The synthesis and application of the GO-Pep-Pdot nanocomplex for MMP-9 measurement [387]. Copyright 2019, the Royal Society of Chemistry.

majority of human cancers. These explorers might be successful in establishing new colonies by traveling to far-off locations, which are the cause of 90 % of human cancer deaths [388]. The ability of cancer cells to form distant metastases allows them to colonize new parts of the body where nutrients and space are, at least initially, not limited. The newly developed metastases are composed of cancer cells mixed with healthy supportive cells conscripted from the host tissue.

Epithelial-mesenchymal transition (EMT) is a developmental regulatory program that has been significantly implicated to the development of altered epithelial cells' capacity to spread, resist apoptosis, and invade other cells [389–392]. The EMT is regulated by many growth factors and signaling pathways, including TGFβ, Wnt, and Notch. These signaling pathways interact to promote EMT and subsequent cell invasion. There are many other factors that induce EMT, e.g., hypoxia, metabolic stress, matrix stiffness, and epigenetic and post-translational modification. The exact contribution of each factor to EMT is unclear and may differ between tumors. The Notch pathway is mainly regulating cell fate decisions, differentiation, and proliferation (Fig. 35) [393–395]. Notch cooperates with the Wnt pathway and TGFβ to induce EMT.

Three Wnt signaling pathways operate in react to the attachment of 19 distinct Wnt ligands to the Frizzled family of cell surface receptors (Fig. 36). These pathways are referred to as the canonical Wnt signaling pathway, noncanonical Wnt/calcium pathway, and noncanonical planar cell polarity (PCP) pathway. The canonical Wnt pathway is activated when a canonical Wnt ligand binds to a Frizzled membrane receptor. This results in the release of β-catenin from a complex formed by glycogen synthase kinase-3β (GSK3β), axis inhibition protein (Axin), and adenomatous polyposis coli (APC). The β-catenin then translocates to the nucleus where it attaches to the T-cell factor (TCF) and lymphoid enhancer-binding factor (LEF) transcription factors which activates genes that drive the EMT.

In cells with invasive or metastatic potential, several groups of proteins involved in anchoring tissue cells to their environment are changed, one of the proteins impacted, are cell adhesion molecules (CAMs). Notable CAMs include members of the immunoglobulin and calcium-dependent cadherin families, both of which mediate cell-to-cell interactions, and integrins, which link cells to ECM substrates. A second general group of substances involved in invasion and metastasis capacity are extracellular proteases: protease genes become up-regulated, protease inhibitor genes down-regulated, and the non-active zymogen forms of proteases converted to active enzymes [396,397].

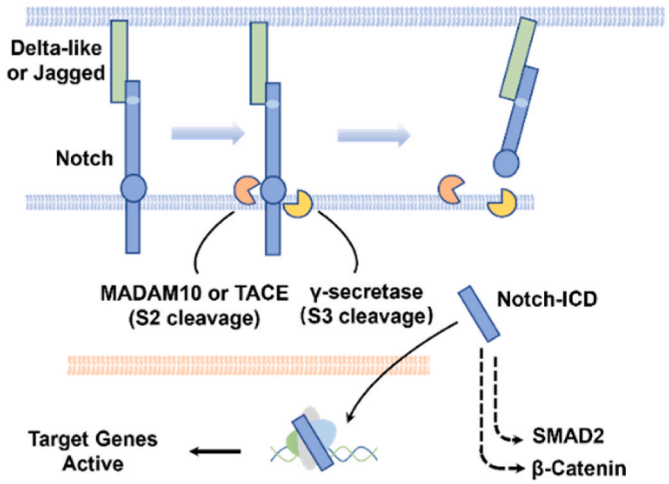

Fig. 35. Outline of the Notch signaling pathway.

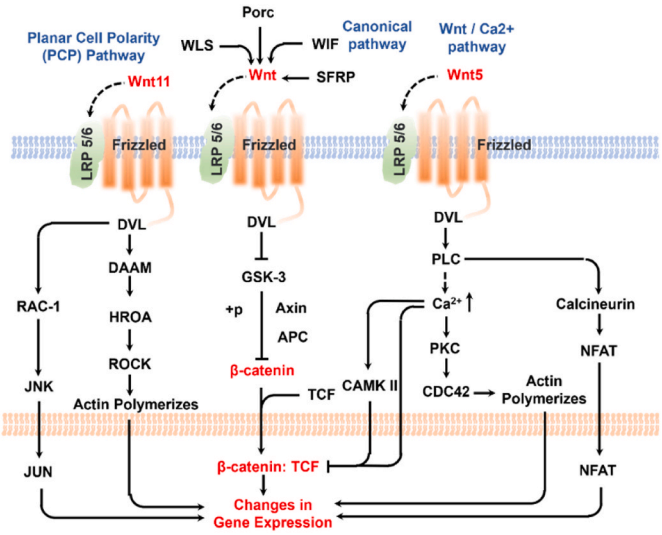

Fig. 36. Outline of the three Wnt signaling pathways.

9.1. *Change in adhesive proteins that bind cells to their surroundings*

Some highly aggressive carcinomas have observable changes in the expression of genes encoding cell-to-cell and cell-to-ECM adhesion molecules. Adhesion molecules that are often related to the cell movement that takes place during embryogenesis and inflammation tend to be up-regulated, whereas those that promoting cytostasis are typically down-regulated.

The best characterized change in carcinoma cells is that involving the loss of E-cadherin (a key molecule involved in cell-to-cell adhesion), which function appears to be eliminated in the majority of epithelial cancers. The mechanism responsible for this may involve mutational inactivation of the E-cadherin or β-catenin genes, transcriptional repression, or proteolysis of the extracellular cadherin domain. However, there is only one study that has suggested that CQDs may prove effective in diagnosing and treating cancer by targeting signaling pathways involving β-catenin [336].

CD44 is an extracellular cell-matrix adhesion glycoprotein known to be overexpressed on the surfaces of various cancers, including breast and lung cancer. Thus, it can be used as a biomarker for diagnosing and treating such cancers [398]. It is essential for various cellular functions, e.g., adhesion, aggregation, migration, and signal transduction [399], CD44 receptor thus is associated with tumor invasion, prognosis, progression, and metastasis. As it is associated with tumor development and progression, it has been used as a target for delivering therapeutic drugs for tumor therapy [399–401]. The cooperation that occurs between CDs and hyaluronic acid (HA) has been used in tumor diagnosis and treatment by numerous researchers [402–427], brief details of which are presented in Tables 7 and 8.

Wang et al. [420] combined a redox/enzyme dual-responsive disulfide-conjugated CD with MSNs (MSN–SS–CD_{HA}) for targeted and regulated antitumor drug delivery and real-time bioimaging. CD_{HA} nanoparticles with diameters of *ca.* 3 nm completely blocked the pore entrances of the Dox-encapsulated MSN nanoparticles (whose pore size is also *ca.* 3 nm). Their *ex vivo* fluorescence images showed that much stronger fluorescence was emitted from the tumor site (compared to normal tissues) when MSN–SS–CD_{HA}-Dox was administered. These nanocarriers also greatly facilitated the accumulation of Dox in the target tissue (Fig. 37a). Abdullah-Al-Nahain et al. [413] fabricated GQD-HA with a particle size of *ca.* 20 nm as a targeting agent. The synthesized GQD-HA was administered to CD44 receptor overexpressed tumor-bearing balb/c female mice and the *in vivo* biodistribution investigated. They thus demonstrated that the GQD-HA led to much brighter fluorescence being emitted from the tumor tissue (Fig. 37b, c).

Table 7
Recent tumor-diagnostic techniques based on detecting CD44 with CQDs.

Materials	Method	λ_{ex} (nm)	λ_{em} (nm)	QY (%)	LOD	LR	Sample	Cell line	Ref.
FA-PEI-HA-CNDs	Confocal fluorescence imaging.	424	531	10.71	NA	NA	Buffer	A-549	[406]
MSN–SS–CD_{HA}	Flow cytometry measurement; Confocal fluorescence imaging; *Ex vivo* imaging.	345	450	39.6	NA	NA	Buffer	A-549	[420]
GQD-HA	Confocal fluorescence imaging; *In vivo*, *ex vivo* fluorescence imaging.	318	440	27	NA	NA	Buffer	A-549	[413]
HA-CDs	Flow cytometry measurement; Confocal fluorescence imaging.	320–500	436–531	8.6	NA	NA	PBS	A-549; 4T1	[417]
GQD-conjugated gemcitabine-loaded HSA	Fluorescence imaging.	340 360–480	430, 540 540	14	NA	NA	Buffer	Panc-1	[419]
HMSN–SS–CD_{PEI}@HA	Flow cytometry measurement; Confocal fluorescence imaging.	360	450	NA	NA	NA	Buffer	A-549	[415]
P-CDs/HA-Dox	Confocal fluorescence imaging.	290–370	370–450	NA	0.65 U mL^{-1}	400 U mL^{-1}	Buffer	HeLa	[425]
HA-nCQDs	Confocal fluorescence images; *In vivo* fluorescent images.	540	600	10.5	NA	NA	Buffer	CHO	[412]
CD(HA)/TiO_2/Cu^{2+}	Wireless sensor; Flow cytometry measurement.	450	505	NA	2.31 cells/mL	NA	Buffer	HeLa	[422]
MnNS:CDs@HA	Magnetic resonance imaging; Confocal fluorescence images.	360	437	17.7	NA	NA	Buffer	HeLa	[405]
PMn@Cdots/HA	Magnetic resonance imaging; Confocal fluorescence images; Flow cytometry measurement.	530, 570	600	36	NA	NA	Buffer	B16F1; HeLa	[410]
HA-functionalized CDs@FcDA	Confocal fluorescence images; Flow cytometry measurement.	450	533	4.38	0.157 μM	0.20–10.0 μM	Buffer	HeLa	[421]

NA: not mentioned.

Table 8
Summary of CDs targeting CD44 cells for cancer therapy.

Materials	Therapeutic agent	Strategy	λ_{ex} (nm)	λ_{em} (nm)	QY (%)	Type of cancer	Cell line	Animal model	Ref.
MSN–SS–CD_{HA}	Dox	Chemotherapy	345	450	39.6	Adenocarcinoma	A-549	Mice	[420]
HA-CD@p-CBA-Dox			488	525	NA	Breast cancer	4T1	Mice	[403]
HMSN–SS–CD_{PEI}@HA			360	450	NA	Adenocarcinoma	A-549	NA	[415]
P-CDs/HA-Dox			290–70	370–450	NA	Human cervical cancer	HeLa	NA	[425]
HA-g-PLA/HCDs		PTT; Chemotherapy	540	570	6	Breast cancer	MDA-MB-231; MCF-7	NA	[426]
HA-CDs	NA	PDT	320–500	436–531	8.6	Adenocarcinoma	A-549; 4T1	NA	[417]
GQD-conjugated gemcitabine-loaded HSA	Gemcitabine	Chemotherapy	340 360–480	430, 540 540	14	Pancreatic cancer	Panc-1	NA	[419]

NA: not mentioned.

Karakocak et al. [424] used confocal microscopy to show that the HA-nCQDs, facilitated by CD44 receptors, experienced enhanced internalization in the target cells (Fig. 37d). To demonstrate the selectivity of the HA-nCQDs towards human tumor cells, patient-derived breast cancer tissues with high CD44 expression were injected in adult mice (Fig. 37e-37g). Following additional investigation using flow cytometry, fluorescence, and MRI, Lin et al. [410] synthesized PMn@Cdots/HA to achieve good *in vivo* and *in vitro* biocompatibility as well as the capacity to specifically target CD44-overexpressing cancer cells (Fig. 37h).

Yang et al. incorporated a gadolinium complex (Gd-DOTA) functionalized with PEG with GQDs to synthesize paramagnetic GQDs (PGQDs) [404]. Their *in vitro* results demonstrate that the relaxivity of the PGQDs can be controlled by regulating the length of the PEG used. Relaxivities *ca.* 16 times those of commercial MRI contrast agents (e.g., Gd-DTPA) were thus obtained (Fig. 38a). Qiu et al. [401] fabricated a single-cell analysis platform that uses solid-state zinc-coadsorbed CQDs (ZnCQDs) as electrochemiluminescent (ECL) probes. The ZnCQDs were used to detect breast cancer cells and measure the degree of CD44 expression. The technique is highly sensitive and can be used to detect single cells. The authors applied it to analyze MDA-MB-231 and MCF-7 cells and obtained linearity ranges of 1–18 and 1–12 cells, respectively. The CD44 expression levels in the two cell lines were also evaluated and found to be 2.8–5.2 times higher in MDA-MB-231 cells than MCF-7 cells (Fig. 38b-38d). Giang et al. [422] investigated a CD(HA)/TiO_2/Cu^{2+} electrochemical biosensor. The surface of the stimulus-responsive biosensor was monitored by wireless sensing to visualize the cell adhesion interaction with the surface and detect cancer cells. The biosensor achieved LOD values of 2.31 cells/mL, using an electrochemical approach, and 70.05 cells/mL, using an optical approach (Fig. 38e).

9.2. Immunoglobulin superfamily mediated adhesion reaction

The processes of invasion and metastasis also seem to be significantly influenced by changes in the expression of CAMs belonging to the immunoglobulin superfamily. The extracellular structure of this molecule contains immunoglobulin-like folds that mediate calcium-dependent intercellular adhesion reactions. Intercellular adhesion molecule (ICAM-1), vascular endothelial cell adhesion molecule (VCAM), nerve adhesion molecule (NCAM) and carcinoembryonic antigen (CEA) are members of the immunoglobulin superfamily associated with tumor metastasis. In CQDs for tumor detection CEA is the focus of attention (Table 9), while other markers are almost not studied.

Yang et al. [428] fabricated PtPd/N-GQDs@Au in an electrochemical immunosensor was for quantitative detection of CEA as well as electrocatalytic activity towards hydrogen peroxide (H2O2) reduction

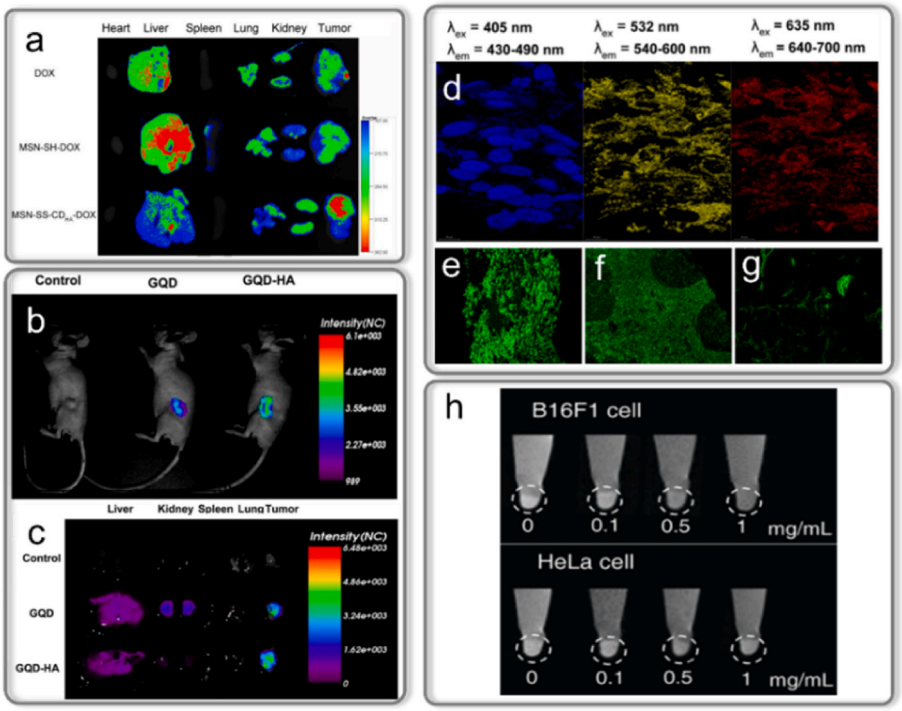

Fig. 37. (a) *Ex vivo* images of various organs and tumors in tumor-bearing mice after injecting them with Dox, MSN–SH–Dox, and MSN–SS–CD_{HA}-Dox [420]. Copyright 2017, Elsevier. (b) *In vivo* fluorescence images of mice after GQD-HA injection (in tail vein). (c) *Ex vivo* images of various organs and tumor cells after dissection [413]. Copyright 2013, American Chemical Society. (d) Confocal microscopy images of Chinese hamster ovary cells exposed to nCQDs conjugated with HA. (e) High-CD44 expressing sample, (f) tonsil tissue, and (g) low-CD44 expressing sample imaged in a tissue microarray (TMA) [424]. Copyright 2021, American Chemical Society. (h) *T2*-Weighted images of B16F1 (upper layer) and HeLa cells (lower layer) incubated with different concentrations of PMn@Cdots/HA for 24 h (7 T MRI system) [410]. Copyright 2019, the Royal Society of Chemistry.

(Fig. 39a and b). In addition, a noval ECL nanomaterial made of CQDs and the dual luminophores perylenetetracarboxylic acid (PTCA) is described by Xu et al. [429] The ECL nanomaterial exhibits significant increases in ECL intensity, which were explained by the synergistic promotion ECL mechanism of PTCA and CQDs. Moreover, a sandwiched CEA immunosensor was made using this ECL nanomaterial to mark secondary antibodies (Fig. 39c).

Green CDs were created by Miao et al. [430], whose abundance in carboxyl groups allowed for substantial ssDNA adsorption on the surface of the CDs through π-π stacking interactions, which effectively quenched fluorescence by generating CDs-aptamer complexes. When the CEA was added, the fluorescence of CDs was immediately recovered owing to the greater binding affinity between CEA and CEA-aptamer than the stacking interactions (Fig. 39d and e). Wang et al. [431] proposed a universal biosensing device based on microfluidic immunofluorescence micro assays chip combined with solid phase GOQDs. The biosensing platform can validated CEA, carbohydrate antigen 125 (CA125), a-fetoprotein (AFP), carbohydrate antigen 199 (CA199) and carbohydrate antigen 153 (CA153). It features a detection limit of 1 pg/mL or 0.01 U/mL, a linear quantification detection regime of 5–6 orders of magnitude. Furthermore, this biosensing chip can perform 5–20 different types of biomarkers from at least 60 people concurrently in 40 min using just 2 mL of each patient's serum, cutting the detection cost and time to at least 1/60 of the time and cost of currently used common methods (Fig. 39f and g).

9.3. Integrins control the bioavailability of ECM components

Invading and metastatic cells have altered integrin expression as well. These cells travel through altering tissue microenvironments, which may expose them to novel matrix elements. As a result, adaptation is necessary for effective colonization of these new places, both nearby and far away. This can be accomplished by changing in the α/β integrin expressed by the migrating cells. For example, carcinoma cells promote invasion by altering the expression of integrins from those that prefer the ECM present in normal epithelium to others (e.g., $\alpha_5\beta_1$ and $\alpha_v\beta_3$) that preferentially attach to the damaged stromal components released by extracellular proteases. In particular, $\alpha_5\beta_1$ binds fibronectin, $\alpha_\gamma\beta_5$ binds vitronectin, and $\alpha_\gamma\beta_3$ binds many substrates, including fibronectin, vitronectin, von Willebrand factor, tenascin, osteopontin, fibrillin, fibrinogen, and thrombospondin.

Integrin-mediated signaling often arises after ligation to a specific matrix protein, it is a result of interaction between integrins and certain activated cytokines or growth-factor receptors. These signaling processes can decide if a cell is in a suitable microenvironment, which will subsequently have an impact on its capacity to survive, migrate, and invade. RGD is the most typical marker of integrin. Reproduced with permission.

Microwaves and a cocktail containing soybean milk (as a green source of carbon) and a capping agent (4,7,10-trioxa-1, 13-tridecanediamine) were used by Liu et al. [443] to synthesize CD nanocomposites (MB-CDs@NH-RGD) capable of targeting integrin $\alpha_v\beta_3$. The CDs can target the $\alpha_v\beta_3$ that is overexpressed in the MDA-MB231 and B16 cell lines. Subsequent irradiation of the CD nanocomposites using a pulsed laser was also shown to produce a significant photothermal effect in the targeted cells. Li et al. [444] reported the development of nanohybrids made from poly(amidoamine) (PAMAM) dendrimers and blue-emitting CDs for monitoring cancer cells *via* fluorescence imaging. The nanohybrids can also be loaded with more than one drug to help overcome the problem of multidrug resistance. Generation 5 (G5) PAMAM dendrimers were covalently modified with arginine-glycine-aspartic (RGD) peptide, which can target $\alpha_v\beta_3$, and the drug efflux inhibitor D-α-tocopheryl polyethylene glycol succinate (TPGS). The functionalized dendrimers G5-RGD-TPGS were complexed with CDs/Dox complexes *via*

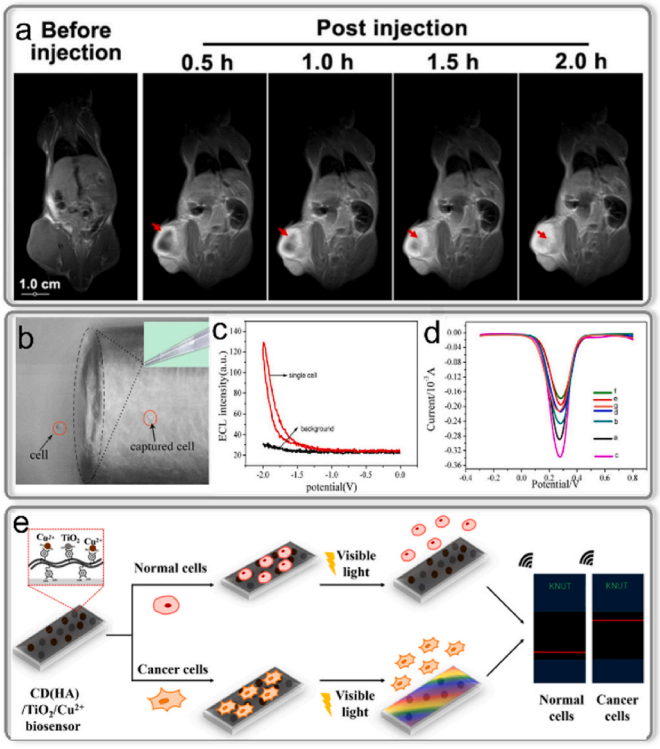

Fig. 38. (a) *In vivo* T_1-weighted magnetic resonance images of A549 tumor-bearing mice before and after being injected with PGQDs-HA (recorded using a 1.5 T human MRI scanner) [404]. Copyright 2018, American Chemical Society. (b) Inverted microscope images showing the capture of a cell. (c) ECL emission from a single cell before and after the introduction of the HA-ZnCQDs/AuNPs@MB probe. (d) DPV response [401]. Copyright 2017, American Chemical Society (e) Mechanism of CD(HA)/TiO_2/Cu^{2+} wireless biosensor for the tumor diagnosis and antifouling properties [422]. Copyright 2021, Elsevier Science SA.

electrostatic interactions to form dual-drug-loaded nanohybrids (Fig. 40a). The nanohybrids were found to inhibit cancer cells due to the presence of TPGS (which inhibits P-glycoprotein by decreasing ATP levels and increasing ROS levels). The cancer cells could also be imaged *in vitro* by detecting the luminescence produced by the CDs in the nanohybrids.

Feng et al. [445] developed pH/redox dual-response CDs (CDs-RGD-Pt(IV)-PEG) for targeting the extracellular microenvironment in tumors and enhanced delivery of anticancer drugs. Hydrolysis of benzoic-imine bonds in the nanocarriers in the tumor extracellular (at pH 6.5–6.8) exposes the inner targeting RGD peptide. The drug in the nanocarriers was effectively delivered to the cancer cells through the RGD-integrin $\alpha_v\beta_3$ (ligand-receptor) interaction. When the loaded cisplatin(IV) prodrug is internally absorbed, it is converted to cytotoxic cisplatin in the cytoplasm of the cancer cells, producing a therapeutic effect (Fig. 40b). Confocal imaging, flow cytometry, and cell viability assays were subsequently performed using the CDs-RGD-Pt(IV)-PEG. Chen et al. [446] produced highly fluorescent CDs on the mesoporous organosilica nanoparticles and further indicated that Dox can be effectively contained within these fluorescent mesoporous silica nanoparticles. Coupling with c(RGDyK) also allowed the nanoconjugates to efficiently target the tumors through their interaction with the integrin $\alpha_v\beta_3$ overexpressed on the tumor vasculatur).

Zheng et al. [447] synthesis a dual mode nanocarrier to transport Dox and regulate the release of the drug in the targeted tumor cells. The nanocarrier consists of a gold nanorod (to act as a heating core), biodegradable mesoporous silica (as a storage chamber), and RGD-modified GQDs (to act as a drug carrier). When exposed to NIR radiation, the internalized nanocarriers rapidly heat their surrounding environment. The high temperature produced also leads to the collapse of the π-π interaction between the Dox and GQDs and instantaneous release of the drug, thereby intensifying the efficacy of the therapeutic effect (Fig. 41a).

In the invasion and metastasis of tumor, angiogenesis is a crucial stage. Recent research has demonstrated that the multi-tyrosine kinase inhibitor sorafenib (SFB) may inhibit angiogenesis and slow the growth of tumors. For this reason, a nanocomposite of GQDs and poly(D,L-lactide-co-glycolide) (PLGA) nanoparticles was functionalized with RGD

Table 9
Recent tumor diagnostic techniques based on CEA detection with CDs.

Materials	Method	λ_{ex} (nm)	λ_{em} (nm)	LOD	LR	Sample	Cell line	Ref.
SiO_2@C-dots	Electrochemical immunosensor	NA	NA	CEA = 0.006 ng/mL PSA = 0.003 ng/mL α-AFP = 0.005 ng/mL	NA	human serum	NA	[432]
PtPd/N-GQDs@Au		NA	NA	2 fg/mL	5 fg/mL - 50 ng/mL	human serum	NA	[428]
SWCNTs@GQDs		360	440	5.3 pg/mL	50–650 pg/mL	human serum	NA	[433]
CQDs	Electrochemi	NA	NA	0.00026 fg/mL	0.001 fg/mL - 1 ng/mL	human serum	NA	[429]
GQDs@AuNP	-luminescence	NA	NA	3.78 fg/mL	0.1 pg/mL −10 ng/mL	human serum	NA	[434]
AuNPs/CQDs-PEI-GO		365	443	1.67 pg/mL	5 pg/mL - 500 ng/mL	human serum	NA	[435]
N-carbon dots/ TiO_2–Pt		360	495	1.0 pg/mL	0.002–200 ng/mL	human serum	MCF-7	[436]
GOx/McAb2/GQDs/ Au@Pt		NA	NA	0.6 pg/mL	1.0 pg/mL −10 ng/mL	human serum	NA	[437]
CDs	Confocal laser scanning microscopy	458	518	1.48 fg/mL	4fg/mL-0.8 pg/mL	NA	HepG2	[438]
GOQDs	Microfluidic chip	352	455	1 pg/mL (CEA, AFP) 0.01–0.05 U/mL (CA125, CA199, CA153)	5 pg/mL - 0.5 mg/mL (CEA, AFP); 0.5–5000 U/mL (CA125, CA199, CA153)	human serum	NA	[431]
CDs	Fluorescence Spectrum	440	367	0.3 ng/mL	1 ng/mL - 0.5 mg/mL	human serum	NA	[430]
o-CDs		428	572	74.5 pg/mL	0.1–80 ng/mL	human serum	NA	[439]
CDs-DNA		450	380	7.32 pg/mL	0.01 e 1 ng/mL	serum	NA	[440]
NIR-CDs-DNA		420	683	0.02 pg/mL	0.1 e 5000 pg/mL	Pleural effusion	NA	[441]
CDs@SiO_2		380	449	794.6 ag/mL	1 fg/mL - 10 ng/mL	real serum samples	NA	[442]

NA: not mentioned.

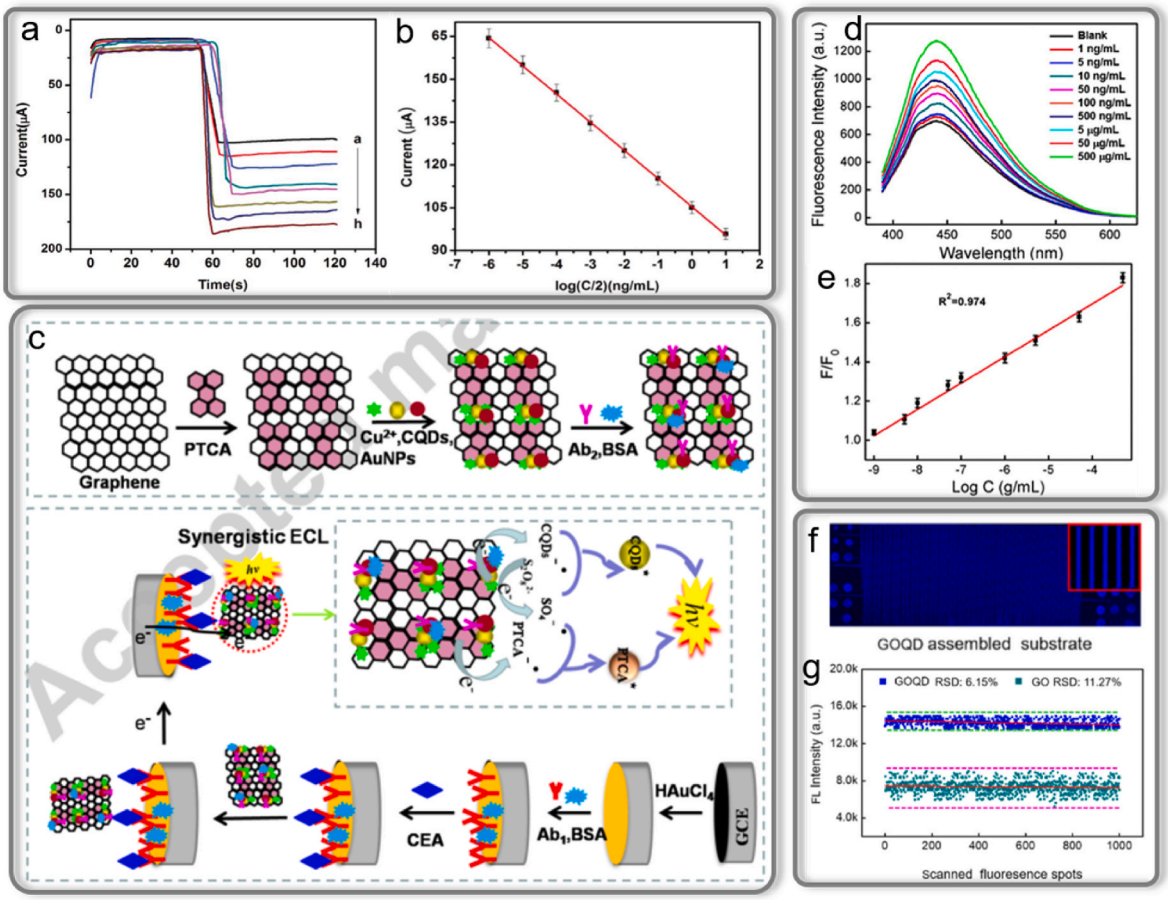

Fig. 39. (a) Amperometric response and (b) calibration curves of the immunosensor to different concentration of CEA [428]. Copyright 2017, Elsevier Advanced Technology. (c) Graphene-PTCA-Cu2+-CQDs/AuNPs/Ab2 layer-by-layer assembly, fabrication of the ECL immunosensor, and the synergistic ECL concept [429]. Copyright 2017, Elsevier Advanced Technology. (d) CDs and CEA-aptamer fluorescence spectra at varied concentrations of CEA. (e) Plot of F/F0 against CEA concentrations from 1 ng mL-1 to 500 μg mL-1 [430]. Copyright 2016, Elsevier Advanced Technology. (f) GOQDs nanosheets assembled substrates. (g) Fluorescence intensity distribution measured along microchannels on two distinct substrates at 1000 sites chosen at random [431]. Copyright 2021, Elsevier.

peptide to enhance SFB distribution for the therapy of angiogenesis (Fig. 41b) [448]. The drug release behavior of the nanocomposite was investigated at 37 °C and pH = 7.4. The photoluminescence from the GQDs in the nanocomposite was used to track the drug-delivery system.

Aimed at overcoming PDT resistance in cancer, Li et al. [449] devised a high-performance nanosystem based on N,S-codoped GQDs labeled with c(RGDfC) peptides. The as-prepared cRGD-GQDs featured high singlet oxygen quantum yield (0.95), good biocompatibility and excellent pH stability (Fig. 42a). Factors indicative of PDT resistance were maintained at low levels after repeated PDT treatment with the cRGD-GQDs.

Ghosh et al. [450] developed a CD-based system aimed at detecting triple-negative breast cancer (TNBC). They synthesized their CDs from sweet lemon peel and conjugated them with different generations of PAMAM dendrimers to generate CD-PAMAM conjugates (CDPs). RGDS peptide was further conjugated to the CDPs to target $\alpha_v\beta_3$ integrin which is overexpressed in TNBC. The results of various tests showed that one particular conjugate (CDP3) is a potential gene carrier system for use in TNBC gene therapy (Fig. 42b–42d). Fan et al. [451] have also developed a biomimetic nano-drug system for TNBC therapy. As shown in Fig. 42e Their system uses GTDC@M-R nanoparticles that are based on erythrocyte membrane (M)-camouflaged graphene oxide quantum dots (GOQDs, G). Transactivator of transcription (TAT, T) and RGD (R) peptides are incorporated into the system to target importin α and β on the nuclear surface, thus allowing gamabufotalin (CS-6, C) and Dox (D) to accumulate in the tumor tissue. The average diameter of the GOQDs is 5 nm and that of the GTDC@M-R NPs is 70 nm. Fluorescence-activated cell sorter analysis showed that the apoptosis rate in the TNBC cells was up to 89 % using this therapy. Zhang et al. [452] developed g-CNQDs-PEG-RGD nanocarriers by covalently grafting graphitic-C_3N_4 quantum dots (g-CNQDs) to RGD through diamine-terminated oligomeric PEG. By noncovalently loading Dox onto the nanocarriers, therapeutic effects could be realized as well as real-time monitoring (Fig. 42f). Ghafary et al. [453] also used GQDs and miRGD to load Dox and curcumin (as hydrophilic and hydrophobic drug models, respectively) for use in tumor therapy.

In summary, the unique targeting effect of RGD peptide in tumor diagnosis and therapy has become a hot research topic and is most aimed at detecting overexpressed $\alpha_v\beta_3$ rather than $\alpha_5\beta_1$ or $\alpha_\gamma\beta_5$.

10. Other emerging tumor feature

There are three other rising attributes that are particularly compelling. The first includes genomic instability in cancer cells, resulting in the generation of random mutations such as chromosomal rearrangements. Among these are rare genetic alterations that can orchestrate hallmark capabilities. The second is the major reprogramming of the cellular energy metabolism in tumors to enable ongoing cell growth and proliferation. The new programs replace the metabolic programs that present in majority of healthy tissues and supply energy for the physiological functions of related cells. The third relates to the fact that cancer cells actively evade attack and elimination by immune cells. This ability

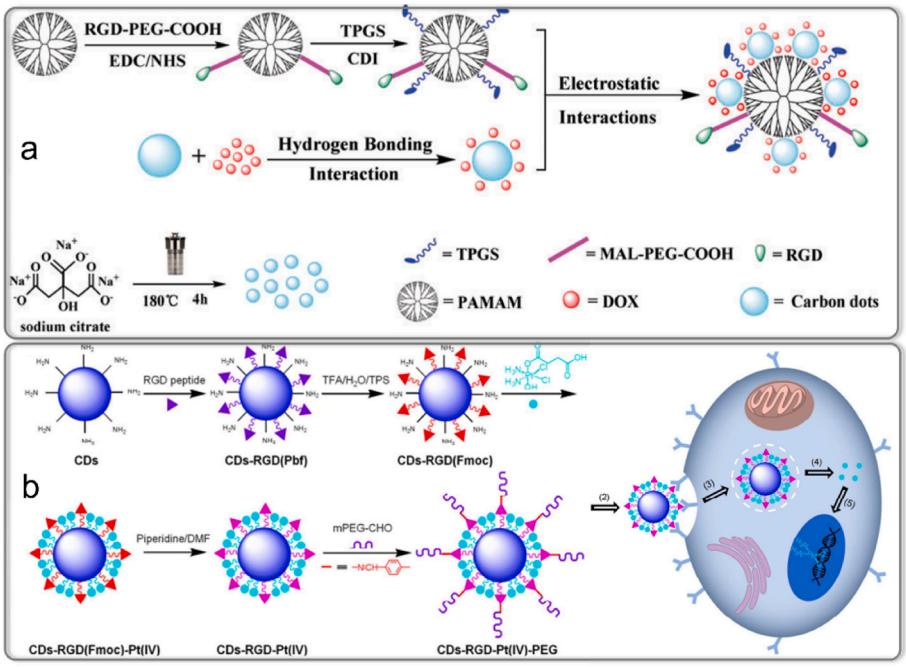

Fig. 40. (b) The development of a dual drug delivery system for precisely delivering medication to cancer cells [444]. Copyright 2019, the Royal Society of Chemistry. (c) The generation of CDs-RGD-Pt(IV)-PEG with its tumor targeting property [445]. Copyright 2016, American Chemical Society. (d) *In vivo* and *ex vivo* images of U87MG tumor-bearing mice injected with RGD-FL-SiO_2 and NH_2-FL-SiO_2 nanoparticles [446]. Copyright 2013, Ivyspring International Publisher.

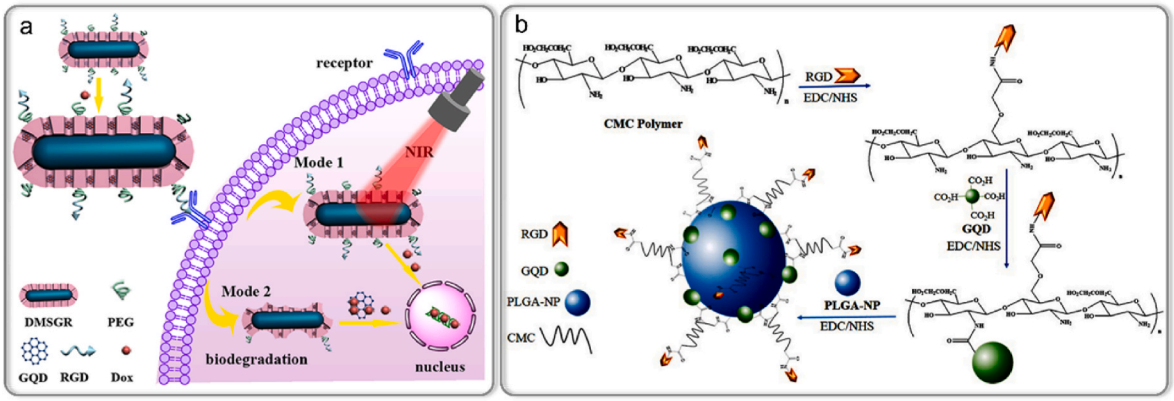

Fig. 41. (a) Dual-mode hierarchical nanocarriers for controlled drug release [447]. Copyright 2017, American Chemical Society. (b) the generation of GQD-CMC-RGD-PLGA-targeted GCRP-NC [448]. Copyright 2022, Elsevier.

emphasizes the immune system's contradictory functions, as it both suppresses and promotes tumor development and progression.

10.1. Genome instability and mutation

Multistep tumor progression can be represented as a collection of clonal expansions that are triggered by the accidental acquisition of an enabling mutant genotype. Some clonal expansions may be driven by non-mutational alterations influencing the management of gene expression since heritable phenotypes, such as the inactivation of tumor suppressor genes, can also be acquired by epigenetic processes (e.g., DNA methylation and histone modification) [454–456]. Genome mutation can be triggered through rendering a cell more susceptible to mutagenic agents, or by producing a malfunction in one or more parts of the genomic maintenance system (or both actions). Additionally, by undermining the surveillance mechanisms that typically maintain genomic integrity and drive genetically damaged cells into senescence or death, the accumulation of mutations can be accelerated [457–459]. In this respect, the role of *TP53* is of paramount importance, leading to it being called the 'guardian of the genome'.

Protein 53 (p53), a tumor suppressor protein encoded in humans by the *TP53* gene, is essential in preventing cancers such as oral and ocular squamous cell carcinoma. The ability to sensitively detect p53 in biological fluids is therefore of great importance in point-of-care diagnostics. Researchers have shown that the therapeutic effects of CDs on tumors can be evaluated by detecting the expression of p53 [22,338,339,460,461]. It has also been shown that p53 can be used as a biomarker to diagnose tumor. Xiao et al. [343] designed a sensitive PL immunoassay technique for detecting p53 in biological fluid that uses CQDs synthesized from grapefruit peel as signal-generating tags. These were then used to label polyclonal anti-p53 antibodies (pAb_2). In the presence of p53, the pAb_2-CQD-SiNP formed 'sandwich' compounds with monoclonal anti-p53 antibodies (mAb_1) coated onto the wells of a microplate (Fig. 43). This strategy allowed the p53 target to be detected with high sensitivity over the range 0.01–50 ng/mL: the LOD was determined to be 2.7 pg/mL.

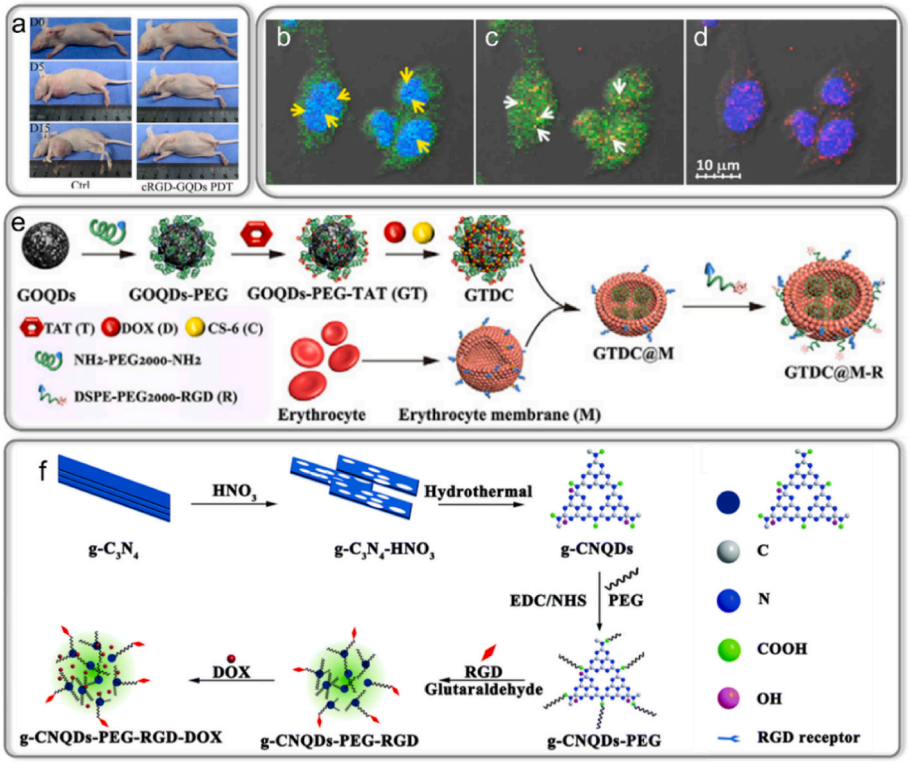

Fig. 42. (a) Photographs of mice after PDT [449]. Copyright 2021, Elsevier Science SA. (b–d) *In vitro* colocalization images of MDA-MB-231 cells transfected with CDP3-RGD [450]. Copyright 2019, Elsevier Science SA. (e) The generation of RGD-modified erythrocyte membrane disguised GTDC@M-R NPs [451]. (Copyright 2020, Elsevier Sci. Ltd. (f) The development of nanocarriers with tumor-targeted drug delivery capability [452]. Copyright 2019, the Royal Society of Chemistry.

10.2. Modulation of metabolic processes

Normal cells convert glucose into pyruvate (through glycolysis in the cytoplasm) and then carbon dioxide (in the mitochondria) when the environment is aerobic, and glycolysis can still take place in anaerobic environments. However, relatively little pyruvate is subsequently dispatched to the oxygen-consuming mitochondria. An anomalous characteristic of cancer cell energy metabolism was first observed by Warburg [462–464]. Warburg found that cancer cells have ability to reprogram their glucose metabolism (and therefore their ability to produce energy) in the presence of oxygen by restricting their energy metabolism primarily to glycolysis, resulting in a condition known as 'aerobic glycolysis' (Fig. 44).

Cancer cells must compensate for the 16-fold lower efficiency of ATP production afforded by glycolysis relative to mitochondria-mediated oxidative phosphorylation. They achieve this in part by up-regulating glucose transporters (GLUTs), notably GLUT1, which significantly boosts glucose importation into the cytoplasm. Recently, an innovative approach for assessing HT-29 cell growth based on glucose consumption was suggested. Moreover, consumption was evaluated in the presence of resveratrol (RSV) in order to evaluate its potential use as an anticancer agent. An enzyme-based sensor for the selective and sensitive voltametric detection of glucose in cancer cells was proposed, which was formed by a hybrid nanocomposite of carbon nanofibers and nitrogen-doped GQDs [465]. The results obtained were compared with those obtained *via* conventional colorimetric assay, and a strong association was emerged between the proliferation rate of the cancer cells and their glucose utilization (Fig. 45a and b). It was also found that the RSV induces a reduction in glucose consumption, demonstrating that the HT-29 cells consume glucose less efficiently in the presence of the drug. Lu et al. [466] synthesized CQDs modified with 2,2,6,6-tetramethyl-piperidinooxy (TEMPO) and glucose for use as GLUT-targeting bimodal MRI/optical imaging contrast agents and used them to detect tumor cells (Fig. 45c).

Due to enhanced glycolysis in cancer cells and proton-pump activity in their plasma membranes, more lactic acid is produced and leaches out, inducing a drop in pH in the environment surrounding the cancer cells [467,468]. For a deeper comprehension of the biological implications of pH gradients, sensitive and focused pH monitoring devices for living cells are consequently crucial. Because of this, many strategies have appeared in which CDs are used to detect pH, including label-free CDs [469–473], nitrogen-doped CDs [474–480], amine-coated CDs [481–488], mesoporous silica-CDs [489–495], and CDs with other materials [496–505].

The diverse nature of the structures of CQDs means that pH may affect the response produced by the CQDs through a variety of mechanisms. A change in pH may, for example, cause a change in the molecular structure of the CQDs, or it might affect their electronic structure. A change in molecular structure could further lead to a change in orientation or distance between a pair of fluorophores serving as donor-acceptor pairs. Similarly, a change in electronic structure could lead to a change in the wavelength or intensity of the fluorescence emitted by the CQDs. Six general paths by which pH may have an effect are shown

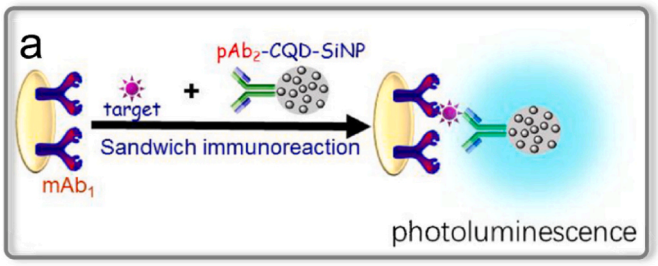

Fig. 43. (a) Schematic illustration of a sandwich-type PL immunoassay technique for targeting p53 protein [343]. Copyright 2018, Elsevier.

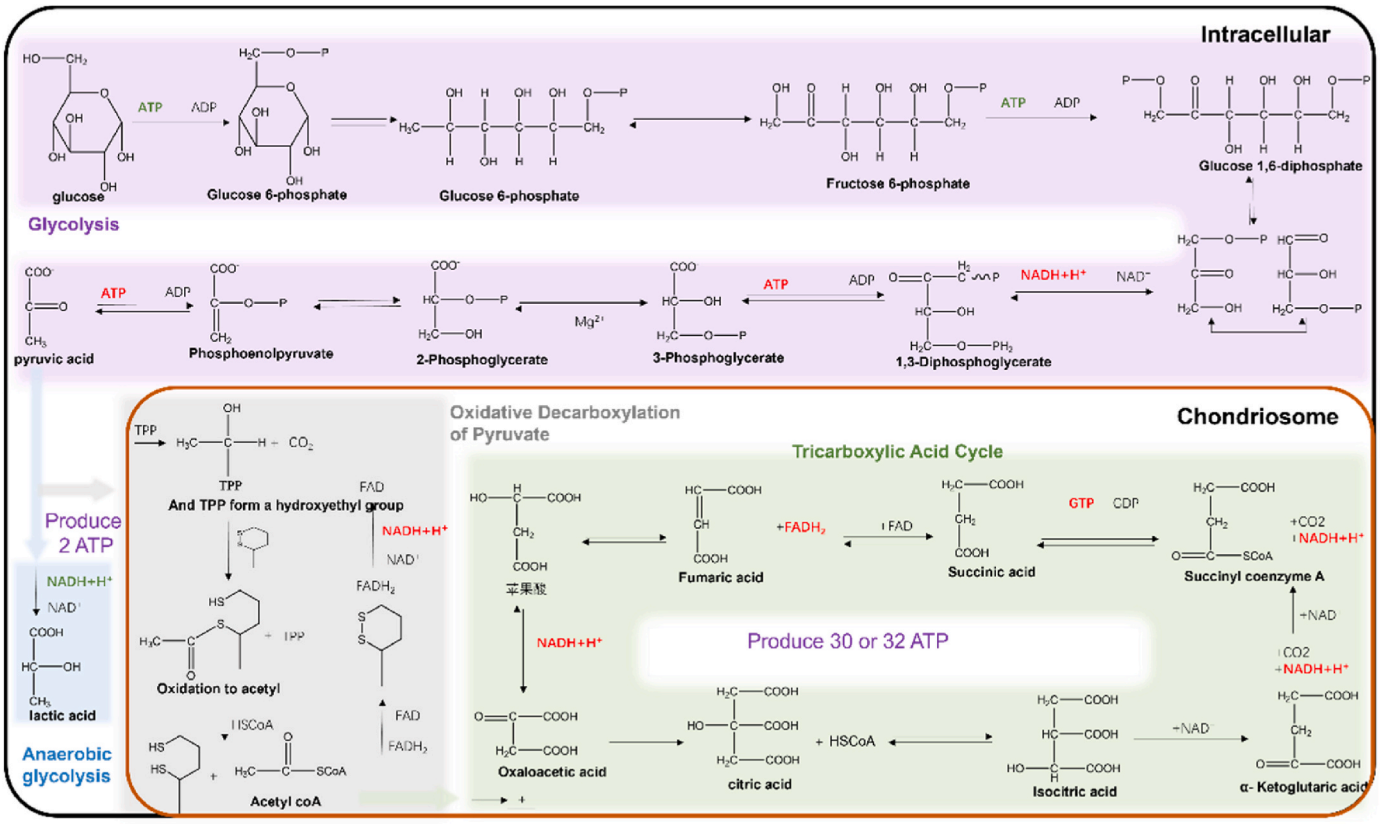

Fig. 44. Schematic representation of the glycolytic pathway.

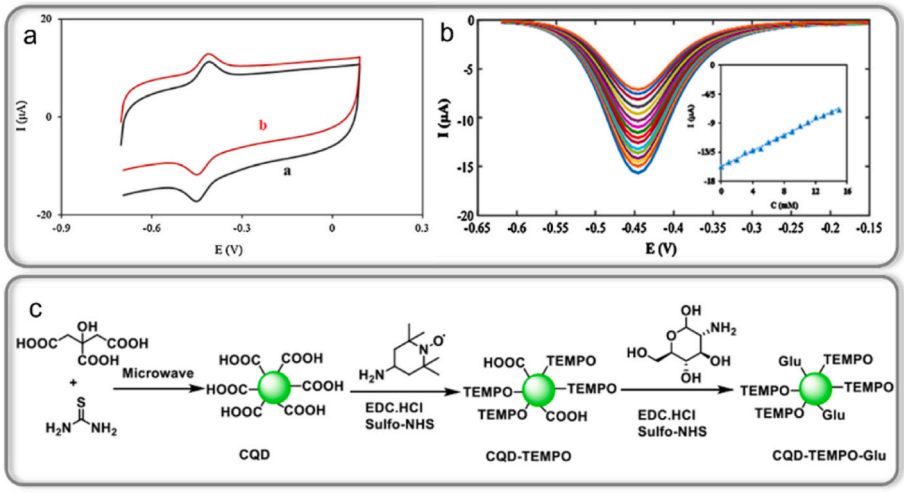

Fig. 45. Cyclic voltammograms of the CNFs-NGQDs-GOx-modified GCE electrode in air-saturated PBS (pH 7.4) in the absence (a) and presence (b) of glucose with the concentration of 2 mM [465]. Copyright 2021, Elsevier Science Inc. (c) Preparation of CQD-TEMPO-Glu [466]. Copyright 2018, Elsevier.

in Fig. 46.

A change in pH can lead to the protonation or deprotonation of functional groups on the surface of the CQDs. This can lead to the formation of delocalized π bonds and increase in n electrons which affects the wavelength of the fluorescence emitted [470,471,501,506,507]. Put briefly, the other 5 mechanisms in Fig. 46 involve: the aggregation or dispersal of CQDs [483,484,508,509]; energy transfer between different elements on the CQDs [505,510]; surface passivation and elimination leading to saturation of functional groups [445,511,512]; energy transfer due to the assembly or separation of aptamers [484,513,514]; occurrence of tautomerism due to the destruction and formation of intramolecular hydrogen-bonds (H-bonds) under the pH change of the solvent surrounding the CQDs (such a change can also alter the wavelength of the fluorescence emission peak) [515,516].

As shown in Fig. 47, a large range in pH have been reported in the literature. However, the majority of the effects involve pH changes in the range 5–7, and this range seems favorable for the diagnosis of tumor and other physiological maladies as this best matches the physiological acidity changes caused by tumor [467,468].

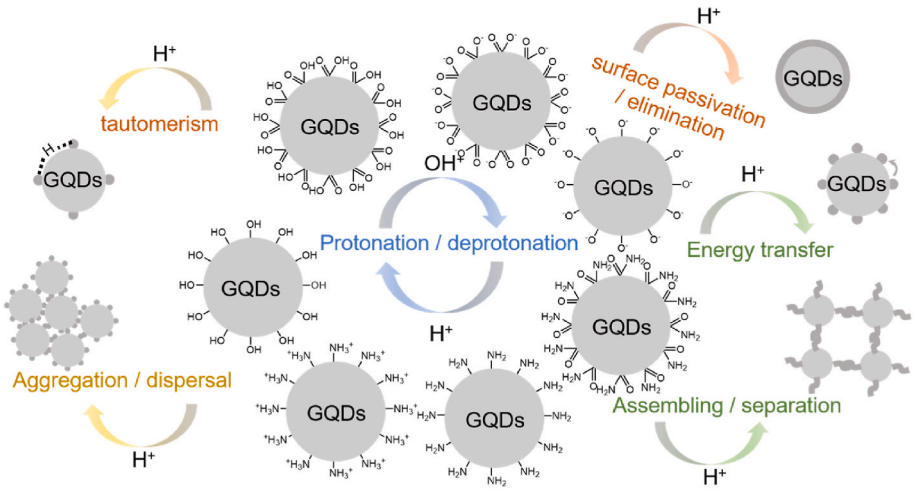

Fig. 46. Schematic diagram showing the classification of pH-based tumor diagnosee methods.

10.3. Evading inflammatory responses and destruction by the immune system

Some tumors are densely infiltrated by immune system cells from both the innate and adaptive arms, mirroring the inflammatory conditions developing in non-neoplastic tissues. It has been found that the inflammatory response induced by tumors has an unanticipated and paradoxical effect: it can accelerate tumorigenesis and progression, assisting incipient neoplasia in establish hallmark capabilities [542–544].

Evaluating the overproduction of intracellular reactive oxygen species (including the superoxide anion, O_2^-, hydrogen peroxide, H_2O_2, and hydroxyl radical, HO•) can be used in tumor diagnosis and several techniques have been devised that take advantage of the unique properties of CQDs (Table 10). Shen et al. [545] fabricated NIR chemiluminescent (CL) CDs for monitoring H_2O_2 and achieved a CL quantum yield of 9.98×10^{-3} E mol^{-1} and a detection limit of 5×10^{-9} M. Peroxalate-modified CDs (P-CDs) were synthesized by integrating the NIR CDs with bis(2,4,5-trichloro-6-carbopentoxyphenyl) oxalate. The functionalized P-CDs are H_2O_2-responsive and can be used as turn-on probes for detecting and imaging H_2O_2 (Fig. 48a and b).

Won et al. [546] developed a stimulus-responsive electrochemical wireless biosensor for use in tumor diagnose. The biosensor was formed by embedding diselenide-containing CDs (dsCDs) in a ureidopyriminone-conjugated gelatin (Gel-UPy) hydrogel. In the presence of ROS or glutathione, the diselenide groups on the dsCDs in the hydrogel are cleaved, initiating the formation of H-bonds (Fig. 48c and d). These H-bonds affect the conductivity and adhesiveness of the Gel-UPy/dsCD hydrogel as well as its ability to self-heal. Cleavage of the diselenide bonds also affects the electrochemical signal from the hydrogel due to the degradation of the dsCDs (Fig. 49e).

Li et al. [547] pyrolyzed a zeolitic imidazolate framework (ZIF-8) filled with glucose to create nanozymes in the form of CDs confined in N-doped carbon (CDs@NC). The CDs@NC nanozymes were found to have peroxidase-like properties and were successfully used to (colorimetrically) detect D-amino acids associated with the early onset of gastric cancer, e.g., D-Proline (D-Pro) and D-Alanine (D-Ala) (Fig. 49a and b). The ability to detect D-Pro and D-Ala sensitively and selectively in clinical saliva samples has enormous potential in early gastric cancer diagnosis and treatment.

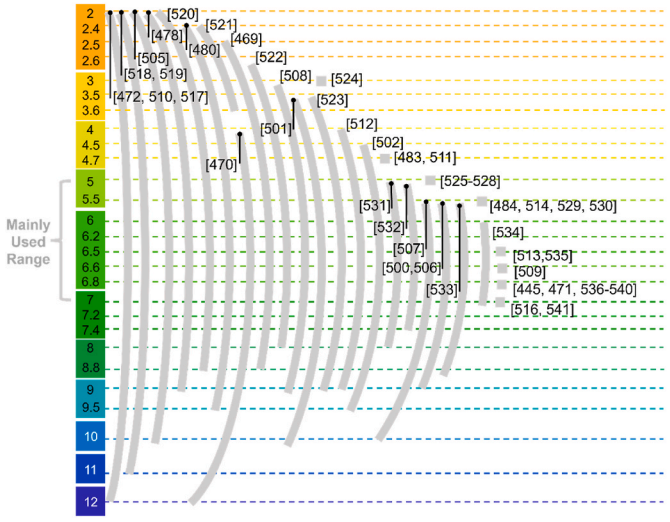

Fig. 47. Cancer diagnosis based on pH detection range. References: [445, 469–472,478,480,483,484,500–502,505–514,516–541].

11. Challenges and perspectives

Although rapid developments have been made, there are still problems to addressed and challenges to conquer.

(i) An unambiguous definition (definition, classification, structure, etc.) of exactly what a CQDs is should be agreed upon by the scientific community in order to have a clear roadmap for future CQDs research. New synthetic routes for developing CQDs with specific structures are urgently needed. Some advanced characterization techniques (e.g., synchrotron-radiation based spectroscopy, neutron scattering spectroscopy, transient absorption spectroscopy, and three-dimensional reconstruction based on cryogenic electron microscopy) may prove helpful when reaching an agreement on the structural definition and classification of CQDs.

(ii) The complete range of physical interactions, which may occur at the interface between a complicated carbon nanostructure and a physiological system, needs to be delineated based on the CQDs definitions as mentioned above. At the same time, this area of research will greatly benefit from the development of new highly efficient tumor diagnostic reagents/microsystems and nanodrugs for tumor therapy. It is worth pointing out that high-throughput screening technology and machine learning have shown remarkable promise in the study of related interaction mechanisms. Furthermore, the artificial intelligence program AlphaFold has shown great promise in predicting protein

Table 10
Recent tumor-diagnostic techniques based on using CDs to detecting ROS.

Materials	Method	λ_{ex} (nm)	λ_{em} (nm)	QY	LOD	LR	Cell line	Ref.
AgNP-DNA@GQDs	Fluorescence spectra.	340	420	17.6 %	0.10 μM	0.4–200 μM	NA	[548]
Hemoglobin-derived Fe^{2+}-containing CDs	Fluorescence imaging; EPR spectra; UV–vis; CD spectra.	230	405	54 %	1 μM	0.4–200 μM	HeLa	[549]
B-PPD CDs	Confocal fluorescence microscopy.	520	606	5.5 %	0.242 mM	3–110 mM Ala	RAW 264.7	[550]
CDs@NC	Steady-state kinetics assays; UV–vis absorption spectra.	NA	NA	NA	7.7 μM for D-Pro; 18.6 μM for D-Ala	20–300 μM for D-Pro; 20–400 μM for D-Ala	NA	[547]
CD-hydrogel	Fluorescence spectra; ^{13}C NMR spectra; FT-IR alkene spectra; Flow cytometry measurements.	488	695	NA	NA	10 and 100 nM	HeLa	[551]
Gel-UPy/dsCD	Resistance change spectra; Electrochemical analysis; *Ex vivo* and *in vivo* imaging.	NA	NA	51.3 %	NA	NA	MDA-MB-231	[546]
C6-8-conjugated CDs	Fluorescence microscopy images; Flow cytometry measurements; Electrophoretic mobility shift assay; *in vitro* and *in vivo* imaging.	378	458	26 %	NA	NA	HeLa	[552]
P-CDs	Photoluminescent and chemiluminescent imaging; *In vivo* CL imaging.	365	642	9.98×10^{-3} E mol^{-1}	5×10^{-9} M	0–100 × 10^{-9} M	HeLa	[545]
NGQD@NC@Pd HNS	CV curves; Amperometric response; Microscope imaging.	NA	NA	2.7 %	20 nM	0–1.4 mM	MDA-MB-231	[553]
C-GQDs	Confocal fluorescence imaging; *In vitro* and *in vivo* imaging.	469	546	12 %	4 nM	0–10 nM	5637, HeLa, HepG2, TPC1, HGC-27, 1590, and ACHN	[554]
Ag@AuNPs-DNA/GQDs	Fluorescence emission spectra; Confocal fluorescence imaging.	520	560	NA	0.49 μM	5–200 μM	MCF-7	[555]
PD(HA/DP)-DiSe	Photoluminescence spectra; Confocal fluorescence imaging; Electrochemical analysis.	NA	NA	50.4 %	9 cells mL^{-1}	10^1–10^6	MDA-MB-231	[556]

NA: not mentioned.

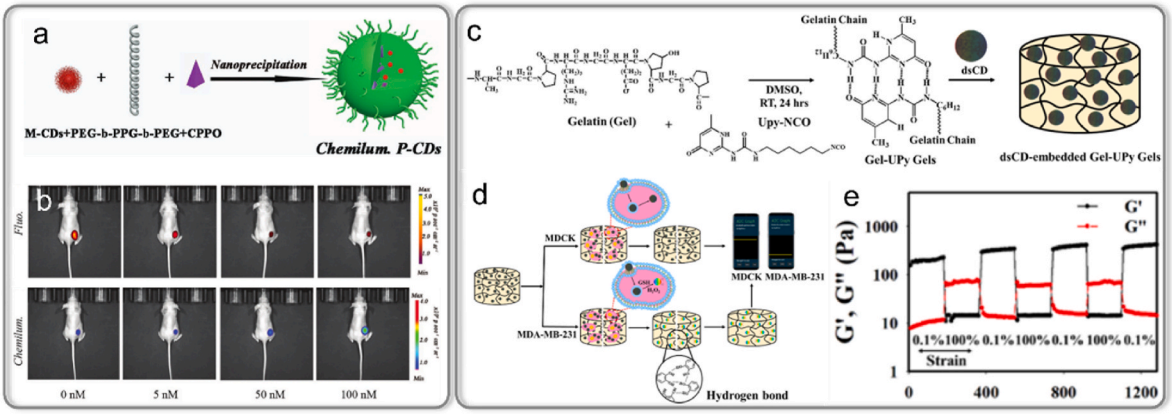

Fig. 48. (a) The preparation of the P-CDs. (b) *In vivo* PL and CL images of mice subcutaneously injected with different concentrations of H_2O_2 [545]. Copyright 2020, American Chemical Society. (c) Chemical structures of Gel-UPy/dsCD hydrogels. (d) Cancer cell reactive self-healing feature of Gel-UPy/dsCD hydrogels (e) Continuous step-strain rheology test performed using MDA-MB-231-treated hydrogel [546]. Copyright 2020, American Chemical Society.

structure and has made some important breakthroughs in recent years. If all of the abovementioned technologies can be effectively combined with appropriate theoretical thermodynamics/kinetics studies, it is very likely that there will be great improvements in our understanding of the interfacial interactions that occur between complex CQDs and various physiological systems.

(iii) The hallmarks of cancer can be used to appreciate the significance of the large number of CQDs-based tumor-diagnostic reagents/microsystems that have been developed. However, highly selective CQDs have not been created for the vast majority of markers (over 95 %, which includes many strongly associated with tumor occurrence). Meanwhile, the design of CQDs that respond to multiple markers remains a challenge. The solution to these problems is to acquire a thorough understanding of the interactions that occur at the interface between the CQDs (with their complicated nanostructures) and the physiological systems involved (which are also complex). Of course, this is the challenge outlined in (ii). However, there is already a diverse range of CQDs-based fluorescent reagents available for tumor diagnosis and treatment, so it is highly likely that the research currently being undertaken on the subcellular mechanisms responsible for tumor development will continue to yield some exciting results.

(iv) CQDs, like other nanomaterials, are faced with the problem that it is not known if their long-term use *in vivo* can lead to toxic effects. This means that the *in vivo* use of CQDs-based contrast agents (including MRI CAs, CT CAs, and tumor-targeting fluorescent reagents) in clinical applications will meet some resistance. On the other hand, their use *in vitro* avoids the problem of undefined

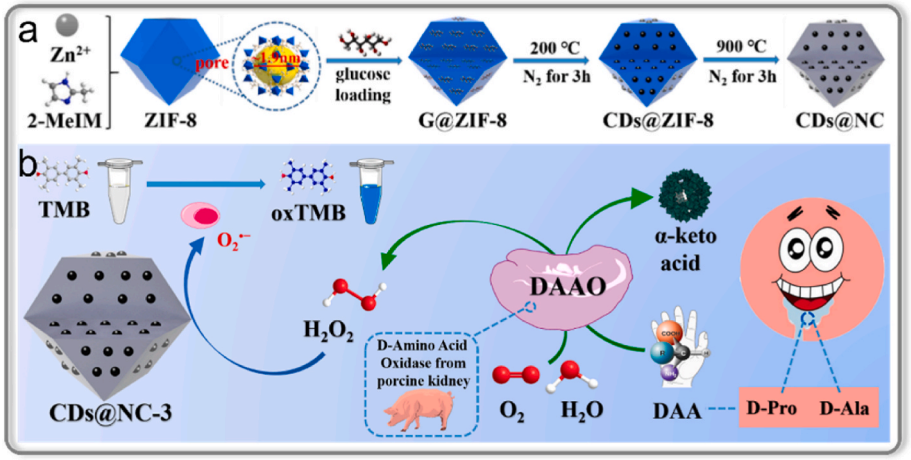

Fig. 49. (a) Synthesis of CDs@NC-3 by two-step generation method with ZIF-8. (b) The detection mechanism of CDs@NC-3 D-Pro and D-Ala [547]. Copyright 2022, Elsevier Science SA.

chronic toxicity *in vivo*. However, even their *in vitro* use with clinical samples can still produce results that are not sufficiently accurate. This may, for example, be because the clinical samples involved (e.g., body fluids or tissue samples) are extremely complex and vary significantly from individual to individual. Moreover, as CQDs are relatively new, industrial methods for their large-scale production are unlikely to be readily available and this limits their widespread application in clinical applications. Thus, their clinical application value needs to be further tapped. (However, the issue of scalability is encountered with virtually all new materials and is not unique to CQDs.)

Based on the above challenges, the potential solutions for the development of tumor diagnosis based on CQDs need: development of detection technologies for complex tumors (such as gliomas); machine learning based structural design of CQDs; breakthroughs in scaled-up, reliable CQDs preparation technology; development of portable, low-cost integrated testing equipment; development of intelligent test result analysis technology based on big data analysis.

In summary, starting from the hallmarks of cancer we have summarized the recent advances made in CQDs-based tumor diagnosis/treatment. There is no doubt that CQDs have contributed much to the progress that has been made in this area of medical research. However, there are still many challenges that need to be overcome if progress is to continue. This review covers tumor diagnosis strategies within the framework of molecular oncology. The clarification of the structure-function relationship of CQDs facilitates the understanding of interfacial interactions of carbon nanostructures, and further impacts on tumor diagnosis. It also goes a long way towards addressing similar problems encountered with other nanomaterials.

Notes

The authors declare no competing financial interests.

Ethics approval and consent to participate

No human or animal experiments were conducted in this review.

Acknowledgments

This work was supported by the Shanghai Science and Technology Committee (grant nos. 21ZR1482800, 23YF1455800), Shanghai Post-doctoral Excellence Program (2022675), and the National Natural Science Foundation of China (grant no. 62174093). S. Yang acknowledge the support from the Youth Innovation Promotion Association of Chinese Academy of Sciences, and the Xinweizhixing Project of SIMIT.

References

[1] S. Zhu, Y. Song, X. Zhao, J. Shao, J. Zhang, B. Yang, The photoluminescence mechanism in carbon dots (graphene quantum dots, carbon nanodots, and polymer dots): current state and future perspective, Nano Res. 8 (2) (2015) 355–381.
[2] X.T. Zheng, A. Ananthanarayanan, K.Q. Luo, P. Chen, Glowing graphene quantum dots and carbon dots: properties, syntheses, and biological applications, Small 11 (14) (2015) 1620–1636.
[3] M.J. Molaei, A review on nanostructured carbon quantum dots and their applications in biotechnology, sensors, and chemiluminescence, Talanta 196 (2019) 456–478.
[4] Y.F. Wang, A.G. Hu, Carbon quantum dots: synthesis, properties and applications, J. Mater. Chem. C 2 (34) (2014) 6921–6939.
[5] M. Moniruzzaman, S.D. Dutta, J. Hexiu, K. Ganguly, K.-T. Lim, J. Kim, Polyphenol derived bioactive carbon quantum dot-incorporated multifunctional hydrogels as an oxidative stress attenuator for antiaging and in vivo wound-healing applications, Biomater. Sci. 10 (13) (2022) 3527–3539.
[6] M. Moniruzzaman, S.D. Dutta, K.-T. Lim, J. Kim, Wet chemistry-based processing of tunable polychromatic carbon quantum dots for multicolor bioimaging and enhanced NIR-triggered photothermal bactericidal efficacy, Appl. Surf. Sci. 597 (2022).
[7] S.D. Dutta, K. Ganguly, J. Hexiu, A. Randhawa, M. Moniruzzaman, K.-T. Lim, A 3D bioprinted nanoengineered hydrogel with photoactivated drug delivery for tumor apoptosis and simultaneous bone regeneration via macrophage immunomodulation, Macromol. Biosci. (2023).
[8] M. Zheng, S.B. Ruan, S. Liu, T.T. Sun, D. Qu, H.F. Zhao, Z.G. Xie, H.L. Gao, X. B. Jing, Z.C. Sun, Self-targeting fluorescent carbon dots for diagnosis of brain cancer cells, ACS Nano 9 (11) (2015) 11455–11461.
[9] F.L. Yuan, S.H. Li, Z.T. Fan, X.Y. Meng, L.Z. Fan, S.H. Yang, Shining carbon dots: synthesis and biomedical and optoelectronic applications, Nano Today 11 (5) (2016) 565–586.
[10] C.Y. Ji, Y.Q. Zhou, R.M. Leblanc, Z.L. Peng, Recent developments of carbon dots in biosensing: a review, ACS Sens. 5 (9) (2020) 2724–2741.
[11] Y.J. Li, S.H. Wu, J.J. Zhang, R.H. Zhou, X.X. Cai, Sulphur doped carbon dots enhance photodynamic therapy via PI3K/Akt signalling pathway, Cell Prolif. 53 (5) (2020).
[12] X.L. Huang, F. Zhang, L. Zhu, K.Y. Choi, N. Guo, J.X. Guo, K. Tackett, P. Anilkumar, G. Liu, Q.M. Quan, H.S. Choi, G. Niu, Y.P. Sun, S. Lee, X.Y. Chen, Effect of injection routes on the biodistribution, clearance, and tumor uptake of carbon dots, ACS Nano 7 (7) (2013) 5684–5693.
[13] S. Havanur, I. Batish, S.P. Cheruku, K. Gourishetti, P.E. JagadeeshBabu, N. Kumar, Poly(N,N-diethyl acrylamide)/functionalized graphene quantum dots hydrogels loaded with doxorubicin as a nano-drug carrier for metastatic lung cancer in mice, Mat Sci Eng C-Mater 105 (2019).
[14] X.A. Miao, X.L. Yan, D. Qu, D.B. Li, F.F. Tao, Z.C. Sun, Red emissive sulfur, nitrogen codoped carbon dots and their application in ion detection and theraonostics, Acs Appl. Mater. Inter. 9 (22) (2017) 18549–18556.
[15] S.D. Dutta, H. Jin, J. Kim, S. Sarkar, J. Mondal, J.M. An, Y.-k. Lee, M. Moniruzzaman, K.-T. Lim, Two-photon excitable membrane targeting polyphenolic carbon dots for long-term imaging and pH-responsive chemotherapeutic drug delivery for synergistic tumor therapy, Biomater. Sci. 10 (7) (2022) 1680–1696.
[16] Q.Y. Jia, J.C. Ge, W.M. Liu, X.L. Zheng, S.Q. Chen, Y.M. Wen, H.Y. Zhang, P. F. Wang, A magnetofluorescent carbon dot assembly as an acidic H2O2-driven

oxygenerator to regulate tumor hypoxia for simultaneous bimodal imaging and enhanced photodynamic therapy, Adv. Mater. 30 (13) (2018).
[17] Z.M. Markovic, B.Z. Ristic, K.M. Arsikin, D.G. Klisic, L.M. Harhaji-Trajkovic, B. M. Todorovic-Markovic, D.P. Kepic, T.K. Kravic-Stevovic, S.P. Jovanovic, M. M. Milenkovic, D.D. Milivojevic, V.Z. Bumbasirevic, M.D. Dramicanin, V. S. Trajkovic, Graphene quantum dots as autophagy-inducing photodynamic agents, Biomaterials 33 (29) (2012) 7084–7092.
[18] H.Y. Fan, X.H. Yu, K. Wang, Y.J. Yin, Y.J. Tang, Y.L. Tang, X.H. Liang, Graphene quantum dots (GQDs)-based nanomaterials for improving photodynamic therapy in cancer treatment, Eur. J. Med. Chem. 182 (2019).
[19] J.P. Li, S.W. Yang, Y. Deng, P.W. Chai, Y.C. Yang, X.Y. He, X.M. Xie, Z.H. Kang, G. Q. Ding, H.F. Zhou, X.Q. Fan, Emancipating target-functionalized carbon dots from autophagy vesicles for a novel visualized tumor therapy, Adv. Funct. Mater. 28 (30) (2018).
[20] H. He, D. Liu, Z.Z. Feng, A.J. Guo, L.H. Liu, X.L. Chen, Antifade carbon dots on a plasmonic substrate for enhanced protein detection in immunotherapy, ACS Sens. 5 (12) (2020) 4027–4034.
[21] Y. Lyu, Y. Fang, Q.Q. Miao, X. Zhen, D. Ding, K.Y. Pu, Intraparticle molecular orbital engineering of semiconducting polymer nanoparticles as amplified theranostics for in vivo photoacoustic imaging and photothermal therapy, ACS Nano 10 (4) (2016) 4472–4481.
[22] S.W. Yang, X.L. Wang, P. He, A.L. Xu, G. Wang, J.L. Duan, Y.Q. Shi, G.Q. Ding, Graphene quantum dots with pyrrole N and pyridine N: superior reactive oxygen species generation efficiency for metal-free sonodynamic tumor therapy, Small 17 (10) (2021).
[23] B.J. Geng, S. Xu, P. Li, X.K. Li, F.L. Fang, D.Y. Pan, L.X. Shen, Platinum crosslinked carbon dot@TiO2-x p-n junctions for relapse-free sonodynamic tumor eradication via high-yield ROS and GSH depletion, Small 18 (6) (2022).
[24] S. Yang, Y. Li, L. Chen, H. Wang, L. Shang, P. He, H. Dong, G. Wang, G. Ding, Fabrication of carbon-based quantum dots via a "Bottom-Up" approach: topology, chirality, and free radical processes in "building blocks", Small (2023), e2205957.
[25] A. Xu, G. Wang, Y. Li, H. Dong, S. Yang, P. He, G. Ding, Carbon-based quantum dots with solid-state photoluminescent: mechanism, implementation, and application, Small 16 (48) (2020).
[26] S. Yang, Y. Li, L. Chen, H. Wang, L. Shang, P. He, H. Dong, G. Wang, G. Ding, Fabrication of carbon-based quantum dots via a "Bottom-Up" approach: topology, chirality, and free radical processes in "building blocks", Small 19 (31) (2023).
[27] W. Su, H. Wu, H.M. Xu, Y. Zhang, Y.C. Li, X.H. Li, L.N. Fan, Carbon dots: a booming material for biomedical applications, Mater. Chem. Front. 4 (3) (2020) 821–836.
[28] D. Iannazzo, I. Ziccarelli, A. Pistone, Graphene quantum dots: multifunctional nanoplatforms for anticancer therapy, J. Mater. Chem. B 5 (32) (2017) 6471–6489.
[29] S. Chung, R.A. Revia, M.Q. Zhang, Graphene quantum dots and their applications in bioimaging, biosensing, and therapy, Adv. Mater. 33 (22) (2021).
[30] D. Hanahan, Hallmarks of cancer: new dimensions, Cancer Discov. 12 (1) (2022) 31–46.
[31] D. Hanahan, R.A. Weinberg, The hallmarks of cancer, Cell 100 (1) (2000) 57–70.
[32] D. Hanahan, R.A. Weinberg, Hallmarks of cancer: the next generation, Cell 144 (5) (2011) 646–674.
[33] S. Anwar, H. Ding, M. Xu, X. Hu, Z. Li, J. Wang, L. Liu, L. Jiang, D. Wang, C. Dong, M. Yan, Q. Wang, H. Bi, Recent advances in synthesis, optical properties, and biomedical applications of carbon dots, ACS Appl. Bio Mater. 2 (6) (2019) 2317–2338.
[34] Y. Huang, L. Li, D.H. Zhang, L.P. Gan, P. Zhao, Y.F. Zhang, Q. Zhang, M.Q. Hua, C. M. Jia, Gadolinium-doped carbon quantum dots loaded magnetite nanoparticles as a bimodal nanoprobe for both fluorescence and magnetic resonance imaging, Magn. Reson. Imag. 68 (2020) 113–120.
[35] L.L. Li, G.H. Wu, G.H. Yang, J. Peng, J.W. Zhao, J.J. Zhu, Focusing on luminescent graphene quantum dots: current status and future perspectives, Nanoscale 5 (10) (2013) 4015–4039.
[36] M.S. Dresselhaus, M. Terrones, Carbon-based nanomaterials from a historical perspective, Proc. IEEE 101 (7) (2013) 1522–1535.
[37] H.W. Kroto, J.R. Heath, S.C. Obrien, R.F. Curl, R.E. Smalley, C-60 - buckminsterfullerene, Nature 318 (6042) (1985) 162–163.
[38] S. Iijima, Helical microtubules of graphitic carbon, Nature 354 (6348) (1991) 56–58.
[39] S. Iijima, T. Ichihashi, SINGLE-SHELL carbon nanotubes of 1-NM diameter, Nature 363 (6430) (1993) 603–605.
[40] V.L. Kuznetsov, A.L. Chuvilin, Y.V. Butenko, I.Y. Malkov, V.M. Titov, ONION-LIKE carbon from ultra-disperse diamond, Chem. Phys. Lett. 222 (4) (1994) 343–348.
[41] S. Iijima, M. Yudasaka, R. Yamada, S. Bandow, K. Suenaga, F. Kokai, K. Takahashi, Nano-aggregates of single-walled graphitic carbon nano-horns, Chem. Phys. Lett. 309 (3–4) (1999) 165–170.
[42] V.V. Danilenko, On the history of the discovery of nanodiamond synthesis, Phys. Solid State 46 (4) (2004) 595–599.
[43] H.W. Kroto, J.R. Heath, S.C. O'Brien, R.F. Curl, R.E. Smalley, C60: buckminsterfullerene, Nature 318 (6042) (1985) 162–163.
[44] R.L. Liu, D.Q. Wu, S.H. Liu, K. Koynov, W. Knoll, Q. Li, An aqueous route to multicolor photoluminescent carbon dots using silica spheres as carriers, Angew. Chem., Int. Ed. 48 (25) (2009) 4598–4601.
[45] J. Geys, A. Nemmar, E. Verbeken, E. Smolders, M. Ratoi, M.F. Hoylaerts, B. Nemery, P.H.M. Hoet, Acute toxicity and prothrombotic effects of quantum dots: impact of surface charge, Environ. Health Perspect. 116 (12) (2008) 1607–1613.
[46] S.W. Yang, W. Li, C.C. Ye, G. Wang, H. Tian, C. Zhu, P. He, G.Q. Ding, X.M. Xie, Y. Liu, Y. Lifshitz, S.T. Lee, Z.H. Kang, M.H. Jiang, C3N-A 2D crystalline, hole-free, tunable-narrow-bandgap semiconductor with ferromagnetic properties, Adv. Mater. 29 (16) (2017).
[47] X. Xu, R. Ray, Y. Gu, H. Ploehn, L. Gearheart, K. Raker, W. Scrivens, CDs were prepared from single-walled carbon nanotubes (SWCNTs) using arc-discharge soot by electrophoresis, J. Am. Chem. Soc. 126 (2004), 12736.
[48] X. Yan, X. Cui, B.S. Li, L.S. Li, Large, solution-processable graphene quantum dots as light absorbers for photovoltaics, Nano Lett. 10 (5) (2010) 1869–1873.
[49] K. Nekoueian, M. Amiri, M. Sillanpaa, F. Marken, R. Boukherroub, S. Szunerits, Carbon-based quantum particles: an electroanalytical and biomedical perspective, Chem. Soc. Rev. 48 (15) (2019) 4281–4316.
[50] Z.F. An, C. Zheng, Y. Tao, R.F. Chen, H.F. Shi, T. Chen, Z.X. Wang, H.H. Li, R. R. Deng, X.G. Liu, W. Huang, Stabilizing triplet excited states for ultralong organic phosphorescence, Nat. Mater. 14 (7) (2015) 685–690.
[51] L.C. Bement, A.S. Madden, B.J. Carter, A.R. Simms, A.L. Swindle, H.M. Alexander, S. Fine, M. Benamara, Quantifying the distribution of nanodiamonds in pre-Younger Dryas to recent age deposits along Bull Creek, Oklahoma Panhandle, USA, Proc. Natl. Acad. Sci. U. S. A. 111 (5) (2014) 1726–1731.
[52] S.W. Yang, J. Sun, X.B. Li, W. Zhou, Z.Y. Wang, P. He, G.Q. Ding, X.M. Xie, Z. H. Kang, M.H. Jiang, Large-scale fabrication of heavy doped carbon quantum dots with tunable-photoluminescence and sensitive fluorescence detection, J. Mater. Chem. A 2 (23) (2014) 8660–8667.
[53] J. Sun, S.W. Yang, Z.Y. Wang, H. Shen, T. Xu, L.T. Sun, H. Li, W.W. Chen, X. Y. Jiang, G.Q. Ding, Z.H. Kang, X.M. Xie, M.H. Jiang, Ultra-high quantum yield of graphene quantum dots: aromatic-nitrogen doping and photoluminescence mechanism, Part. Part. Syst. Char. 32 (4) (2015) 434–440.
[54] E.T. Thostenson, Z.F. Ren, T.W. Chou, Advances in the science and technology of carbon nanotubes and their composites: a review, Compos. Sci. Technol. 61 (13) (2001) 1899–1912.
[55] J.I. Tapia, E. Larios, C. Bittencourt, M.J. Yacaman, M. Quintana, Carbon nano-allotropes produced by ultrasonication of few-layer graphene and fullerene, Carbon 99 (2016) 541–546.
[56] S.W. Zhang, J.X. Li, M.Y. Zeng, J.Z. Xu, X.K. Wang, W.P. Hu, 撤稿声明: polymer nanodots of graphitic carbon nitride as effective fluorescent probes for the detection of Fe3+ and Cu2+ ions (Retraction of Vol 6, Pg 4157, 2014), Nanoscale 13 (36) (2021), 15481-15481.
[57] M.X. Li, T. Chen, J.J. Gooding, J.Q. Liu, Review of carbon and graphene quantum dots for sensing, ACS Sens. 4 (7) (2019) 1732–1748.
[58] P. Namdari, B. Negahdari, A. Eatemadi, Synthesis, properties and biomedical applications of carbon-based quantum dots: an updated review, Biomed. Pharmacother. 87 (2017) 209–222.
[59] P.J.G. Luo, F. Yang, S.T. Yang, S.K. Sonkar, L.J. Yang, J.J. Broglie, Y. Liu, Y. P. Sun, Carbon-based quantum dots for fluorescence imaging of cells and tissues, RSC Adv. 4 (21) (2014) 10791–10807.
[60] D. Yoo, Y. Park, B. Cheon, M.H. Park, Carbon dots as an effective fluorescent sensing platform for metal ion detection, Nanoscale Res. Lett. 14 (1) (2019).
[61] X. Yan, X. Cui, L.S. Li, Synthesis of large, stable colloidal graphene quantum dots with tunable size, J. Am. Chem. Soc. 132 (17) (2010) 5944. -+.
[62] Y. Yan, J. Gong, J. Chen, Z. Zeng, W. Huang, K. Pu, J. Liu, P. Chen, Recent advances on graphene quantum dots: from chemistry and physics to applications, Adv. Mater. 31 (21) (2019).
[63] V.C. Hoang, K. Dave, V.G. Gomes, Carbon quantum dot-based composites for energy storage and electrocatalysis: mechanism, applications and future prospects, Nano Energy 66 (2019).
[64] S. Liu, J.Q. Tian, L. Wang, Y.W. Zhang, X.Y. Qin, Y.L. Luo, A.M. Asiri, A.O. Al-Youbi, X.P. Sun, Hydrothermal treatment of grass: a low-cost, green route to nitrogen-doped, carbon-rich, photoluminescent polymer nanodots as an effective fluorescent sensing platform for label-free detection of Cu(II) ions, Adv. Mater. 24 (15) (2012) 2037–2041.
[65] S.J. Zhu, Y.B. Song, X.H. Zhao, J.R. Shao, J.H. Zhang, B. Yang, The photoluminescence mechanism in carbon dots (graphene quantum dots, carbon nanodots, and polymer dots): current state and future perspective, Nano Res. 8 (2) (2015) 355–381.
[66] Y.B. Song, S.J. Zhu, J.R. Shao, B. Yang, Polymer carbon dots-A highlight reviewing their unique structure, bright emission and probable photoluminescence mechanism, J. Polym. Sci., Part A: Polym. Chem. 55 (4) (2017) 610–615.
[67] Y.B. Song, S.J. Zhu, B. Yang, Bioimaging based on fluorescent carbon dots, RSC Adv. 4 (52) (2014) 27184–27200.
[68] Y. Li, Z. Shi, L. Shang, Q. Tao, Q. Tang, H.-J. Krause, S. Yang, G. Ding, H. Dong, Graphene quantum dots-based magnetic relaxation switch involving magnetic separation for enhanced performances of endoglin detection using ultra-low-field nuclear magnetic resonance relaxometry, Sensor. Actuator. B Chem. 380 (2023).
[69] Z.H. Kang, S.T. Lee, Carbon dots: advances in nanocarbon applications, Nanoscale 11 (41) (2019) 19214–19224.
[70] Z. Ma, H. Ming, H. Huang, Y. Liu, Z.H. Kang, One-step ultrasonic synthesis of fluorescent N-doped carbon dots from glucose and their visible-light sensitive photocatalytic ability, New J. Chem. 36 (4) (2012) 861–864.
[71] F. Li, Y.Y. Li, X. Yang, X.X. Han, Y. Jiao, T.T. Wei, D.Y. Yang, H.P. Xu, G.J. Nie, Highly fluorescent chiral N-S-doped carbon dots from cysteine: affecting cellular energy metabolism, Angew. Chem., Int. Ed. 57 (9) (2018) 2377–2382.
[72] F. Li, T.Y. Li, C.X. Sun, J.H. Xia, Y. Jiao, H.P. Xu, Selenium-doped carbon quantum dots for free-radical scavenging, Angew. Chem., Int. Ed. 56 (33) (2017) 9910–9914.

[73] X.C. Yuan, Z.M. Liu, Z.Y. Guo, Y.H. Ji, M. Jin, X.P. Wang, Cellular distribution and cytotoxicity of graphene quantum dots with different functional groups, Nanoscale Res. Lett. 9 (2014).
[74] M.J. Sweetman, S.M. Hickey, D.A. Brooks, J.D. Hayball, S.E. Plush, A practical guide to prepare and synthetically modify graphene quantum dots, Adv. Funct. Mater. 29 (14) (2019).
[75] X. Hai, J. Feng, X.W. Chen, J.H. Wang, Tuning the optical properties of graphene quantum dots for biosensing and bioimaging, J. Mater. Chem. B 6 (20) (2018) 3219–3234.
[76] M.A. Sk, A. Ananthanarayanan, L. Huang, K.H. Lim, P. Chen, Revealing the tunable photoluminescence properties of graphene quantum dots, J. Mater. Chem. C 2 (34) (2014) 6954–6960.
[77] Y.F. Shen, Y. Liang, Y.P. Wang, C.L. Liu, X.Y. Ren, A comparative study on impact factors of emission: surface state, carbonaceous core, and size based on series of exactly designed P, S co-doped carbon dots, J. Nanoparticle Res. 20 (9) (2018).
[78] H. Ding, S.B. Yu, J.S. Wei, H.M. Xiong, Full-color light-emitting carbon dots with a surface-state-controlled luminescence mechanism, ACS Nano 10 (1) (2016) 484–491.
[79] Y.Q. Dong, J.W. Shao, C.Q. Chen, H. Li, R.X. Wang, Y.W. Chi, X.M. Lin, G. N. Chen, Blue luminescent graphene quantum dots and graphene oxide prepared by tuning the carbonization degree of citric acid, Carbon 50 (12) (2012) 4738–4743.
[80] F.L. Yuan, T. Yuan, L.Z. Sui, Z.B. Wang, Z.F. Xi, Y.C. Li, X.H. Li, L.Z. Fan, Z.A. Tan, A.M. Chen, M.X. Jin, S.H. Yang, Engineering triangular carbon quantum dots with unprecedented narrow bandwidth emission for multicolored LEDs, Nat. Commun. 9 (2018).
[81] Y.H. Chen, M.T. Zheng, Y. Xiao, H.W. Dong, H.R. Zhang, J.L. Zhuang, H. Hu, B. F. Lei, Y.L. Liu, A self-quenching-resistant carbon-dot powder with tunable solid-state fluorescence and construction of dual-fluorescence morphologies for white light-emission, Adv. Mater. 28 (2) (2016) 312–318.
[82] K. Jiang, Y.H. Wang, C.Z. Cai, H.W. Lin, Conversion of carbon dots from fluorescence to ultralong room-temperature phosphorescence by heating for security applications, Adv. Mater. 30 (26) (2018).
[83] H. Gonçalves, P.A.S. Jorge, J.R.A. Fernandes, J.C.G. Esteves da Silva, Hg(II) sensing based on functionalized carbon dots obtained by direct laser ablation, Sensor. Actuator. B Chem. 145 (2) (2010) 702–707.
[84] L. Liu, Y. Li, L. Zhan, Y. Liu, C. Huang, One-step synthesis of fluorescent hydroxyls-coated carbon dots with hydrothermal reaction and its application to optical sensing of metal ions, Sci. China Chem. 54 (8) (2011) 1342–1347.
[85] Y. Liu, C.-y. Liu, Z.-y. Zhang, Synthesis of highly luminescent graphitized carbon dots and the application in the Hg2+ detection, Appl. Surf. Sci. 263 (2012) 481–485.
[86] J.J. Liu, X.L. Zhang, Z.X. Cong, Z.T. Chen, H.H. Yang, G.N. Chen, Glutathione-functionalized graphene quantum dots as selective fluorescent probes for phosphate-containing metabolites, Nanoscale 5 (5) (2013) 1810–1815.
[87] Z. Qian, X. Shan, L. Chai, J. Ma, J. Chen, H. Feng, Si-doped carbon quantum dots: a facile and general preparation strategy, bioimaging application, and multifunctional sensor, ACS Appl. Mater. Interfaces 6 (9) (2014) 6797–6805.
[88] M.L. Bhaisare, A. Talib, M.S. Khan, S. Pandey, H.-F. Wu, Synthesis of fluorescent carbon dots via microwave carbonization of citric acid in presence of tetraoctylammonium ion, and their application to cellular bioimaging, Microchim. Acta 182 (13–14) (2015) 2173–2181.
[89] G. Oza, M. Ravichandran, V.I. Merupo, S. Shinde, A. Mewada, J.T. Ramirez, S. Velumani, M. Sharon, M. Sharon, Camphor-mediated synthesis of carbon nanoparticles, graphitic shell encapsulated carbon nanocubes and carbon dots for bioimaging, Sci. Rep. 6 (2016), 21286.
[90] R. Hu, L. Li, W.J. Jin, Controlling speciation of nitrogen in nitrogen-doped carbon dots by ferric ion catalysis for enhancing fluorescence, Carbon 111 (2017) 133–141.
[91] M.L. Mueller, X. Yan, J.A. McGuire, L.S. Li, Triplet States and electronic relaxation in photoexcited graphene quantum dots, Nano Lett. 10 (7) (2010) 2679–2682.
[92] Q. Wang, H. Zheng, Y. Long, L. Zhang, M. Gao, W. Bai, Microwave–hydrothermal synthesis of fluorescent carbon dots from graphite oxide, Carbon 49 (9) (2011) 3134–3140.
[93] X. Wu, F. Tian, W.X. Wang, J. Chen, M. Wu, J.X. Zhao, Fabrication of highly fluorescent graphene quantum dots using L-glutamic acid for in vitro/in vivo imaging and sensing, J. Mater. Chem. C 1 (31) (2013) 4676–4684.
[94] C.P. Chen, Y.C. Huang, S.Y. Liou, P.J. Wu, S.Y. Kuo, Y.H. Chan, Near-infrared fluorescent semiconducting polymer dots with high brightness and pronounced effect of positioning alkyl chains on the comonomers, ACS Appl. Mater. Interfaces 6 (23) (2014) 21585–21595.
[95] Y. Zhao, X. Liu, Y. Yang, L. Kang, Z. Yang, W. Liu, L. Chen, Carbon dots: from intense absorption in visible range to excitation-independent and excitation-dependent photoluminescence, Fullerenes, Nanotub. Carbon Nanostruct. 23 (11) (2015) 922–929.
[96] D. Chen, I.C. Wu, Z. Liu, Y. Tang, H. Chen, J. Yu, C. Wu, D.T. Chiu, Semiconducting polymer dots with bright narrow-band emission at 800 nm for biological applications, Chem. Sci. 8 (5) (2017) 3390–3398.
[97] Y. Xiu, Q. Gao, G.D. Li, K.X. Wang, J.S. Chen, Preparation and tunable photoluminescence of carbogenic nanoparticles confined in a microporous magnesium-aluminophosphate, Inorg. Chem. 49 (13) (2010) 5859–5867.
[98] P. Anilkumar, X. Wang, L. Cao, S. Sahu, J.H. Liu, P. Wang, K. Korch, K. N. Tackett 2nd, A. Parenzan, Y.P. Sun, Toward quantitatively fluorescent carbon-based "quantum" dots, Nanoscale 3 (5) (2011) 2023–2027.
[99] W. Kwon, S.W. Rhee, Facile synthesis of graphitic carbon quantum dots with size tunability and uniformity using reverse micelles, Chem. Commun. 48 (43) (2012) 5256–5258.
[100] D. Qu, M. Zheng, P. Du, Y. Zhou, L. Zhang, D. Li, H. Tan, Z. Zhao, Z. Xie, Z. Sun, Highly luminescent S, N co-doped graphene quantum dots with broad visible absorption bands for visible light photocatalysts, Nanoscale 5 (24) (2013) 12272–12277.
[101] F. Li, C. Liu, J. Yang, Z. Wang, W. Liu, F. Tian, Mg/N double doping strategy to fabricate extremely high luminescent carbon dots for bioimaging, RSC Adv. 4 (7) (2014) 3201–3205.
[102] Z. Xie, Q. Du, Y. Wu, X. Hao, C. Liu, Full-band UV shielding and highly daylight luminescent silane-functionalized graphene quantum dot nanofluids and their arbitrary polymerized hybrid gel glasses, J. Mater. Chem. C 4 (41) (2016) 9879–9886.
[103] W. Xuan, L. Ruiyi, F. Saiying, L. Zaijun, W. Guangli, G. Zhiguo, L. Junkang, D-penicillamine-functionalized graphene quantum dots for fluorescent detection of Fe3+ in iron supplement oral liquids, Sensor. Actuator. B Chem. 243 (2017) 211–220.
[104] J. Liu, Y. Liu, N.Y. Liu, Y.Z. Han, X. Zhang, H. Huang, Y. Lifshitz, S.T. Lee, J. Zhong, Z.H. Kang, Metal-free efficient photocatalyst for stable visible water splitting via a two-electron pathway, Science 347 (6225) (2015) 970–974.
[105] H. Huang, S. Yang, Y. Liu, Y. Yang, H. Li, J.A. McLeod, G. Ding, J. Huang, Z. Kang, Photocatalytic polymerization from amino acid to protein by carbon dots at room temperature, ACS Appl. Bio Mater. 2 (11) (2019) 5144–5153.
[106] B.P. Jiang, B. Zhou, Z.X. Lin, H. Liang, X.C. Shen, Recent advances in carbon nanomaterials for cancer phototherapy, Chem. Eur J. 25 (16) (2019) 3993–4004.
[107] B. Zhou, Z.X. Guo, Z.X. Lin, L.Z. Zhang, B.P. Jiang, X.C. Shen, Recent insights into near-infrared light-responsive carbon dots for bioimaging and cancer phototherapy, Inorg. Chem. Front. 6 (5) (2019) 1116–1128.
[108] K. Ghosal, A. Ghosh, Carbon dots: the next generation platform for biomedical applications, Mat Sci Eng C-Mater 96 (2019) 887–903.
[109] Q.Y. Jia, Z.Y. Zhao, K. Liang, F.C. Nan, Y. Li, J. Wang, J.C. Ge, P.F. Wang, Recent advances and prospects of carbon dots in cancer nanotheranostics, Mater. Chem. Front. 4 (2) (2020) 449–471.
[110] S. Yang, X. Wang, P. He, A. Xu, G. Wang, J. Duan, Y. Shi, G. Ding, Graphene quantum dots with pyrrole N and pyridine N: superior reactive oxygen species generation efficiency for metal-free sonodynamic tumor therapy, Small 17 (10) (2021).
[111] J. Ge, M. Lan, B. Zhou, W. Liu, L. Guo, H. Wang, Q. Jia, G. Niu, X. Huang, H. Zhou, X. Meng, P. Wang, C.-S. Lee, W. Zhang, X. Han, A graphene quantum dot photodynamic therapy agent with high singlet oxygen generation, Nat. Commun. 5 (2014).
[112] L. Cheng, C. Wang, L.Z. Feng, K. Yang, Z. Liu, Functional nanomaterials for phototherapies of cancer, Chem. Rev. 114 (21) (2014) 10869–10939.
[113] R. Vankayala, K.C. Hwang, Near-infrared-light-activatable nanomaterial-mediated phototheranostic nanomedicines: an emerging paradigm for cancer treatment, Adv. Mater. 30 (23) (2018).
[114] T. Xu, S.J. Zhao, C.W. Lin, X.L. Zheng, M.H. Lan, Recent advances in nanomaterials for sonodynamic therapy, Nano Res. 13 (11) (2020) 2898–2908.
[115] Y.Q. Li, H. Dong, Q. Tao, C.C. Ye, M.M. Yu, J.P. Li, H.F. Zhou, S.W. Yang, G. Q. Ding, X.M. Xie, Enhancing the magnetic relaxivity of MRI contrast agents via the localized superacid microenvironment of graphene quantum dots, Biomaterials 250 (2020).
[116] H.F. Su, Y. Liao, F.S. Wu, X.Z. Sun, H.J. Liu, K. Wang, X.J. Zhu, Cetuximab-conjugated iodine doped carbon dots as a dual fluorescent/CT probe for targeted imaging of lung cancer cells, Colloids Surf., B 170 (2018) 194–200.
[117] L.L. Yue, H.L. Li, Q. Liu, D. Guo, J. Chen, Q. Sun, Y.Z. Xu, F.S. Wu, Manganese-doped carbon quantum dots for fluorometric and magnetic resonance (dual mode) bioimaging and biosensing, Microchim. Acta 186 (5) (2019).
[118] S. Naahidi, M. Jafari, F. Edalat, K. Raymond, A. Khademhosseini, P. Chen, Biocompatibility of engineered nanoparticles for drug delivery, J. Contr. Release 166 (2) (2013) 182–194.
[119] J. Peng, W. Gao, B.K. Gupta, Z. Liu, R. Romero-Aburto, L.H. Ge, L. Song, L. B. Alemany, X.B. Zhan, G.H. Gao, S.A. Vithayathil, B.A. Kaipparettu, A.A. Marti, T. Hayashi, J.J. Zhu, P.M. Ajayan, Graphene quantum dots derived from carbon fibers, Nano Lett. 12 (2) (2012) 844–849.
[120] S.J. Zhu, J.H. Zhang, C.Y. Qiao, S.J. Tang, Y.F. Li, W.J. Yuan, B. Li, L. Tian, F. Liu, R. Hu, H.N. Gao, H.T. Wei, H. Zhang, H.C. Sun, B. Yang, Strongly green-photoluminescent graphene quantum dots for bioimaging applications, Chem. Commun. 47 (24) (2011) 6858–6860.
[121] W. Bing, H.J. Sun, Z.Q. Yan, J.S. Ren, X.G. Qu, Programmed bacteria death induced by carbon dots with different surface charge, Small 12 (34) (2016) 4713–4718.
[122] A.T. Young, N. Cornwell, M.A. Daniele, Neuro-nano interfaces: utilizing nano-coatings and nanoparticles to enable next-generation electrophysiological recording, neural stimulation, and biochemical modulation, Adv. Funct. Mater. 28 (12) (2018).
[123] M.H. Lan, S.J. Zhao, Z.Y. Zhang, L. Yan, L. Guo, G.L. Niu, J.F. Zhang, J.F. Zhao, H. Y. Zhang, P.F. Wang, G.Y. Zhu, C.S. Lee, W.J. Zhang, Two-photon-excited near-infrared emissive carbon dots as multifunctional agents for fluorescence imaging and photothermal therapy, Nano Res. 10 (9) (2017) 3113–3123.
[124] W.Q. Kong, J. Liu, R.H. Liu, H. Li, Y. Liu, H. Huang, K.Y. Li, J. Liu, S.T. Lee, Z. H. Kang, Quantitative and real-time effects of carbon quantum dots on single living HeLa cell membrane permeability, Nanoscale 6 (10) (2014) 5116–5120.

[125] A.H. Loo, Z. Sofer, D. Bousa, P. Ulbrich, A. Bonanni, M. Pumera, Carboxylic carbon quantum dots as a fluorescent sensing platform for DNA detection, Acs Appl. Mater. Inter. 8 (3) (2016) 1951–1957.
[126] J.H. Zhu, M.M. Li, S.P. Liu, Z.F. Liu, Y.F. Li, X.L. Hu, Fluorescent carbon dots for auramine O determination and logic gate operation, Sensor Actuat. B-Chem. 219 (2015) 261–267.
[127] C.L. Xia, S.J. Zhu, T.L. Feng, M.X. Yang, B. Yang, Evolution and synthesis of carbon dots: from carbon dots to carbonized polymer dots, Adv. Sci. 6 (23) (2019).
[128] P. Piotrowski, W. Pacuski, Photoluminescence of CdTe quantum wells doped with cobalt and iron, J. Lumin. 221 (2020).
[129] G.M. Li, X.N. Fei, H.F. Liu, J. Gao, J.Y. Nie, Y.B. Wang, Z.D. Tian, C.C. He, J. L. Wang, C. Ji, D. Oron, G.L. Yang, Fluorescence and optical activity of chiral CdTe quantum dots in their interaction with amino acids, ACS Nano 14 (4) (2020) 4196–4205.
[130] M.X. Jiao, X.D. Huang, L.Z. Ma, Y. Li, P.S. Zhang, X.J. Wei, L.H. Jing, X.L. Luo, A. L. Rogach, M.Y. Gao, Biocompatible off-stoichiometric copper indium sulfide quantum dots with tunable near-infrared emission via aqueous based synthesis, Chem. Commun. 55 (100) (2019) 15053–15056.
[131] Z.M. Luo, G.Q. Qi, K.Y. Chen, M. Zou, L.H. Yuwen, X.W. Zhang, W. Huang, L. H. Wang, Microwave-assisted preparation of white fluorescent graphene quantum dots as a novel phosphor for enhanced white-light-emitting diodes, Adv. Funct. Mater. 26 (16) (2016) 2739–2744.
[132] M. Zhang, L.L. Bai, W.H. Shang, W.J. Xie, H. Ma, Y.Y. Fu, D.C. Fang, H. Sun, L. Z. Fan, M. Han, C.M. Liu, S.H. Yang, Facile synthesis of water-soluble, highly fluorescent graphene quantum dots as a robust biological label for stem cells, J. Mater. Chem. 22 (15) (2012) 7461–7467.
[133] D.B. Shinde, V.K. Pillai, Electrochemical preparation of luminescent graphene quantum dots from multiwalled carbon nanotubes, Chem. Eur J. 18 (39) (2012) 12522–12528.
[134] D.Y. Pan, J.C. Zhang, Z. Li, M.H. Wu, Hydrothermal route for cutting graphene sheets into blue-luminescent graphene quantum dots, Adv. Mater. 22 (6) (2010) 734–+.
[135] Z.A. Qiao, Y.F. Wang, Y. Gao, H.W. Li, T.Y. Dai, Y.L. Liu, Q.S. Huo, Commercially activated carbon as the source for producing multicolor photoluminescent carbon dots by chemical oxidation, Chem. Commun. 46 (46) (2010) 8812–8814.
[136] L.B. Tang, R.B. Ji, X.K. Cao, J.Y. Lin, H.X. Jiang, X.M. Li, K.S. Teng, C.M. Luk, S. J. Zeng, J.H. Hao, S.P. Lau, Deep ultraviolet photoluminescence of water-soluble self-passivated graphene quantum dots, ACS Nano 6 (6) (2012) 5102–5110.
[137] S. Ranjit, N.M. Midde, N. Sinha, B.J. Patters, M.A. Rahman, T.J. Cory, P.S.S. Rao, S. Kumar, Effect of polyaryl hydrocarbons on cytotoxicity in monocytic cells: potential role of cytochromes P450 and oxidative stress pathways, PLoS One 11 (9) (2016).
[138] Y.H. Deng, D.X. Zhao, X. Chen, F. Wang, H. Song, D.Z. Shen, Long lifetime pure organic phosphorescence based on water soluble carbon dots, Chem. Commun. 49 (51) (2013) 5751–5753.
[139] G. Wang, G.L. Guo, D. Chen, Z.D. Liu, X.H. Zheng, A.L. Xu, S.W. Yang, G.Q. Ding, Facile and highly effective synthesis of controllable lattice sulfur-doped graphene quantum dots via hydrothermal treatment of durian, Acs Appl. Mater. Inter. 10 (6) (2018) 5750–5759.
[140] C. Zhu, S.W. Yang, G. Wang, R.W. Mo, P. He, J. Sun, Z.F. Di, N.Y. Yuan, J.N. Ding, G.Q. Ding, X.M. Xie, Negative induction effect of graphite N on graphene quantum dots: tunable band gap photoluminescence, J. Mater. Chem. C 3 (34) (2015) 8810–8816.
[141] G. Wang, P. He, A.L. Xu, Q.L. Guo, J.R. Li, Z.H. Wang, Z.D. Liu, D. Chen, S. W. Yang, G.Q. Ding, Promising fast energy transfer system between graphene quantum dots and the application in fluorescent bioimaging, Langmuir 35 (3) (2019) 760–766.
[142] Y.Q. Dong, R.X. Wang, H. Li, J.W. Shao, Y.W. Chi, X.M. Lin, G.N. Chen, Polyamine-functionalized carbon quantum dots for chemical sensing, Carbon 50 (8) (2012) 2810–2815.
[143] S.J. Zhu, Q.N. Meng, L. Wang, J.H. Zhang, Y.B. Song, H. Jin, K. Zhang, H.C. Sun, H.Y. Wang, B. Yang, Highly photoluminescent carbon dots for multicolor patterning, sensors, and bioimaging, Angew. Chem., Int. Ed. 52 (14) (2013) 3953–3957.
[144] H.J. Sun, L. Wu, W.L. Wei, X.G. Qu, Recent advances in graphene quantum dots for sensing, Mater. Today 16 (11) (2013) 433–442.
[145] H. Yoon, Y.H. Chang, S.H. Song, E.S. Lee, S.H. Jin, C. Park, J. Lee, B.H. Kim, H. J. Kang, Y.H. Kim, S. Jeon, Intrinsic photoluminescence emission from subdomained graphene quantum dots, Adv. Mater. 28 (26) (2016) 5255–+.
[146] Q.Q. Li, S. Zhang, L.M. Dai, L.S. Li, Nitrogen-doped colloidal graphene quantum dots and their size-dependent electrocatalytic activity for the oxygen reduction reaction, J. Am. Chem. Soc. 134 (46) (2012) 18932–18935.
[147] L. Jiang, H.Z. Ding, S.Y. Lu, T. Geng, G.J. Xiao, B. Zou, H. Bi, Photoactivated fluorescence enhancement in F,N-doped carbon dots with piezochromic behavior, Angew. Chem., Int. Ed. 59 (25) (2020) 9986–9991.
[148] S.H. Li, Y.C. Li, J. Cao, J. Zhu, L.Z. Fan, X.H. Li, Sulfur-doped graphene quantum dots as a novel fluorescent probe for highly selective and sensitive detection of Fe3+, Anal. Chem. 86 (20) (2014) 10201–10207.
[149] B. Hui, W. Qian, Y. Siwei, Y. Changjie, W. Haoran, L. Lei, J. Zhiwen, W. Gang, L. Shengzhong, Nitrogen-doped graphene quantum dots for 80% photoluminescence quantum yield for inorganic gamma-CsPbI3 perovskite solar cells with efficiency beyond 16, J. Mater. Chem. A 7 (10) (2019) 5740–5747.
[150] X.L. Gan, S.W. Yang, J. Zhang, G. Wang, P. He, H.R. Sun, H.B. Yuan, L.T. Yu, G. Q. Ding, Y.J. Zhu, Graphite-N doped graphene quantum dots as semiconductor additive in perovskite solar cells, Acs Appl. Mater. Inter. 11 (41) (2019) 37796–37803.
[151] J.J. Liu, D.W. Li, K. Zhang, M.X. Yang, H.C. Sun, B. Yang, One-step hydrothermal synthesis of nitrogen-doped conjugated carbonized polymer dots with 31% efficient red emission for in vivo imaging, Small 14 (15) (2018).
[152] H. Huang, S.W. Yang, Y. Liu, Y.C. Yang, H. Li, J.A. McLeod, G.Q. Ding, J. Huang, Z.H. Kang, Photocatalytic polymerization from amino acid to protein by carbon dots at room temperature, ACS Appl. Bio Mater. 2 (11) (2019) 5144–5153.
[153] Y.Q. Li, H. Dong, Q. Tao, C.C. Ye, M.M. Yu, J.P. Li, H.F. Zhou, S.W. Yang, G. Q. Ding, X.M. Xie, Enhancing the magnetic relaxivity of MRI contrast agents via the localized superacid microenvironment of graphene quantum dots, Biomaterials 250 (2020), 120056.
[154] L. Jiang, H.H. Ding, M.S. Xu, X.L. Hu, S.L. Li, M.Z. Zhang, Q. Zhang, Q.Y. Wang, S. Y. Lu, Y.P. Tian, H. Bi, UV-Vis-NIR full-range responsive carbon dots with large multiphoton absorption cross sections and deep-red fluorescence at nucleoli and in vivo, Small 16 (19) (2020).
[155] J.M. Wang, X.L. Hu, H.Z. Ding, X. Huang, M.S. Xu, Z.Z. Li, D. Wang, X. Yang, Y. Lu, Y.J. Xu, Y. Chen, P.C. Morais, Y.P. Tian, R.Q. Zhang, H. Bi, Fluorine and nitrogen Co-doped carbon dot complexation with Fe(III) as a T-1 contrast agent for magnetic resonance imaging, Acs Appl. Mater. Inter. 11 (20) (2019) 18203–18212.
[156] J.J. Du, N. Xu, J.L. Fan, W. Sun, X.J. Peng, Carbon dots for in vivo bioimaging and theranostics, Small 15 (32) (2019).
[157] Z.Z. Li, D. Wang, M.S. Xu, J.M. Wang, X.L. Hu, S. Anwar, A.C. Tedesco, P. C. Morais, H. Bi, Fluorine-containing graphene quantum dots with a high singlet oxygen generation applied for photodynamic therapy, J. Mater. Chem. B 8 (13) (2020) 2598–2606.
[158] Y. Su, S.Y. Lu, P.L. Gao, M. Zheng, Z.G. Xie, BODIPY@carbon dot nanocomposites for enhanced photodynamic activity, Mater. Chem. Front. 3 (9) (2019) 1747–1753.
[159] P. Devi, S. Saini, K.H. Kim, The advanced role of carbon quantum dots in nanomedical applications, Biosens. Bioelectron. 141 (2019).
[160] M. Zheng, S. Liu, J. Li, D. Qu, H.F. Zhao, X.G. Guan, X.L. Hu, Z.G. Xie, X.B. Jing, Z. C. Sun, Integrating oxaliplatin with highly luminescent carbon dots: an unprecedented theranostic agent for personalized medicine, Adv. Mater. 26 (21) (2014) 3554–3560.
[161] P.C. Hsu, P.C. Chen, C.M. Ou, H.Y. Chang, H.T. Chang, Extremely high inhibition activity of photoluminescent carbon nanodots toward cancer cells, J. Mater. Chem. B 1 (13) (2013) 1774–1781.
[162] F. Bray, J. Ferlay, I. Soerjomataram, R.L. Siegel, L.A. Torre, A. Jemal, Global cancer statistics 2018: GLOBOCAN estimates of incidence and mortality worldwide for 36 cancers in 185 countries, CA A Cancer J. Clin. 68 (6) (2018) 394–424.
[163] Cancer Research Report – Current Trends & Future Directions, Elsvier, 2017.
[164] A. Umar, B.K. Dunn, P. Greenwald, Future directions in cancer prevention, Nat. Rev. Cancer 12 (12) (2012) 835–848.
[165] K.D. Miller, L. Nogueira, T. Devasia, A.B. Mariotto, K.R. Yabroff, A. Jemal, J. Kramer, R.L. Siegel, Cancer treatment and survivorship statistics, 2022, CA A Cancer J. Clin. 72 (5) (2022) 409–436.
[166] A.B. Bourlinos, A. Bakandritsos, A. Kouloumpis, D. Gournis, M. Krysmann, E. P. Giannelis, K. Polakova, K. Safarova, K. Hola, R. Zboril, Gd(III)-doped carbon dots as a dual fluorescent-MRI probe, J. Mater. Chem. 22 (44) (2012) 23327–23330.
[167] R.C. Lv, P.P. Yang, F. He, S.L. Gai, C.X. Li, Y.L. Dai, G.X. Yang, J. Lin, A yolk-like multifunctional platform for multimodal imaging and synergistic therapy triggered by a single near-infrared light, ACS Nano 9 (2) (2015) 1630–1647.
[168] Y.Y. Yao, G. Gedda, W.M. Girma, C.L. Yen, Y.C. Ling, J.Y. Chang, Magnetofluorescent carbon dots derived from crab shell for targeted dual-modality bioimaging and drug delivery, Acs Appl. Mater. Inter. 9 (16) (2017) 13887–13899.
[169] X.L. Liu, H. Jiang, J. Ye, C.Q. Zhao, S.P. Gao, C.Y. Wu, C.H. Li, J.C. Li, X.M. Wang, Nitrogen-doped carbon quantum dot stabilized magnetic iron oxide nanoprobe for fluorescence, magnetic resonance, and computed tomography triple-modal in vivo bioimaging, Adv. Funct. Mater. 26 (47) (2016) 8694–8706.
[170] Y. Su, S. Liu, Y.Y. Guan, Z.G. Xie, M. Zheng, X.B. Jing, Renal clearable Hafnium-doped carbon dots for CT/Fluorescence imaging of orthotopic liver cancer, Biomaterials (2020) 255.
[171] M.M. Zhang, H.X. Ju, L. Zhang, M.Z. Sun, Z.W. Zhou, Z.Y. Dai, L.R. Zhang, A. H. Gong, C.Y. Wu, F.Y. Du, Engineering iodine-doped carbon dots as dual-modal probes for fluorescence and X-ray CT imaging, Int. J. Nanomed. 10 (2015).
[172] M. Hernandez-Rivera, I. Kumar, S.Y. Cho, B.Y. Cheong, M.X. Pulikkathara, S. E. Moghaddam, K.H. Whitmire, L.J. Wilson, High-performance hybrid bismuth-carbon nanotube based contrast agent for X-ray CT imaging, Acs Appl. Mater. Inter. 9 (7) (2017) 5709–5716.
[173] S. Badrigilan, B. Shaabani, N. Gharehaghaji, A. Mesbahi, Iron oxide/bismuth oxide nanocomposites coated by graphene quantum dots: "Three-in-one" theranostic agents for simultaneous CT/MR imaging-guided in vitro photothermal therapy, Photodiagnosis Photodyn. Ther. 25 (2019) 504–514.
[174] Y. Xuan, R.-Y. Zhang, D.-H. Zhao, X.-S. Zhang, J. An, K. Cheng, X.-L. Hou, X.-L. Song, Y.-D. Zhao, X.-Q. Yang, Ultrafast synthesis of gold nanosphere cluster coated by graphene quantum dot for active targeting PA/CT imaging and near-infrared laser/pH-triggered chemo-photothermal synergistic tumor therapy, Chem. Eng. J. 369 (2019) 87–99.
[175] J. Wahsner, E.M. Gale, A. Rodriguez-Rodriguez, P. Caravan, Chemistry of MRI contrast agents: current challenges and new Frontiers, Chem. Rev. 119 (2) (2019) 957–1057.

[176] V.M. Runge, Critical questions regarding gadolinium deposition in the brain and body after injections of the gadolinium-based contrast agents, safety, and clinical recommendations in consideration of the EMA's pharmacovigilance and risk assessment committee recommendation for suspension of the marketing authorizations for 4 linear agents, Invest. Radiol. 52 (6) (2017) 317–323.
[177] P. Caravan, J.J. Ellison, T.J. McMurry, R.B. Lauffer, Gadolinium(III) chelates as MRI contrast agents: structure, dynamics, and applications, Chem. Rev. 99 (9) (1999) 2293–2352.
[178] R.B. Lauffer, Paramagnetic metal-complexes as water proton relaxation agents for nmr imaging - theory and design, Chem. Rev. 87 (5) (1987) 901–927.
[179] P. Marckmann, L. Skov, K. Rossen, A. Dupont, M.B. Damholt, J.G. Heaf, H. S. Thomsen, Nephrogenic systemic fibrosis: suspected causative role of gadodiamide used for contrast-enhanced magnetic resonance imaging, J. Am. Soc. Nephrol. 17 (9) (2006) 2359–2362.
[180] C.L. Huang, C.C. Huang, F.D. Mai, C.L. Yen, S.H. Tzing, H.T. Hsieh, Y.C. Lingd, J. Y. Chang, Application of paramagnetic graphene quantum dots as A platform for simultaneous dual-modality bioimaging and tumor-targeted drug delivery, J. Mater. Chem. B 3 (4) (2015) 651–664.
[181] X.Y. Ren, X.X. Yuan, Y.P. Wang, C.L. Liu, Y. Qin'a, L.P. Guo, L.H. Liu, Facile preparation of Gd3+ doped carbon quantum dots: photoluminescence materials with magnetic resonance response as magnetic resonance/fluorescence bimodal probes, Opt. Mater. 57 (2016) 56–62.
[182] F.H. Wang, K. Bae, Z.W. Huang, J.M. Xue, Two-Photon graphene quantum dot modified Gd2O3 nanocomposites as A dual-mode MRI contrast agent and cell labelling agent, Nanoscale 10 (12) (2018) 5642–5649.
[183] Y. Li, H. Dong, Q. Tao, C. Ye, M. Yu, J. Li, H. Zhou, S. Yang, G. Ding, X. Xie, Enhancing the magnetic relaxivity of MRI contrast agents via the localized superacid microenvironment of graphene quantum dots, Biomaterials 250 (2020), 120056.
[184] B. Monzavi-Karbassi, A. Pashov, T. Kieber-Emmons, Tumor-associated glycans and immune surveillance, Vaccines 1 (2) (2013) 174–203.
[185] H. Denk, R. Eckerstorfer, G. Tappeiner, J.H. Holzner, Carcinoembryonic antigen (cea) in gastrointestinal and extragastrointestinal tumors and its relationship to tumor-cell differentiation, Int. J. Cancer 10 (2) (1972) 262–272.
[186] M.K. Boehm, M.O. Mayans, J.D. Thornton, R.H.J. Begent, P.A. Keep, S.J. Perkins, Extended glycoprotein structure of the seven domains in human carcinoembryonic antigen by X-ray and neutron solution scattering and an automated curve fitting procedure: implications for cellular adhesion, J. Mol. Biol. 259 (4) (1996) 718–736.
[187] Z. Farka, T. Juriik, D. Kovaar, L. Trnkova, P. Sklaadal, Nanoparticle-based immunochemical biosensors and assays: recent advances and challenges, Chem. Rev. 117 (15) (2017) 9973–10042.
[188] E. Bengtén, M. Wilson, N. Miller, L.W. Clem, L. Pilström, G.W. Warr, Immunoglobulin isotypes: structure, function, and genetics, in: L. Du Pasquier, G. W. Litman (Eds.), Origin and Evolution of the Vertebrate Immune System, Springer Berlin Heidelberg, Berlin, Heidelberg, 2000, pp. 189–219.
[189] P. E, Collected Studies on Immunity, J. Wiley & sons, 1906.
[190] R. Ralhan, N. Nath, S. Agarwal, M. Mathur, B. Wasylyk, N.K. Shukla, Circulating p53 antibodies as early markers of oral cancer: correlation with p53 alterations, Clin. Cancer Res. 4 (9) (1998) 2147–2152.
[191] S. Kobold, T. Luetkens, Y. Cao, C. Bokemeyer, D. Atanackovic, Prognostic and diagnostic value of spontaneous tumor-related antibodies, Clin. Dev. Immunol. 2010 (2010), 721531.
[192] E.L. Sievers, F.R. Appelbaum, R.T. Spielberger, S.J. Forman, D. Flowers, F. O. Smith, K. Shannon-Dorcy, M.S. Berger, I.D. Bernstein, Selective ablation of acute myeloid leukemia using antibody-targeted chemotherapy: A phase I study of an anti-CD33 calicheamicin immunoconjugate, Blood 93 (11) (1999) 3678–3684.
[193] T.E. Witzig, L.I. Gordon, F. Cabanillas, M.S. Czuczman, C. Emmanouilides, R. Joyce, B.L. Pohlman, N.L. Bartlett, G.A. Wiseman, N. Padre, A.J. Grillo-Lopez, P. Multani, C.A. White, Randomized controlled trial of yttrium-90-labeled ibritumomab tiuxetan radioimmunotherapy versus rituximab immunotherapy for patients with relapsed or refractory low-grade, follicular, or transformed B-cell non-Hodgkin's lymphoma, J. Clin. Oncol. 20 (10) (2002) 2453–2463.
[194] M.S. Kaminski, J. Estes, K.R. Zasadny, I.R. Francis, C.W. Ross, M. Tuck, D. Regan, S. Fisher, J. Gutierrez, S. Kroll, R. Stagg, G. Tidmarsh, R.L. Wahl, Radioimmunotherapy with iodine I-131 tositumomab for relapsed or refractory B-cell non-Hodgkin lymphoma: updated results and long-term follow-up of the University of Michigan experience, Blood 96 (4) (2000) 1259–1266.
[195] D.P. Bartel, MicroRNAs: genomics, biogenesis, mechanism, and function, Cell 116 (2) (2004) 281–297.
[196] V. Ambros, The functions of animal microRNAs, Nature 431 (7006) (2004) 350–355.
[197] B.D. Harfe, MicroRNAs in vertebrate development, Curr. Opin. Genet. Dev. 15 (4) (2005) 410–415.
[198] M. Furuno, K.C. Pang, N. Ninomiya, S. Fukuda, M.C. Frith, C. Bult, C. Kai, J. Kawai, P. Carninci, Y. Hayashizaki, J.S. Mattick, H. Suzuki, Clusters of internally primed transcripts reveal novel long noncoding RNAs, PLoS Genet. 2 (4) (2006) 537–553.
[199] G.A. Calin, C.M. Croce, MicroRNA signatures in human cancers, Nat. Rev. Cancer 6 (11) (2006) 857–866.
[200] E. Berezikov, E. Cuppen, R.H.A. Plasterk, Approaches to microRNA discovery, Nat. Genet. 38 (2006) S2–S7.
[201] C.M. Croce, G.A. Calin, miRNAs, cancer, and stem cell division, Cell 122 (1) (2005) 6–7.
[202] C. Caldas, J.D. Brenton, Sizing up miRNAs as cancer genes, Nat. Med. 11 (7) (2005) 712–714.
[203] C.Z. Chen, MicroRNAs as oncogenes and tumor suppressors, N. Engl. J. Med. 353 (17) (2005) 1768–1771.
[204] J. Lu, G. Getz, E.A. Miska, E. Alvarez-Saavedra, J. Lamb, D. Peck, A. Sweet-Cordero, B.L. Ebet, R.H. Mak, A.A. Ferrando, J.R. Downing, T. Jacks, H. R. Horvitz, T.R. Golub, MicroRNA expression profiles classify human cancers, Nature 435 (7043) (2005) 834–838.
[205] P. Mandel, Les acides nucleiques du plasma sanguin chez 1 homme, C. R. Seances Soc. Biol. Fil. 142 (1948) 241–243.
[206] K.L. Reckamp, V.O. Melnikova, C. Karlovich, L.V. Sequist, D.R. Camidge, H. Wakelee, M. Perol, G.R. Oxnard, K. Kosco, P. Croucher, E. Samuelsz, C. R. Vibat, S. Guerrero, J. Geis, D. Berz, E. Mann, S. Matheny, L. Rolfe, M. Raponi, M.G. Erlander, S. Gadgeel, A highly sensitive and quantitative test platform for detection of NSCLC EGFR mutations in urine and plasma, J. Thorac. Oncol. 11 (10) (2016) 1690–1700.
[207] Y.X. Wang, S. Springer, M. Zhang, K.W. McMahon, I. Kinde, L. Dobbyn, J. Ptak, H. Brem, K. Chaichana, G.L. Gallia, Z.L. Gokaslan, M.L. Groves, G.I. Jallo, M. Lim, A. Olivi, A. Quinones-Hinojosa, D. Rigamonti, G.J. Riggins, D.M. Sciubba, J. D. Weingart, J.P. Wolinsky, X.B. Ye, S.M. Oba-Shinjo, S.K.N. Marie, M. Holdhoff, N. Agrawal, L.A. Diaz, N. Papadopoulos, K.W. Kinzler, B. Vogelstein, C. Bettegowda, Detection of tumor-derived DNA in cerebrospinal fluid of patients with primary tumors of the brain and spinal cord, Proc. Natl. Acad. Sci. U. S. A. 112 (31) (2015) 9704–9709.
[208] K.B. Sriram, V. Relan, B.E. Clarke, E.E. Duhig, M.N. Windsor, K.S. Matar, R. Naidoo, L. Passmore, E. McCaul, D. Courtney, I.A. Yang, R.V. Bowman, K. M. Fong, Pleural fluid cell-free DNA integrity index to identify cytologically negative malignant pleural effusions including mesotheliomas, BMC Cancer 12 (2012) 428.
[209] S.K. Mithani, I.M. Smith, S.Y. Zhou, A. Gray, W.M. Koch, A. Maitra, J.A. Califano, Mitochondrial resequencing arrays detect tumor-specific mutations in salivary rinses of patients with head and neck cancer, Clin. Cancer Res. 13 (24) (2007) 7335–7340.
[210] S.A. Leon, B. Shapiro, D.M. Sklaroff, M.J. Yaros, Free DNA in serum of cancer-patients and effect of therapy, Cancer Res. 37 (3) (1977) 646–650.
[211] C. Kohler, R. Radpour, Z. Barekati, R. Asadollahi, J. Bitzer, E. Wight, N. Burki, C. Diesch, W. Holzgreve, X.Y. Zhong, Levels of plasma circulating cell free nuclear and mitochondrial DNA as potential biomarkers for breast tumors, Mol. Cancer 8 (2009) 105.
[212] V. Casadio, D. Calistri, M. Tebaldi, S. Bravaccini, R. Gunelli, G. Martorana, A. Bertaccini, L. Serra, E. Scarpi, D. Amadori, R. Silvestrini, W. Zoli, Urine Cell-Free DNA integrity as a marker for early bladder cancer diagnosis: preliminary data, Urol. Oncol-Semin Ori. 31 (8) (2013) 1744–1750.
[213] E. Heitzer, I.S. Haque, C.E.S. Roberts, M.R. Speicher, Current and future perspectives of liquid biopsies in genomics-driven oncology, Nat. Rev. Genet. 20 (2) (2019) 71–88.
[214] O.E. Bryzgunova, M.Y. Konoshenko, P.P. Laktionov, Concentration of cell-free DNA in different tumor types, Expert Rev. Mol. Diagn. (2020) 1–13.
[215] S. Cristiano, A. Leal, J. Phallen, J. Fiksel, V. Adleff, D.C. Bruhm, S.O. Jensen, J. E. Medina, C. Hruban, J.R. White, D.N. Palsgrove, N. Niknafs, V. Anagnostou, P. Forde, J. Naidoo, K. Marrone, J. Brahmer, B.D. Woodward, H. Husain, K.L. van Rooijen, M.B.W. Orntoft, A.H. Madsen, C.J.H. van de Velde, M. Verheij, A. Cats, C.J.A. Punt, G.R. Vink, N.C.T. van Grieken, M. Koopman, R.J.A. Fijneman, J. S. Johansen, H.J. Nielsen, G.A. Meijer, C.L. Andersen, R.B. Scharpf, V. E. Velculescu, Genome-wide cell-free DNA fragmentation in patients with cancer, Nature 570 (7761) (2019) 385–389.
[216] M. Stroun, P. Anker, P. Maurice, J. Lyautey, C. Lederrey, M. Beljanski, Neoplastic characteristics of the DNA found in the plasma of cancer-patients, Oncology 46 (5) (1989) 318–322.
[217] F. Mouliere, B. Robert, E.A. Peyrotte, M. Del Rio, M. Ychou, F. Molina, C. Gongora, A.R. Thierry, High fragmentation characterizes tumour-derived circulating DNA, PLoS One 6 (9) (2011), e23418.
[218] G.D. Sorenson, D.M. Pribish, F.H. Valone, V.A. Memoli, D.J. Bzik, S.L. Yao, Soluble normal and mutated DNA-sequences from single-copy genes in human blood, Cancer Epidem Biomar 3 (1) (1994) 67–71.
[219] F. Diehl, M. Li, D. Dressman, Y.P. He, D. Shen, S. Szabo, L.A. Diaz, S.N. Goodman, K.A. David, H. Juhl, K.W. Kinzler, B. Vogelstein, Detection and quantification of mutations in the plasma of patients with colorectal tumors, Proc. Natl. Acad. Sci. U. S. A. 102 (45) (2005) 16368–16373.
[220] H. Kimura, K. Kasahara, M. Kawaishi, H. Kunitoh, T. Tamura, B. Holloway, K. Nishio, Detection of epidermal growth factor receptor mutations in serum as a predictor of the response to gefitinib in patients with non-small-cell lung cancer, Clin. Cancer Res. 12 (13) (2006) 3915–3921.
[221] G. Sozzi, K. Musso, C. Ratcliffe, P. Goldstraw, M.A. Pierotti, U. Pastorino, Detection of microsatellite alterations in plasma DNA of non-small cell lung cancer patients: a prospect for early diagnosis, Clin. Cancer Res. 5 (10) (1999) 2689–2692.
[222] J.C. Ahn, P.C. Teng, P.J. Chen, E. Posadas, H.R. Tseng, S.C. Lu, J.D. Yang, Detection of circulating tumor cells and their implications as a biomarker for diagnosis, prognostication, and therapeutic monitoring in hepatocellular carcinoma, Hepatology 73 (1) (2021) 422–436.
[223] K. Pantel, C. Alix-Panabieres, Real-time liquid biopsy in cancer patients: fact or fiction? Cancer Res. 73 (21) (2013) 6384–6388.
[224] S.L. Stott, R.J. Lee, S. Nagrath, M. Yu, D.T. Miyamoto, L. Ulkus, E.J. Inserra, M. Ulman, S. Springer, Z. Nakamura, A.L. Moore, D.I. Tsukrov, M.E. Kempner, D. M. Dahl, C.L. Wu, A.J. Iafrate, M.R. Smith, R.G. Tompkins, L.V. Sequist, M. Toner,

D.A. Haber, S. Maheswaran, Isolation and characterization of circulating tumor cells from patients with localized and metastatic prostate cancer, Sci. Transl. Med. 2 (25) (2010) 25ra23.
[225] D.R. Parkinson, N. Dracopoli, B.G. Petty, C. Compton, M. Cristofanilli, A. Deisseroth, D.F. Hayes, G. Kapke, P. Kumar, J.S.H. Lee, M.C. Liu, R. McCormack, S. Mikulski, L. Nagahara, K. Pantel, S. Pearson-White, E. A. Punnoose, L.T. Roadcap, A.E. Schade, H.I. Scher, C.C. Sigman, G.J. Kelloff, Considerations in the development of circulating tumor cell technology for clinical use, J. Transl. Med. 10 (2012) 138.
[226] C. Bayarri-Lara, F.G. Ortega, A.C.L. de Guevara, J.L. Puche, J.R. Zafra, D. de Miguel-Perez, A.S.P. Ramos, C.F. Giraldo-Ospina, J.A.N. Gomez, M. Delgado-Rodriguez, J.A. Lorente, M.J. Serrano, Circulating tumor cells identify early recurrence in patients with non-small cell lung cancer undergoing radical resection, PLoS One 11 (2) (2016), e0148659.
[227] C. Alix-Panabieres, K. Pantel, Challenges in circulating tumour cell research, Nat. Rev. Cancer 14 (9) (2014) 623–631.
[228] C. Thery, M. Ostrowski, E. Segura, Membrane vesicles as conveyors of immune responses, Nat. Rev. Immunol. 9 (8) (2009) 581–593.
[229] J. Skog, T. Wurdinger, S. van Rijn, D.H. Meijer, L. Gainche, M. Sena-Esteves, W. T. Curry, B.S. Carter, A.M. Krichevsky, X.O. Breakefield, Glioblastoma microvesicles transport RNA and proteins that promote tumour growth and provide diagnostic biomarkers, Nat. Cell Biol. 10 (12) (2008) 1470–U209.
[230] Z.Y. Wei, A.O. Batagov, S. Schinelli, J.T. Wang, Y. Wang, R. El Fatimy, R. Rabinovsky, L. Balaj, C.C. Chen, F. Hochberg, B. Carter, X.O. Breakefield, A. M. Krichevsky, Coding and noncoding landscape of extracellular RNA released by human glioma stem cells, Nat. Commun. 8 (2017) 1145.
[231] L. Balaj, R. Lessard, L.X. Dai, Y.J. Cho, S.L. Pomeroy, X.O. Breakefield, J. Skog, Tumour microvesicles contain retrotransposon elements and amplified oncogene sequences, Nat. Commun. 2 (2011) 180.
[232] M. Yáñez-Mó, P.R.M. Siljander, Z. Andreu, A. Bedina Zavec, F.E. Borràs, E. I. Buzas, K. Buzas, E. Casal, F. Cappello, J. Carvalho, E. Colás, A. Cordeiro-da Silva, S. Fais, J.M. Falcon-Perez, I.M. Ghobrial, B. Giebel, M. Gimona, M. Graner, I. Gursel, M. Gursel, N.H.H. Heegaard, A. Hendrix, P. Kierulf, K. Kokubun, M. Kosanovic, V. Kralj-Iglic, E.-M. Krämer-Albers, S. Laitinen, C. Lässer, T. Lener, E. Ligeti, A. Linē, G. Lipps, A. Llorente, J. Lötvall, M. Manček-Keber, A. Marcilla, M. Mittelbrunn, I. Nazarenko, E.N.M. Nolte-'t Hoen, T.A. Nyman, L. O'Driscoll, M. Olivan, C. Oliveira, É. Pállinger, H.A. del Portillo, J. Reventós, M. Rigau, E. Rohde, M. Sammar, F. Sánchez-Madrid, N. Santarém, K. Schallmoser, M. Stampe Ostenfeld, W. Stoorvogel, R. Stukelj, S.G. Van der Grein, M. Helena Vasconcelos, M.H.M. Wauben, O. De Wever, Biological properties of extracellular vesicles and their physiological functions, J. Extracell. Vesicles 4 (1) (2015), 27066.
[233] J.C. Akers, D. Gonda, R. Kim, B.S. Carter, C.C. Chen, Biogenesis of extracellular vesicles (EV): exosomes, microvesicles, retrovirus-like vesicles, and apoptotic bodies, J. Neuro Oncol. 113 (1) (2013) 1–11.
[234] C. Thery, L. Zitvogel, S. Amigorena, Exosomes: composition, biogenesis and function, Nat. Rev. Immunol. 2 (8) (2002) 569–579.
[235] H.L. Shao, H. Im, C.M. Castro, X. Breakefield, R. Weissleder, H.H. Lee, New technologies for analysis of extracellular vesicles, Chem. Rev. 118 (4) (2018) 1917–1950.
[236] B. Hugel, M. Carmen, M.C. Martinez, C. Kunzelmann, J.M. Freyssinet, Membrane microparticles: two sides of the coin, Physiology 20 (2005) 22–27.
[237] R.F.A. Zwaal, A.J. Schroit, Pathophysiologic implications of membrane phospholipid asymmetry in blood cells, Blood 89 (4) (1997) 1121–1132.
[238] S. Elmore, Apoptosis: a review of programmed cell death, Toxicol. Pathol. 35 (4) (2007) 495–516.
[239] C.Q. Ding, A.W. Zhu, Y. Tian, Functional surface engineering of C-dots for fluorescent biosensing and in vivo bioimaging, Accounts Chem. Res. 47 (1) (2014) 20–30.
[240] J. Schlessinger, Cell signaling by receptor tyrosine kinases: from basic principles to cancer therapy, Cancer Res. 72 (2012).
[241] E. Witsch, M. Sela, Y. Yarden, Roles for growth factors in cancer progression, Physiology 25 (2) (2010) 85–101.
[242] N.E. Hynes, G. MacDonald, ErbB receptors and signaling pathways in cancer, Curr. Opin. Cell Biol. 21 (2) (2009) 177–184.
[243] R. Perona, Cell signalling: growth factors and tyrosine kinase receptors, Clin. Transl. Oncol. 8 (2) (2006) 77–82.
[244] J.B. Yu, C.F. Wu, X.J. Zhang, F.M. Ye, M.E. Gallina, Y. Rong, I.C. Wu, W. Sun, Y. H. Chan, D.T. Chiu, Stable functionalization of small semiconducting polymer dots via covalent cross-linking and their application for specific cellular imaging, Adv. Mater. 24 (26) (2012) 3498–3504.
[245] X.J. Wang, X. Sun, H. He, H. Yang, J. Lao, Y.Z. Song, Y.Q. Xia, H. Xu, X.D. Zhang, F. Huang, A two-component active targeting theranostic agent based on graphene quantum dots, J. Mater. Chem. B 3 (17) (2015) 3583–3590.
[246] J. Noh, D. Kim, G. Jang, J. Kim, M.B. Heo, N.E. Lee, C.Y. Kim, E. Lee, Y.J. Kim, Y. T. Lim, T.S. Lee, Fabrication, biofunctionalization, and simultaneous multicolor emission of hybrid "dots-on-spheres" structures for specific targeted imaging of cancer cells, RSC Adv. 4 (78) (2014) 41378–41386.
[247] E.M. Reyes-Reyes, F.R. Salipur, M. Shams, M.K. Forsthoefel, P.J. Bates, Mechanistic studies of anticancer aptamer AS1411 reveal a novel role for nucleolin in regulating Rac1 activation, Mol. Oncol. 9 (7) (2015) 1392–1405.
[248] C.I. Bargmann, R.A. Weinberg, Oncogenic activation of the neu-encoded receptor protein by point mutation and deletion, EMBO J. 7 (7) (1988) 2043–2052.
[249] D.J. Slamon, G.M. Clark, S.G. Wong, W.J. Levin, A. Ullrich, W.L. Mcguire, Human-breast cancer - correlation of relapse and survival with amplification of the her-2 neu oncogene, Science 235 (4785) (1987) 177–182.
[250] R. Colomer, S. Montero, A. Lluch, B. Ojeda, A. Barnadas, A. Casado, B. Massuti, H. Cortes-Funes, B. Lloveras, Circulating HER2 extracellular domain and resistance to chemotherapy in advanced breast cancer, Clin. Cancer Res. 6 (6) (2000) 2356–2362.
[251] W.J. Allard, J. Matera, M.C. Miller, M. Repollet, M.C. Connelly, C. Rao, A.G. J. Tibbe, J.W. Uhr, L.W.M.M. Terstappen, Tumor cells circulate in the peripheral blood of all major carcinomas but not in healthy subjects or patients with nonmalignant diseases, Clin. Cancer Res. 10 (20) (2004) 6897–6904.
[252] G. Gastl, G. Spizzo, P. Obrist, M. Dunser, G. Mikuz, Ep-CAM overexpression in breast cancer as a predictor of survival, Lancet 356 (9246) (2000) 1981–1982.
[253] M. Varga, P. Obrist, S. Schneeberger, G. Muhlmann, C. Felgel-Farnholz, D. Fong, M. Zitt, T. Brunhuber, G. Schafer, G. Gastl, G. Spizzo, Overexpression of epithelial cell adhesion molecule antigen in gallbladder carcinoma is an independent marker for poor survival, Clin. Cancer Res. 10 (9) (2004) 3131–3136.
[254] D. Fong, M. Steurer, P. Obrist, V. Barbieri, R. Margreiter, A. Amberger, K. Laimer, G. Gastl, A. Tzankov, G. Spizzo, Ep-CAM expression in pancreatic and ampullary carcinomas: frequency and prognostic relevance, J. Clin. Pathol. 61 (1) (2008) 31–35.
[255] L.L. Liu, D. Fu, Y.S. Ma, X.Z. Shen, The power and the promise of liver cancer stem cell markers, Stem Cell. Dev. 20 (12) (2011) 2023–2030.
[256] P. Dalerba, S.J. Dylla, I.K. Park, R. Liu, X.H. Wang, R.W. Cho, T. Hoey, A. Gurney, E.H. Huang, D.M. Simeone, A.A. Shelton, G. Parmiani, C. Castelli, M.F. Clarke, Phenotypic characterization of human colorectal cancer stem cells, Proc. Natl. Acad. Sci. U. S. A. 104 (24) (2007) 10158–10163.
[257] M. Munz, C. Kieu, B. Mack, B. Schmitt, R. Zeidler, O. Gires, The carcinoma-associated antigen EpCAM upregulates c-myc and induces cell proliferation, Oncogene 23 (34) (2004) 5748–5758.
[258] M. Munz, P.A. Baeuerle, O. Gires, The emerging role of EpCAM in cancer and stem cell signaling, Cancer Res. 69 (14) (2009) 5627–5629.
[259] D. Maetzel, S. Denzel, B. Mack, M. Canis, P. Went, M. Benk, C. Kieu, P. Papior, P. A. Baeuerle, M. Munz, O. Gires, Nuclear signalling by tumour-associated antigen EpCAM, Nat. Cell Biol. 11 (2) (2009) 162–U117.
[260] A. Chaves-Perez, B. Mack, D. Maetzel, H. Kremling, C. Eggert, U. Harreus, O. Gires, EpCAM regulates cell cycle progression via control of cyclin D1 expression, Oncogene 32 (5) (2013) 641–650.
[261] Q. Li, J.A. Zhang, W. Sun, J.B. Yu, C.F. Wu, W.P. Qin, D.T. Chiu, Europium-complex-Grafted polymer dots for amplified quenching and cellular imaging applications, Langmuir 30 (28) (2014) 8607–8614.
[262] J.Y. Shi, J. Lyu, F. Tian, M. Yang, A fluorescence turn-on biosensor based on graphene quantum dots (GQDs) and molybdenum disulfide (MoS2) nanosheets for epithelial cell adhesion molecule (EpCAM) detection, Biosens. Bioelectron. 93 (2017) 182–188.
[263] Y. Zhang, K.W. Chang, B. Xu, J.L. Chen, L.L. Yan, S.Q. Ma, C.F. Wu, W.J. Tian, Highly efficient near-infrared organic dots based on novel AEE fluorogen for specific cancer cell imaging, RSC Adv. 5 (46) (2015) 36837–36844.
[264] Y. Zhang, J.B. Yu, M.E. Gallina, W. Sun, Y. Rong, D.T. Chiu, Highly luminescent, fluorinated semiconducting polymer dots for cellular imaging and analysis, Chem. Commun. 49 (74) (2013) 8256–8258.
[265] F.C. Cui, J. Ji, J.D. Sun, J. Wang, H.M. Wang, Y.Z. Zhang, H. Ding, Y. Lu, D. Xu, X. Sun, A novel magnetic fluorescent biosensor based on graphene quantum dots for rapid, efficient, and sensitive separation and detection of circulating tumor cells, Anal. Bioanal. Chem. 411 (5) (2019) 985–995.
[266] I.C. Wu, J.B. Yu, F.M. Ye, Y. Rong, M.E. Gallina, B.S. Fujimoto, Y. Zhang, Y. H. Chan, W. Sun, X.H. Zhou, C.F. Wu, D.T. Chiu, Squaraine-based polymer dots with narrow, bright near-infrared fluorescence for biological applications, J. Am. Chem. Soc. 137 (1) (2015) 173–178.
[267] Y.H. Chan, M.E. Gallina, X.J. Zhang, I.C. Wu, Y.H. Jin, W. Sun, D.T. Chiu, Reversible photoswitching of spiropyran-conjugated semiconducting polymer dots, Anal. Chem. 84 (21) (2012) 9431–9438.
[268] W. Sun, J.B. Yu, R.P. Deng, Y. Rong, B. Fujimoto, C.F. Wu, H.J. Zhang, D.T. Chiu, Semiconducting polymer dots doped with europium complexes showing ultranarrow emission and long luminescence lifetime for time-gated cellular imaging, Angew. Chem., Int. Ed. 52 (43) (2013) 11294–11297.
[269] L. Wang, Y. Yin, A. Jain, H.S. Zhou, Aqueous phase synthesis of highly luminescent, nitrogen-doped carbon dots and their application as bioimaging agents, Langmuir 30 (47) (2014) 14270–14275.
[270] Q. Zhang, S.N. Deng, J.L. Liu, X.X. Zhong, J. He, X.F. Chen, B.W. Feng, Y.F. Chen, K. Ostrikov, Cancer-targeting graphene quantum dots: fluorescence quantum yields, stability, and cell selectivity, Adv. Funct. Mater. 29 (5) (2019).
[271] Z. Chen, X.C. Wang, H. Li, C. Li, Q.H. Lu, G. Yang, J.G. Long, L.J. Meng, Controllable and mass fabrication of highly luminescent N-doped carbon dots for bioimaging applications, RSC Adv. 5 (29) (2015) 22343–22349.
[272] Q.L. Liu, S.H. Xu, C.X. Niu, M.F. Li, D.C. He, Z.L. Lu, L. Ma, N. Na, F. Huang, H. Jiang, J. Ouyang, Distinguish cancer cells based on targeting turn-on fluorescence imaging by folate functionalized green emitting carbon dots, Biosens. Bioelectron. 64 (2015) 119–125.
[273] X.Y. Tan, Y.C. Li, X.H. Li, S.X. Zhou, L.Z. Fan, S.H. Yang, Electrochemical synthesis of small-sized red fluorescent graphene quantum dots as a bioimaging platform, Chem. Commun. 51 (13) (2015) 2544–2546.
[274] Y.C. Song, W. Shi, W. Chen, X.H. Li, H.M. Ma, Fluorescent carbon nanodots conjugated with folic acid for distinguishing folate-receptor-positive cancer cells from normal cells, J. Mater. Chem. 22 (25) (2012) 12568–12573.
[275] B. Sun, B. Zhao, D.D. Wang, Y.B. Wang, Q. Tang, S.J. Zhu, B. Yang, H.C. Sun, Fluorescent non-conjugated polymer dots for targeted cell imaging, Nanoscale 8 (18) (2016) 9837–9841.

[276] F.W. Cao, L.Q. Xiong, Folic acid functionalized PFBT fluorescent polymer dots for tumor imaging, Chin. J. Chem. 34 (6) (2016) 570–575.
[277] J.L. Zhang, X.W. Zhao, M. Xian, C. Dong, S.M. Shuang, Folic acid-conjugated green luminescent carbon dots as a nanoprobe for identifying folate receptor-positive cancer cells, Talanta 183 (2018) 39–47.
[278] S.X. Feng, J.Q. Pan, C.R. Li, Y.Y. Zheng, Folic acid-conjugated nitrogen-doped graphene quantum dots as a fluorescent diagnostic material for MCF-7 cells, Nanotechnology 31 (13) (2020).
[279] Y. Zhang, Y.J. Chen, X. Li, J.B. Zhang, J.L. Chen, B. Xu, X.Q. Fu, W.J. Tian, Folic acid-functionalized AIE Pdots based on amphiphilic PCL-b-PEG for targeted cell imaging, Polym. Chem-Uk 5 (12) (2014) 3824–3830.
[280] R.Y. Li, X. Wang, Z.J. Li, H.Y. Zhu, J.K. Liu, Folic acid-functionalized graphene quantum dots with tunable fluorescence emission for cancer cell imaging and optical detection of Hg2+, New J. Chem. 42 (6) (2018) 4352–4360.
[281] N. Prabhakar, T. Nareoja, E. von Haartman, D. Sen Karaman, S.A. Burikov, T. A. Dolenko, T. Deguchi, V. Mamaeva, P.E. Hanninen, I.I. Vlasov, O. A. Shenderova, J.M. Rosenholm, Functionalization of graphene oxide nanostructures improves photoluminescence and facilitates their use as optical probes in preclinical imaging, Nanoscale 7 (23) (2015) 10410–10420.
[282] X.Q. Su, C.Y. Chan, J.Y. Shi, M.K. Tsang, Y. Pan, C.M. Cheng, O. Gerile, M. Yang, A graphene quantum dot@Fe3O4@SiO2 based nanoprobe for drug delivery sensing and dual-modal fluorescence and MRI imaging in cancer cells, Biosens. Bioelectron. 92 (2017) 489–495.
[283] S.K. Bhunia, A.R. Maity, S. Nandi, D. Stepensky, R. Jelinek, Imaging cancer cells expressing the folate receptor with carbon dots produced from folic acid, Chembiochem 17 (7) (2016) 614–619.
[284] S.S. Liu, H.J. Cao, Z.Y. Wang, W.W. Tu, Z.H. Dai, Label-free photoelectrochemical cytosensing via resonance energy transfer using gold nanoparticle-enhanced carbon dots, Chem. Commun. 51 (75) (2015) 14259–14262.
[285] C.X. Wang, Z.Z. Xu, H.H. Lin, Y.J. Huang, C. Zhang, Large scale synthesis of highly stable fluorescent carbon dots using silica spheres as carriers for targeted bioimaging of cancer cells, Part. Part. Syst. Char. 32 (10) (2015) 944–951.
[286] X.J. Wang, X. Sun, J. Lao, H. He, T.T. Cheng, M.Q. Wang, S.J. Wang, F. Huang, Multifunctional graphene quantum dots for simultaneous targeted cellular imaging and drug delivery, Colloids Surf., B 122 (2014) 638–644.
[287] D. Lei, W. Yang, Y.Q. Gong, J. Jing, H.L. Nie, B. Yu, X.L. Zhang, Non-covalent decoration of carbon dots with folic acid via a polymer-assisted strategy for fast and targeted cancer cell fluorescence imaging, Sensor Actuat. B-Chem. 230 (2016) 714–720.
[288] X.D. Yang, Y. Wang, X.R. Shen, C.Y. Su, J.H. Yang, M.J. Piao, F. Jia, G.H. Gao, L. Zhang, Q. Lin, One-step synthesis of photoluminescent carbon dots with excitation independent emission for selective bioimaging and gene delivery, J. Colloid Interface Sci. 492 (2017) 1–7.
[289] J. Wang, J. Liu, PEI-folic acid modified carbon nanodots for cancer cell-targeted delivery and two-photon excitation imaging, RSC Adv. 6 (24) (2016) 19662–19668.
[290] X.D. Yang, X. Yang, Z.Y. Li, S.Y. Li, Y.X. Han, Y. Chen, X.Y. Bu, C.Y. Su, H. Xu, Y. N. Jiang, Q. Lin, Photoluminescent carbon dots synthesized by microwave treatment for selective image of cancer cells, J. Colloid Interface Sci. 456 (2015) 1–6.
[291] I.P.J. Lai, S.G. Harroun, S.Y. Chen, B. Unnikrishnan, Y.J. Li, C.C. Huang, Solid-state synthesis of self-functional carbon quantum dots for detection of bacteria and tumor cells, Sensor Actuat. B-Chem. 228 (2016) 465–470.
[292] H.F. Liu, Z.H. Li, Y.Q. Sun, X. Geng, Y.L. Hu, H.M. Meng, J. Ge, L.B. Qu, Synthesis of luminescent carbon dots with ultrahigh quantum yield and inherent folate receptor-positive cancer cell targetability, Sci. Rep-Uk 8 (2018).
[293] S. Kadian, G. Manik, N. Das, P. Roy, Targeted bioimaging and sensing of folate receptor-positive cancer cells using folic acid-conjugated sulfur-doped graphene quantum dots, Microchim. Acta 187 (8) (2020).
[294] J. Soleymani, M. Hasanzadeh, M.H. Somi, S.A. Ozkan, A. Jouyban, Targeting and sensing of some cancer cells using folate bioreceptor functionalized nitrogen-doped graphene quantum dots, Int. J. Biol. Macromol. 118 (2018) 1021–1034.
[295] Y. Xuan, R.Y. Zhang, X.S. Zhang, J. An, K. Cheng, C. Li, X.L. Hou, Y.D. Zhao, Targeting N-doped graphene quantum dot with high photothermal conversion efficiency for dual-mode imaging and therapy in vitro, Nanotechnology 29 (35) (2018).
[296] K. Sun, H.B. Chen, L. Wang, S.Y. Yin, H.Y. Wang, G.X. Xu, D.N. Chen, X.J. Zhang, C.F. Wu, W.P. Qin, Size-dependent property and cell labeling of semiconducting polymer dots, Acs Appl. Mater. Inter. 6 (13) (2014) 10802–10812.
[297] P.J. Wu, S.Y. Kuo, Y.C. Huang, C.P. Chen, Y.H. Chan, Polydiacetylene-enclosed near-infrared fluorescent semiconducting polymer dots for bioimaging and sensing, Anal. Chem. 86 (10) (2014) 4831–4839.
[298] Y. Rong, J.Z. Yu, X.J. Zhang, W. Sun, F.M. Ye, I.C. Wu, Y. Zhang, S. Hayden, Y. Zhang, C.F. Wu, D.T. Chiu, Yellow fluorescent semiconducting polymer dots with high brightness, small size, and narrow emission for biological applications, ACS Macro Lett. 3 (10) (2014) 1051–1054.
[299] H. Ding, Y.J. Cai, L.Z. Gao, M.M. Liang, B.P. Miao, H.W. Wu, Y. Liu, N. Xie, A. F. Tang, K.L. Fan, X.Y. Yan, G.H. Nie, Exosome-like nanozyme vesicles for H2O2-responsive catalytic photoacoustic imaging of xenograft nasopharyngeal carcinoma, Nano Lett. 19 (1) (2019) 203–209.
[300] M.E. Hatley, D.M. Patrick, M.R. Garcia, J.A. Richardson, R. Bassel-Duby, E. van Rooij, E.N. Olson, Modulation of K-Ras-Dependent lung tumorigenesis by MicroRNA-21, Cancer Cell 18 (3) (2010) 282–293.
[301] D.P. Bartel, MicroRNAs: target recognition and regulatory functions, Cell 136 (2) (2009) 215–233.
[302] K. Ruan, X.G. Fang, G.L. Ouyang, MicroRNAs: novel regulators in the hallmarks of human cancer, Cancer Lett. 285 (2) (2009) 116–126.
[303] C.Z. Chen, L. Li, H.F. Lodish, D.P. Bartel, MicroRNAs modulate hematopoietic lineage differentiation, Science 303 (5654) (2004) 83–86.
[304] Y.L. Wang, D.N. Keys, J.K. Au-Young, C.F. Chen, MicroRNAs in embryonic stem cells, J. Cell. Physiol. 218 (2) (2009) 251–255.
[305] H.F. Dong, J.P. Lei, L. Ding, Y.Q. Wen, H.X. Ju, X.J. Zhang, MicroRNA: function, detection, and bioanalysis, Chem. Rev. 113 (8) (2013) 6207–6233.
[306] M.V. Joglekar, V.M. Joglekar, A.A. Hardikar, Expression of islet-specific microRNAs during human pancreatic development, Gene Expr. Patterns 9 (2) (2009) 109–113.
[307] P.S. Mitchell, R.K. Parkin, E.M. Kroh, B.R. Fritz, S.K. Wyman, E.L. Pogosova-Agadjanyan, A. Peterson, J. Noteboom, K.C. O'Briant, A. Allen, D.W. Lin, N. Urban, C.W. Drescher, B.S. Knudsen, D.L. Stirewalt, R. Gentleman, R. L. Vessella, P.S. Nelson, D.B. Martin, M. Tewari, Circulating microRNAs as stable blood-based markers for cancer detection, Proc. Natl. Acad. Sci. U. S. A. 105 (30) (2008) 10513–10518.
[308] I.M. Pedersen, D. Otero, E. Kao, A.V. Miletic, C. Hother, E. Ralfkiaer, R.C. Rickert, K. Gronbaek, M. David, Onco-miR-155 targets SHIP1 to promote TNFalpha-dependent growth of B cell lymphomas, EMBO Mol. Med. 1 (5) (2009) 288–295.
[309] E. Tili, J.J. Michaille, D. Wernicke, H. Alder, S. Costinean, S. Volinia, C.M. Croce, Mutator activity induced by microRNA-155 (miR-155) links inflammation and cancer, Proc. Natl. Acad. Sci. U. S. A. 108 (12) (2011) 4908–4913.
[310] W. Kong, L.L. He, M. Coppola, J.P. Guo, N.N. Esposito, D. Coppola, J.Q. Cheng, MicroRNA-155 regulates cell survival, growth, and chemosensitivity by targeting FOXO3a in breast cancer (vol 285, pg 17869, 2010), J. Biol. Chem. 291 (43) (2016), 22855-22855.
[311] S.A. Jiang, H.W. Zhang, M.H. Lu, X.H. He, Y. Li, H. Gu, M.F. Liu, E.D. Wang, MicroRNA-155 functions as an OncomiR in breast cancer by targeting the suppressor of cytokine signaling 1 gene, Cancer Res. 70 (8) (2010) 3119–3127.
[312] T.X. Hu, L. Zhang, W. Wen, X.H. Zhang, S.F. Wang, Enzyme catalytic amplification of miRNA-155 detection with graphene quantum dot-based electrochemical biosensor, Biosens. Bioelectron. 77 (2016) 451–456.
[313] Y. Cao, H.F. Dong, Z. Yang, X.M. Zhong, Y. Chen, W.H. Dai, X.J. Zhang, Aptamer-conjugated graphene quantum dots/porphyrin derivative theranostic agent for intracellular cancer-related MicroRNA detection and fluorescence-guided photothermal/photodynamic synergetic therapy, Acs Appl. Mater. Inter. 9 (1) (2017) 159–166.
[314] F. Yang, T.T. Zhang, S.S. Li, P. Song, K. Zhang, Q.Y. Guan, B. Kang, J.J. Xu, H. Y. Chen, Endogenous MicroRNA-triggered and real-time monitored drug release via cascaded energy transfer payloads, Anal. Chem. 89 (19) (2017) 10239–10247.
[315] F.F. Zheng, P.H. Zhang, Y. Xi, J.J. Chen, L.L. Li, J.J. Zhu, Aptamer/graphene quantum dots nanocomposite capped fluorescent mesoporous silica nanoparticles for intracellular drug delivery and real-time monitoring of drug release, Anal. Chem. 87 (23) (2015) 11739–11745.
[316] E.J. Joo, G.B. ten Dam, T.H. van Kuppevelt, T. Toida, R.J. Linhardt, Y.S. Kim, Nucleolin: acharan sulfate-binding protein on the surface of cancer cells, Glycobiology 15 (1) (2005) 1–9.
[317] S. Christian, J. Pilch, M.E. Akerman, K. Porkka, P. Laakkonen, E. Ruoslahti, Nucleolin expressed at the cell surface is a marker of endothelial cells in angiogenic blood vessels, J. Cell Biol. 163 (4) (2003) 871–878.
[318] Y. Huang, H. Shi, H. Zhou, X. Song, S. Yuan, Y. Luo, The angiogenic function of nucleolin is mediated by vascular endothelial growth factor and nonmuscle myosin, Blood 107 (9) (2006) 3564–3571.
[319] S. Larrucea, R. Cambronero, C. Gonzalez-Rubio, B. Fraile, C. Gamallo, G. Fontan, M. Lopez-Trascasa, Internalization of factor J and cellular signalization after factor J-cell interaction, Biochem. Bioph. Res. Co 266 (1) (1999) 51–57.
[320] S. Larrucea, C. Gonzalez-Rubio, R. Cambronero, B. Ballou, P. Bonay, E. Lopez-Granados, P. Bouvet, G. Fontan, M. Fresno, M. Lopez-Trascasa, Cellular adhesion mediated by factor J, a complement inhibitor - evidence for nucleolin involvement, J. Biol. Chem. 273 (48) (1998) 31718–31725.
[321] G. Harms, R. Kraft, G. Grelle, B. Volz, J. Dernedde, R. Tauber, Identification of nucleolin as a new L-selectin ligand, Biochem. J. 360 (2001) 531–538.
[322] D. Legrand, K. Vigie, E.A. Said, E. Elass, M. Masson, M.C. Slomianny, M. Carpentier, J.P. Briand, J. Mazurier, A.G. Hovanessian, Surface nucleolin participates in both the binding and endocytosis of lactoferrin in target cells, Eur. J. Biochem. 271 (2) (2004) 303–317.
[323] K. Hirano, Y. Miki, Y. Hirai, R. Sato, T. Itoh, A. Hayashi, M. Yamanaka, S. Eda, M. Beppu, A multifunctional shuttling protein nucleolin is a macrophage receptor for apoptotic cells, J. Biol. Chem. 280 (47) (2005) 39284–39293.
[324] M. Srivastava, H.B. Pollard, Molecular dissection of nucleolin's role in growth and cell proliferation: new insights, Faseb. J. 13 (14) (1999) 1911–1922.
[325] Y.C. Mi, S.D. Thomas, X.H. Xu, L.K. Casson, D.M. Miller, P.J. Bates, Apoptosis in leukemia cells is accompanied by alterations in the levels and localization of nucleolin, J. Biol. Chem. 278 (10) (2003) 8572–8579.
[326] P.J. Bates, D.A. Laber, D.M. Miller, S.D. Thomas, J.O. Trent, Discovery and development of the G-rich oligonucleotide AS1411 as a novel treatment for cancer, Exp. Mol. Pathol. 86 (3) (2009) 151–164.
[327] A.G. Hovanessian, F. Puvion-Dutilleul, S. Nisole, J. Svab, E. Perret, J.S. Deng, B. Krust, The cell-surface-expressed nucleolin is associated with the actin cytoskeleton, Exp. Cell Res. 261 (2) (2000) 312–328.
[328] F. Mongelard, P. Bouvet, AS-1411, a guanosine-rich oligonucleotide aptamer targeting nucleolin for the potential treatment of cancer, including acute myeloid leukemia, Curr. Opin. Mol. Therapeut. 12 (1) (2010) 107–114.
[329] C.R. Ireson, L.R. Kelland, Discovery and development of anticancer aptamers, Mol. Cancer Therapeut. 5 (12) (2006) 2957–2962.

[330] H. Motaghi, M.A. Mehrgardi, P. Bouvet, Carbon dots-AS1411 aptamer nanoconjugate for ultrasensitive spectrofluorometric detection of cancer cells, Sci. Rep-Uk 7 (2017).
[331] V.K. Bajpai, I. Khan, S. Shukla, S.M. Kang, F. Aziz, K.M. Tripathi, D. Saini, H. J. Cho, N.S. Heo, S.K. Sonkar, L. Chen, Y.S. Huh, Y.K. Han, Multifunctional N-P-doped carbon dots for regulation of apoptosis and autophagy in B16F10 melanoma cancer cells and in vitro imaging applications, Theranostics 10 (17) (2020) 7841–7856.
[332] Z.L. Wang, L.L. Liu, W.H. Bu, M.D. Zheng, N.Q. Jin, K. Zhang, X.W. Xu, D. Zhou, B. Yang, H.C. Sun, Carbon dots induce epithelial-mesenchymal transition for promoting cutaneous wound healing via activation of TGF-beta/p38/snail pathway, Adv. Funct. Mater. 30 (43) (2020).
[333] Z.H. Lu, S.J. Liu, Y.G. Le, Z.N. Qin, M.W. He, F.B. Xu, Y. Zhu, J.M. Zhao, C.B. Mao, L. Zheng, An injectable collagen-genipin-carbon dot hydrogel combined with photodynamic therapy to enhance chondrogenesis, Biomaterials 218 (2019), 119190, 233 (2020).
[334] W.K. Meng, A. Rey-Rico, M. Claudel, G. Schmitt, S. Speicher-Mentges, F. Pons, L. Lebeau, J.K. Venkatesan, M. Cucchiarini, rAAV-mediated overexpression of SOX9 and TGF-beta via carbon dot-guided vector delivery enhances the biological activities in human bone marrow-derived mesenchymal stromal cells, Nanomaterials-Basel 10 (5) (2020).
[335] Y.Q. Xie, H.Y. Fan, W.F. Lu, Q. Yang, A. Nurkesh, T. Yeleussizov, A. Maipas, J. Lu, L. Manarbek, Z.B. Chen, E. Benassi, Nuclear MET requires ARF and is inhibited by carbon nanodots through binding to phospho-tyrosine in prostate cancer, Oncogene 38 (16) (2019) 2967–2983.
[336] Y.Q. Xie, Q.L. Sun, A.A. Nurkesh, J. Lu, S. Kauanova, J.H. Feng, D. Tursynkhan, Q. Yang, A. Kassymbek, M. Karibayev, K. Duisenova, H.Y. Fan, X. Wang, L. Manarbek, A. Maipas, Z.B. Chen, M.P. Balanay, Dysregulation of YAP by ARF stimulated with tea-derived carbon nanodots, Sci. Rep-Uk 7 (2017).
[337] D. Wang, L. Zhu, J.F. Chen, L.M. Dai, Can graphene quantum dots cause DNA damage in cells? Nanoscale 7 (21) (2015) 9894–9901.
[338] P.T.M. Phuong, H.J. Won, A.I. Robby, S.G. Kim, G.B. Im, S.H. Bhang, G. Lee, S. Y. Park, NIR-vis-Induced pH-sensitive TiO2 immobilized carbon dot for controllable membrane-nuclei targeting and photothermal therapy of cancer cells, Acs Appl. Mater. Inter. 12 (34) (2020) 37929–37942.
[339] C.L. Li, C.M. Ou, C.C. Huang, W.C. Wu, Y.P. Chen, T.E. Lin, L.C. Ho, C.W. Wang, C.C. Shih, H.C. Zhou, Y.C. Lee, W.F. Tzeng, T.J. Chiou, S.T. Chu, J. Cang, H. T. Chang, Carbon dots prepared from ginger exhibiting efficient inhibition of human hepatocellular carcinoma cells, J. Mater. Chem. B 2 (28) (2014) 4564–4571.
[340] S. Wang, F. Zhang, C.Y. Chen, C.Q. Cai, Ultrasensitive graphene quantum dots-based catalytic hairpin assembly amplification resonance light scattering assay for p53 mutant DNA detection, Sensor Actuat. B-Chem. 291 (2019) 42–47.
[341] D.D. Su, N. Li, Y. Liu, M.K. Wang, X.G. Su, Ratiometric fluorescence strategy for p53 gene assay by using nitrogen doped graphene quantum dots and berberine as fluorescence reporters, Anal. Chim. Acta 1084 (2019) 78–84.
[342] M. Hasanzadeh, H.N. Baghban, N. Shadjou, A. Mokhtarzadeh, Ultrasensitive electrochemical immunosensing of tumor suppressor protein p53 in unprocessed human plasma and cell lysates using a novel nanocomposite based on poly-cysteine/graphene quantum dots/gold nanoparticle, Int. J. Biol. Macromol. 107 (2018) 1348–1363.
[343] P. Xiao, Y. Ke, J. Lu, Z.R. Huang, X.F. Zhu, B. Wei, L.L. Huang, Photoluminescence immunoassay based on grapefruit peel-extracted carbon quantum dots encapsulated into silica nanospheres for p53 protein, Biochem. Eng. J. 139 (2018) 109–116.
[344] Q. Lu, W. Wei, Z. Zhou, Z. Zhou, Y. Zhang, S. Liu, Electrochemiluminescence resonance energy transfer between graphene quantum dots and gold nanoparticles for DNA damage detection, Analyst 139 (10) (2014) 2404–2410.
[345] X.Y. Wang, L. Liu, Z.Y. Wang, Z.H. Dai, Highly sensitive electrochemiluminescent DNA biosensor based on hydrazide-modified graphene quantum dots and hemin/G-quadruplex DNAzyme, J. Electroanal. Chem. 781 (2016) 351–355.
[346] L. Wang, P.F. Liu, Z.J. Liu, H.X. Cao, S.Y. Ye, K.R. Zhao, G.X. Liang, J.J. Zhu, A dual-potential ratiometric electrochemiluminescence biosensor based on Au@CDs nanoflowers, Au@luminol nanoparticles and an enzyme-free DNA nanomachine for ultrasensitive p53 DNA detection, Sensor Actuat. B-Chem. 327 (2021).
[347] H.F. Dong, W.H. Dai, H.X. Ju, H.T. Lu, S.Y. Wang, L.P. Xu, S.F. Zhou, Y. Zhang, X. J. Zhang, Multifunctional poly(L-lactide)-polyethylene glycol-grafted graphene quantum dots for intracellular MicroRNA imaging and combined specific-gene-targeting agents delivery for improved therapeutics, Acs Appl. Mater. Inter. 7 (20) (2015) 11015–11023.
[348] B.M. Ryan, N. O'Donovan, M.J. Duffy, Survivin: a new target for anti-cancer therapy, Cancer Treat Rev. 35 (7) (2009) 553–562.
[349] D.C. Altieri, Validating survivin as a cancer therapeutic target, Nat. Rev. Cancer 3 (1) (2003) 46–54.
[350] B.H. Joshi, C. Hogaboam, P. Dover, S.R. Husain, R.K. Puri, Role of interleukin-13 in cancer, pulmonary fibrosis, and other T(H)2-type diseases, Vitam. Horm. 74 (2006) 479–504.
[351] A.L. Andrews, T. Nasir, F. Bucchieri, J.W. Holloway, S.T. Holgate, D.E. Davies, IL-13 receptor alpha 2: a regulator of IL-13 and IL-4 signal transduction in primary human fibroblasts, J. Allergy Clin. Immunol. 118 (4) (2006) 858–865.
[352] V. Serafin, A. Valverde, G. Martinez-Garcia, E. Martinez-Perinan, F. Comba, M. Garranzo-Asensio, R. Barderas, P. Yanez-Sedeno, S. Campuzano, J. M. Pingarron, Graphene quantum dots-functionalized multi-walled carbon nanotubes as nanocarriers in electrochemical immunosensing. Determination of IL-13 receptor alpha 2 in colorectal cells and tumor tissues with different metastatic potential, Sensor Actuat. B-Chem. 284 (2019) 711–722.
[353] W.E. Wright, O.M. Pereirasmith, J.W. Shay, Reversible cellular senescence - implications for immortalization of normal human-diploid fibroblasts, Mol. Cell Biol. 9 (7) (1989) 3088–3092.
[354] J.W. Shay, W.E. Wright, Hayflick, his limit, and cellular ageing, Nat. Rev. Mol. Cell Biol. 1 (1) (2000) 72–76.
[355] M.A. Blasco, Telomeres and human disease: ageing, cancer and beyond, Nat. Rev. Genet. 6 (8) (2005) 611–622.
[356] T. Nikitina, C.L. Woodcock, Closed chromatin loops at the ends of chromosomes, J. Cell Biol. 166 (2) (2004) 161–165.
[357] S. Lejnine, V.L. Makarov, J.P. Langmore, Conserved nucleoprotein structure at the ends of vertebrate and invertebrate chromosomes, Proc. Natl. Acad. Sci. U. S. A. 92 (6) (1995) 2393–2397.
[358] S. Huang, L.M. Wang, C.S. Huang, W. Su, Q. Xiao, Label-free and ratiometric fluorescent nanosensor based on amino-functionalized graphene quantum dots coupling catalytic G-quadruplex/hemin DNAzyme for ultrasensitive recognition of human telomere DNA, Sensor Actuat. B-Chem. 245 (2017) 648–655.
[359] J.R. Williamson, M.K. Raghuraman, T.R. Cech, Mono-valent cation induced structure of telomeric DNA - the G-quartet model, Cell 59 (5) (1989) 871–880.
[360] I. Draskovic, A.L. Vallejo, Telomere recombination and alternative telomere lengthening mechanisms, Front Biosci-Landmrk 18 (2013) 1–U414.
[361] A.J. Cesare, R.R. Reddel, Alternative lengthening of telomeres: models, mechanisms and implications, Nat. Rev. Genet. 11 (5) (2010) 319–330.
[362] E.T. Sugarman, G. Zhang, J.W. Shay, In perspective: an update on telomere targeting in cancer, Mol. Carcinog. 58 (9) (2019) 1581–1588.
[363] H.S. Lee, M. Carmena, M. Liskovykh, E. Peat, J.H. Kim, M. Oshimura, H. Masumoto, M.P. Teulade-Fichou, Y. Pommier, W.C. Earnshaw, V. Larionov, N. Kouprina, Systematic analysis of compounds specifically targeting telomeres and telomerase for clinical implications in cancer therapy, Cancer Res. 78 (21) (2018) 6282–6296.
[364] G. Pennarun, C. Granotier, L.R. Gauthier, D. Gomez, F. Hoffschir, E. Mandine, J. F. Riou, J.L. Mergny, P. Mailliet, F.D. Boussin, Apoptosis related to telomere instability and cell cycle alterations in human glioma cells treated by new highly selective G-quadruplex ligands, Oncogene 24 (18) (2005) 2917–2928.
[365] J.F. Riou, L. Guittat, P. Mailliet, A. Laoui, E. Renou, O. Petitgenet, F. Megnin-Chanet, C. Helene, J.L. Mergny, Cell senescence and telomere shortening induced by a new series of specific G-quadruplex DNA ligands, Proc. Natl. Acad. Sci. U. S. A. 99 (5) (2002) 2672–2677.
[366] M.Y. Kim, M. Gleason-Guzman, E. Izbicka, D. Nishioka, L.H. Hurley, The different biological effects of telomestatin and TMPyP4 can be attributed to their selectivity for interaction with intramolecular or intermolecular G-quadruplex structures, Cancer Res. 63 (12) (2003) 3247–3256.
[367] S.M. Gowan, R. Heald, M.F.G. Stevens, L.R. Kelland, Potent inhibition of telomerase by small-molecule pentacyclic acridines capable of interacting with G-quadruplexes, Mol. Pharmacol. 60 (5) (2001) 981–988.
[368] H. Da, H. Liu, Y. Zheng, R. Yuan, Y. Chai, A highly sensitive VEGF165 photoelectrochemical biosensor fabricated by assembly of aptamer bridged DNA networks, Biosens. Bioelectron. 101 (2018) 213–218.
[369] N. Ferrara, H.P. Gerber, J. LeCouter, The biology of VEGF and its receptors, Nat. Med. 9 (6) (2003) 669–676.
[370] N. Ferrara, Vascular endothelial growth factor: basic science and clinical progress, Endocr. Rev. 25 (4) (2004) 581–611.
[371] H. Basiri, A.A. Mehrizi, A. Ghaee, M. Farokhi, M. Chekini, E. Kumacheva, Carbon dots conjugated with vascular endothelial growth factor for protein tracking in angiogenic therapy, Langmuir 36 (11) (2020) 2893–2900.
[372] I. Garner, R. Vichare, R. Paulson, R. Appavu, S.K. Panguluri, R. Tzekov, N. Sahiner, R. Ayyala, M.R. Biswal, Carbon dots fabrication: ocular imaging and therapeutic potential, Front. Bioeng. Biotechnol. 8 (2020).
[373] H.M. Da, H.Y. Liu, Y.N. Zheng, R. Yuan, Y.Q. Chai, A highly sensitive VEGF(165) photoelectrochemical biosensor fabricated by assembly of aptamer bridged DNA networks, Biosens. Bioelectron. 101 (2018) 213–218.
[374] F. Yan, X. Sun, T. Ma, Y. Zhang, Y. Jiang, R. Wang, C. Ma, J. Wei, L. Chen, Y. Cui, A viscosity-dependent carbon dots with anti-VEGF properties for monitoring and promoting apoptosis in cancerous cell, Chem. Eng. J. 407 (2021).
[375] J. Cui, L. Kan, Z. Li, L. Yang, M. Wang, L. He, Y. Lou, Y. Xue, Z. Zhang, Porphyrin-based covalent organic framework as bioplatfrom for detection of vascular endothelial growth factor 165 through fluorescence resonance energy transfer, Talanta 228 (2021), 122060.
[376] J. Dong, X. Yao, S. Sun, Y. Zhong, C. Qian, D. Yang, In vivo targeting of breast cancer with a vasculature-specific GQDs/hMSN nanoplatform, RSC Adv. 9 (20) (2019) 11576–11584.
[377] H. Yang, M. Xu, S. Li, X. Shen, T.T. Li, J. Yan, C.C. Zhang, C.H. Wu, H.J. Zeng, Y. Y. Liu, Chitosan hybrid nanoparticles as a theranostic platform for targeted doxorubicin/VEGF shRNA co-delivery and dual-modality fluorescence imaging, RSC Adv. 6 (35) (2016) 29685–29696.
[378] N. Turner, R. Grose, Fibroblast growth factor signalling: from development to cancer, Nat. Rev. Cancer 10 (2) (2010) 116–129.
[379] G. Hwang, H. Kim, H. Yoon, C. Song, D.K. Lim, T. Sim, J. Lee, In situ imaging of quantum dot-AZD4547 conjugates for tracking the dynamic behavior of fibroblast growth factor receptor 3, Int. J. Nanomed. 12 (2017) 5345–5357.
[380] A. Tiron, C.S. Stan, G. Luta, C.M. Uritu, I.C. Vacarean-Trandafir, G.D. Stanciu, A. Coroaba, C.E. Tiron, Manganese-doped N-Hydroxyphthalimide-Derived carbon dots-theranostics applications in experimental breast cancer models, Pharmaceutics 13 (11) (2021).

[381] G. Luta, M. Butura, A. Tiron, C.E. Tiron, Enhancing anti-tumoral potential of CD-NHF by modulating PI3K/Akt Axis in U87 ex vivo glioma model, Int. J. Mol. Sci. 22 (8) (2021).
[382] N. Özcan, C. Karaman, N. Atar, O. Karaman, M.L. Yola, A novel molecularly imprinting biosensor including graphene quantum dots/multi-walled carbon nanotubes composite for interleukin-6 detection and electrochemical biosensor validation, ECS J. Solid State Sci. Technol. 9 (12) (2020).
[383] S.S. Wang, C.Y. Li, M. Qian, H.L. Jiang, W. Shi, J. Chen, U. Lachelt, E. Wagner, W. Y. Lu, Y. Wang, R.Q. Huang, Augmented glioma-targeted theranostics using multifunctional polymer-coated carbon nanodots, Biomaterials 141 (2017) 29–39.
[384] N.E. Sounni, A. Paye, L. Host, A. Noel, MT-MMPs as regulators of vessel stability associated with angiogenesis, Front. Pharmacol. 2 (2011).
[385] E.I. Deryugina, J.P. Quigley, Pleiotropic roles of matrix metalloproteinases in tumor angiogenesis: contrasting, overlapping and compensatory functions, Bba-Mol Cell Res 1803 (1) (2010) 103–120.
[386] D. Chen, B. Li, T. Lei, D. Na, M. Nie, Y. Yang, Xie Congjia, Z. He, J. Wang, Selective mediation of ovarian cancer SKOV3 cells death by pristine carbon quantum dots/Cu2O composite through targeting matrix metalloproteinases, angiogenic cytokines and cytoskeleton, J. Nnanobiotechnol. 19 (1) (2021) 68.
[387] Q. Li, Y. Wang, G. Yu, Y. Liu, K. Tang, C. Ding, H. Chen, S. Yu, Fluorescent polymer dots and graphene oxide based nanocomplexes for "off-on" detection of metalloproteinase-9, Nanoscale 11 (43) (2019) 20903–20909.
[388] M.B. Sporn, The war on cancer, Lancet 347 (9012) (1996) 1377–1381.
[389] M. Yilmaz, G. Christofori, EMT, the cytoskeleton, and cancer cell invasion, Cancer Metastasis Rev. 28 (1–2) (2009) 15–33.
[390] M.W. Klymkowsky, P. Savagner, Epithelial-mesenchymal transition A cancer researcher's conceptual friend and foe, Am. J. Pathol. 174 (5) (2009) 1588–1593.
[391] J.P. Thiery, H. Acloque, R.Y.J. Huang, M.A. Nieto, Epithelial-mesenchymal transitions in development and disease, Cell 139 (5) (2009) 871–890.
[392] K. Polyak, R.A. Weinberg, Transitions between epithelial and mesenchymal states: acquisition of malignant and stem cell traits, Nat. Rev. Cancer 9 (4) (2009) 265–273.
[393] S.J. Bray, Notch signalling in context, Nat. Rev. Mol. Cell Biol. 17 (11) (2016) 722–735.
[394] R. Kopan, Notch: a membrane-bound transcription factor, J. Cell Sci. 115 (6) (2002) 1095–1097.
[395] B.A. Osborne, L.M. Minter, Notch signalling during peripheral T-cell activation and differentiation, Nat. Rev. Immunol. 7 (1) (2007) 64–75.
[396] A.F. Chambers, L.M. Matrisian, Changing views of the role of matrix metalloproteinases in metastasis, J. Natl. Cancer Inst. 89 (17) (1997) 1260–1270.
[397] L.M. Coussens, W.W. Raymond, G. Bergers, M. Laig-Webster, O. Behrendtsen, Z. Werb, G.H. Caughey, D. Hanahan, Inflammatory mast cells up-regulate angiogenesis during squamous epithelial carcinogenesis, Gene Dev. 13 (11) (1999) 1382–1397.
[398] A. Pecak, L. Skalniak, K. Pels, M. Ksiazek, M. Madej, D. Krzemien, S. Malicki, B. Wladyka, A. Dubin, T.A. Holak, G. Dubin, Anti-CD44 DNA aptamers selectively target cancer cells, Nucleic Acid Therapeut. 30 (5) (2020) 289–298.
[399] S.Y. Lee, M.S. Kang, W.Y. Jeong, D.W. Han, K.S. Kim, Hyaluronic acid-based theranostic nanomedicines for targeted cancer therapy, Cancers 12 (4) (2020).
[400] Z.A. Nima, M. Mahmood, Y. Xu, T. Mustafa, F. Watanabe, D.A. Nedosekin, M. A. Juratli, T. Fahmi, E.I. Galanzha, J.P. Nolan, A.G. Basnakian, V.P. Zharov, A. S. Biris, Circulating tumor cell identification by functionalized silver-gold nanorods with multicolor, super-enhanced SERS and photothermal resonances, Sci. Rep-Uk 4 (2014).
[401] Y.Y. Qiu, B. Zhou, X.J. Yang, D.P. Long, Y. Hao, P.H. Yang, Novel single-cell analysis platform based on a solid-state zinc-coadsorbed carbon quantum dots electrochemiluminescence probe for the evaluation of CD44 expression on breast cancer cells, Acs Appl. Mater. Inter. 9 (20) (2017) 16849–16857.
[402] J. Tao, S. Feng, B. Liu, J. Pan, C. Li, Y. Zheng, Hyaluronic acid conjugated nitrogen-doped graphene quantum dots for identification of human breast cancer cells, Biomed. Mater. 16 (5) (2021).
[403] J. Li, M. Li, L. Tian, Y. Qiu, Q. Yu, X. Wang, R. Guo, Q. He, Facile strategy by hyaluronic acid functional carbon dot-doxorubicin nanoparticles for CD44 targeted drug delivery and enhanced breast cancer therapy, Int. J. Pharm. 578 (2020).
[404] Y.Q. Yang, S.Z. Chen, H.D. Li, Y.P. Yuan, Z.Y. Zhang, J.S. Xie, D.W. Hwang, A. D. Zhang, M.L. Liu, X. Zhou, Engineered paramagnetic graphene quantum dots with enhanced relaxivity for tumor imaging, Nano Lett. 19 (1) (2019) 441–448.
[405] K. Dehvari, S.-H. Chiu, J.-S. Lin, W.M. Girma, Y.-C. Ling, J.-Y. Chang, Heteroatom doped carbon dots with nanoenzyme like properties as theranostic platforms for free radical scavenging, imaging, and chemotherapy, Acta Biomater. 114 (2020) 343–357.
[406] F. Du, X. Zhao, W. Lu, Z. Guo, S. Shuang, C. Dong, Dual-ligand functionalized carbon nanodots as green fluorescent nanosensors for cellular dual receptor-mediated targeted imaging, Analyst 144 (22) (2019) 6729–6735.
[407] M. Zhang, X. Zhao, Z. Fang, Y. Niu, J. Lou, Y. Wu, S. Zou, S. Xia, M. Sun, F. Du, Fabrication of HA/PEI-functionalized carbon dots for tumor targeting, intracellular imaging and gene delivery, RSC Adv. 7 (6) (2017) 3369–3375.
[408] M. Zhang, Z. Fang, X. Zhao, Y. Niu, J. Lou, L. Zhao, Y. Wu, S. Zou, F. Du, Q. Shao, Hyaluronic acid functionalized nitrogen-doped carbon quantum dots for targeted specific bioimaging, RSC Adv. 6 (107) (2016) 104979–104984.
[409] D. Long, C. Chen, C. Cui, Z. Yao, P. Yang, A high precision MUA-spaced single-cell sensor for cellular receptor assay based on bifunctional Au@Cu-PbCQD nanoprobes, Nanoscale 10 (39) (2018) 18597–18605.
[410] J.S. Lin, Y.W. Tsai, K. Dehvari, C.C. Huang, J.Y. Chang, A carbon dot based theranostic platform for dual-modal imaging and free radical scavenging, Nanoscale 11 (43) (2019) 20917–20931.
[411] E. Campbell, M.T. Hasan, R. Gonzalez-Rodriguez, T. Truly, B.H. Lee, K.N. Green, G. Akkaraju, A.V. Naumov, Graphene quantum dot formulation for cancer imaging and redox-based drug delivery, Nanomedicine 37 (2021), 102408.
[412] O. Kearns, A. Camisasca, S. Giordani, Hyaluronic acid-conjugated carbon nanomaterials for enhanced tumour targeting ability, Molecules 27 (1) (2021).
[413] N. Abdullah Al, J.E. Lee, I. In, H. Lee, K.D. Lee, J.H. Jeong, S.Y. Park, Target delivery and cell imaging using hyaluronic acid-functionalized graphene quantum dots, Mol. Pharm. 10 (10) (2013) 3736–3744.
[414] J.M. Mehta, N.K. Jain, D.S. Chauhan, R. Prasad, M.K. Kumawat, M. Dhanka, A. Shanavas, R. Srivastava, Emissive radiodense stealth plasmonic nanohybrid as X-ray contrast and photo-ablative agent of cancer cells, Mater. Today Commun. 27 (2021).
[415] Q. Zhao, S. Wang, Y. Yang, X. Li, D. Di, C. Zhang, T. Jiang, S. Wang, Hyaluronic acid and carbon dots-gated hollow mesoporous silica for redox and enzyme-triggered targeted drug delivery and bioimaging, Mater. Sci. Eng., C 78 (2017) 475–484.
[416] Y. Kazemi, S. Dehghani, R. Nosrati, S.M. Taghdisi, K. Abnous, M. Alibolandi, M. Ramezani, Recent progress in the early detection of cancer based on CD44 biomarker; nano-biosensing approaches, Life Sci. 300 (2022), 120593.
[417] L. Zhang, Z. Lin, Y.-X. Yu, B.-P. Jiang, X.-C. Shen, Multifunctional hyaluronic acid-derived carbon dots for self-targeted imaging-guided photodynamic therapy, J. Mater. Chem. B 6 (41) (2018) 6534–6543.
[418] B. Demir, H. Moulahoum, F. Ghorbanizamani, F.B. Barlas, O. Yesiltepe, Z. P. Gumus, K. Meral, D. Odaci Demirkol, S. Timur, Carbon dots and curcumin-loaded CD44-Targeted liposomes for imaging and tracking cancer chemotherapy: a multi-purpose tool for theranostics, J. Drug Deliv. Sci. Technol. 62 (2021).
[419] P. Nigam, S. Waghmode, M. Louis, S. Wangnoo, P. Chavan, D. Sarkar, Graphene quantum dots conjugated albumin nanoparticles for targeted drug delivery and imaging of pancreatic cancer, J. Mater. Chem. B 2 (21) (2014) 3190–3195.
[420] Y. Wang, Y. Cui, Y. Zhao, B. He, X. Shi, D. Di, Q. Zhang, S. Wang, Fluorescent carbon dot-gated multifunctional mesoporous silica nanocarriers for redox/enzyme dual-responsive targeted and controlled drug delivery and real-time bioimaging, Eur. J. Pharm. Biopharm. 117 (2017) 105–115.
[421] X. Lu, X. Wang, A. Li, T. Zhou, L. Zhang, J. Qu, Z. Mao, X. Gu, X. Zhang, S. Jing, Ferrocenylseleno-dopamine functionalized carbon dots for redox-gated imaging and drug delivery in cancer cells, Dyes Pigments 205 (2022).
[422] N.N. Giang, H.J. Won, G. Lee, S.Y. Park, Cancer cells targeted visible light and alkaline Phosphatase-Responsive TiO2/Cu2+ carbon Dots-Coated wireless electrochemical biosensor, Chem. Eng. J. 417 (2021).
[423] B.Z. Youyi Qiu, Xiaojuan Yang, Dongping Long, Hao Yan, Peihui Yang, Novel single-cell analysis platform based on a solid-state zinc-coadsorbed carbon quantum dots electrochemiluminescence probe for the evaluation of CD44 expression on breast cancer cells, Acs Appl. Mater. Inter. (2017).
[424] B.B. Karakocak, A. Laradji, T. Primeau, M.Y. Berezin, S. Li, N. Ravi, Hyaluronan-conjugated carbon quantum dots for bioimaging use, Acs Appl. Mater. Inter. 13 (1) (2021) 277–286.
[425] N. Gao, W. Yang, H. Nie, Y. Gong, J. Jing, L. Gao, X. Zhang, Turn-on theranostic fluorescent nanoprobe by electrostatic self-assembly of carbon dots with doxorubicin for targeted cancer cell imaging, in vivo hyaluronidase analysis, and targeted drug delivery, Biosens. Bioelectron. 96 (2017) 300–307.
[426] N. Mauro, M.A. Utzeri, S.E. Drago, A. Nicosia, S. Costa, G. Cavallaro, G. Giammona, Hyaluronic acid dressing of hydrophobic carbon nanodots: a self-assembling strategy of hybrid nanocomposites with theranostic potential, Carbohydr. Polym. 267 (2021), 118213.
[427] J. Fang, Y. Liu, Y. Chen, D. Ouyang, G. Yang, T. Yu, Graphene quantum dots-gated hollow mesoporous carbon nanoplatform for targeting drug delivery and synergistic chemo-photothermal therapy, Int. J. Nanomed. 13 (2018) 5991–6007.
[428] Y.Y. Yang, Q. Liu, Y. Liu, J.J. Cui, H. Liu, P. Wang, Y.Y. Li, L. Chen, Z.D. Zhao, Y. H. Dong, A novel label-free electrochemical immunosensor based on functionalized nitrogen-doped graphene quantum dots for carcinoembryonic antigen detection, Biosens. Bioelectron. 90 (2017) 31–38.
[429] L.L. Xu, W. Zhang, L. Shang, R.N. Ma, L.P. Jia, W.L. Jia, H.S. Wang, L. Niu, Perylenetetracarboxylic acid and carbon quantum dots assembled synergistic electrochemiluminescence nanomaterial for ultra-sensitive carcinoembryonic antigen detection, Biosens. Bioelectron. 103 (2018) 6–11.
[430] H. Miao, L. Wang, Y. Zhuo, Z.N. Zhou, X.M. Yang, Label-free fluorimetric detection of CEA using carbon dots derived from tomato juice, Biosens. Bioelectron. 86 (2016) 83–89.
[431] C.H. Wang, Y. Zhang, W. Tang, C. Wang, Y.K. Han, L. Qiang, J.W. Gao, H. Liu, L. Han, Ultrasensitive, high-throughput and multiple cancer biomarkers simultaneous detection in serum based on graphene oxide quantum dots integrated microfluidic biosensing platform, Anal. Chim. Acta 1178 (2021).
[432] Y. Zhang, W.Y. Liu, S.G. Ge, M. Yan, S.W. Wang, J.H. Yu, N.Q. Li, X.R. Song, Multiplexed sandwich immunoassays using flow-injection electrochemiluminescence with designed substrate spatial-resolved technique for detection of tumor markers, Biosens. Bioelectron. 41 (2013) 684–690.
[433] Y.N. Luo, Y.X. Wang, H.Y. Yan, Y. Wu, C.Z. Zhu, D. Du, Y.H. Lin, SWCNTs@GQDs composites as nanocarriers for enzyme-free dual-signal amplification electrochemical immunoassay of cancer biomarker, Anal. Chim. Acta 1042 (2018) 44–51.
[434] G.M. Nie, Y. Wang, Y. Tang, D. Zhao, Q.F. Guo, A graphene quantum dots based electrochemiluminescence immunosensor for carcinoembryonic antigen detection

using poly(5-formylindole)/reduced graphene oxide nanocomposite, Biosens. Bioelectron. 101 (2018) 123–128.
[435] N.L. Li, L.P. Jia, R.N. Ma, W.L. Jia, Y.Y. Lu, S.S. Shi, H.S. Wang, A novel sandwiched electrochemiluminescence immunosensor for the detection of carcinoembryonic antigen based on carbon quantum dots and signal amplification, Biosens. Bioelectron. 89 (2017) 453–460.
[436] L. Li, T. Wang, Y. Zhang, C.X. Xu, L.N. Zhang, X. Cheng, H. Liu, X.D. Chen, J. H. Yu, Editable TiO2 nanomaterial-modified paper in situ for highly efficient detection of carcinoembryonic antigen by photoelectrochemical method, Acs Appl. Mater. Inter. 10 (17) (2018) 14594–14601.
[437] L. Li, W.P. Li, C. Ma, H.M. Yang, S.G. Ge, J.H. Yu, Paper-based Electrochemiluminescence Immunodevice for Carcinoembryonic Antigen Using Nanoporous Gold-Chitosan Hybrids and Graphene Quantum Dots Functionalized Au@Pt, Sensor Actuat B-Chem, 2014, pp. 314–322.
[438] X.T. Ji, H.Y. Lv, X.X. Sun, C.F. Ding, Green-emitting carbon dot loaded silica nanoparticles coated with DNA-cross-linked hydrogels for sensitive carcinoembryonic antigen detection and effective targeted cancer therapy, Chem. Commun. 55 (100) (2019) 15101–15104.
[439] Y.J. Zhan, S.T. Yang, F. Luo, L.H. Guo, Y.B. Zeng, B. Qiu, Z.Y. Lin, Emission wavelength switchable carbon dots combined with biomimetic inorganic nanozymes for a two-photon fluorescence immunoassay, Acs Appl. Mater. Inter. 12 (27) (2020) 30085–30094.
[440] W.W. Xiang, Z.J. Zhang, W.Q. Weng, B.D. Wu, J. Cheng, L. Shi, H.W. Sun, L. Gao, K.Q. Shi, Highly sensitive detection of carcinoembryonic antigen using copper-free click chemistry on the surface of azide cofunctionalized graphene oxide, Anal. Chim. Acta 1127 (2020) 156–162.
[441] K. Shao, L.F. Wang, Y.T. Wen, T. Wang, Y.J. Teng, Z.L. Shen, Z.F. Pan, Near-infrared carbon dots-based fluorescence turn on aptasensor for determination of carcinoembryonic antigen in pleural effusion, Anal. Chim. Acta 1068 (2019) 52–59.
[442] K.X. Wang, Y.D. Ding, W.Q. Yang, X.K. Wen, H.Y. Zhao, Y.M. Liu, X. Hong, Fluorescence-infrared absorption dual-mode nanoprobes based on carbon dots@ SiO2 nanorods for ultrasensitive and reliable detection of carcinoembryonic antigen, Talanta 230 (2021).
[443] Z. Liu, W. Chen, Y. Li, Q. Xu, Integrin alphavbeta3-targeted C-dot nanocomposites as multifunctional agents for cell targeting and photoacoustic imaging of superficial malignant tumors, Anal. Chem. 88 (23) (2016) 11955–11962.
[444] D. Li, Y. Fan, M. Shen, I. Banyai, X. Shi, Design of dual drug-loaded dendrimer/ carbon dot nanohybrids for fluorescence imaging and enhanced chemotherapy of cancer cells, J. Mater. Chem. B 7 (2) (2019) 277–285.
[445] T. Feng, X. Ai, H. Ong, Y. Zhao, Dual-responsive carbon dots for tumor extracellular microenvironment triggered targeting and enhanced anticancer drug delivery, Acs Appl. Mater. Inter. 8 (29) (2016) 18732–18740.
[446] H. Chen, Z. Zhen, W. Tang, T. Todd, Y.J. Chuang, L. Wang, Z. Pan, J. Xie, Label-free luminescent mesoporous silica nanoparticles for imaging and drug delivery, Theranostics 3 (9) (2013) 650–657.
[447] F. Zheng, P. Zhang, Y. Xi, X. Chen, Z. He, T. Meng, J. Chen, L. Li, J.J. Zhu, Hierarchical nanocarriers for precisely regulating the therapeutic process via dual-mode controlled drug release in target tumor cells, Acs Appl. Mater. Inter. 9 (42) (2017) 36655–36664.
[448] Z. Rahiminezhad, A. Tamaddon, A. Dehshahri, S. Borandeh, S.S. Abolmaali, H. Najafi, N. Azarpira, PLGA-graphene quantum dot nanocomposites targeted against alphavbeta3 integrin receptor for sorafenib delivery in angiogenesis, Biomater. Adv. 137 (2022), 212851.
[449] Y. Li, R. Zhou, D. Xiao, S. Shi, S. Peng, S. Wu, P. Wu, Y. Lin, Polypeptide uploaded efficient nanophotosensitizers to overcome photodynamic resistance for enhanced anticancer therapy, Chem. Eng. J. 403 (2021).
[450] S. Ghosh, K. Ghosal, S.A. Mohammad, K. Sarkar, Dendrimer functionalized carbon quantum dot for selective detection of breast cancer and gene therapy, Chem. Eng. J. 373 (2019) 468–484.
[451] J. Fan, B. Liu, Y. Long, Z. Wang, C. Tong, W. Wang, P. You, X. Liu, Sequentially-targeted biomimetic nano drug system for triple-negative breast cancer ablation and lung metastasis inhibition, Acta Biomater. 113 (2020) 554–569.
[452] W.X. Zhang, J. Dong, G.Y. Dang, H.W. Ji, P. Jiao, B.L. Sun, M.F. Yang, Y.Y. Li, L. Liu, L.F. Dong, Multifunctional nanocarriers based on graphitic-C3N4 quantum dots for tumor-targeted, traceable and pH-responsive drug delivery, New J. Chem. 43 (43) (2019) 17078–17089.
[453] S.M. Ghafary, E. Rahimjazi, H. Hamzehil, S.M.M. Mousavi, M. Nikkhah, S. Hosseinkhani, Design and preparation of a theranostic peptideticle for targeted cancer therapy: peptide-based codelivery of doxorubicin/curcumin and graphene quantum dots, Nanomed-Nanotechnol. 42 (2022).
[454] M. Berdasco, M. Esteller, Aberrant epigenetic landscape in cancer: how cellular identity goes awry, Dev. Cell 19 (5) (2010) 698–711.
[455] M. Esteller, Cancer epigenomics: DNA methylomes and histone-modification maps, Nat. Rev. Genet. 8 (4) (2007) 286–298.
[456] P.A. Jones, S.B. Baylin, The epigenomics of cancer, Cell 128 (4) (2007) 683–692.
[457] S.P. Jackson, J. Bartek, The DNA-damage response in human biology and disease, Nature 461 (7267) (2009) 1071–1078.
[458] M.B. Kastan, DNA damage responses: mechanisms and roles in human disease, Mol. Cancer Res. 6 (4) (2008) 517–524.
[459] A. Sigal, V. Rotter, Oncogenic mutations of the p53 tumor suppressor: the demons of the guardian of the genome, Cancer Res. 60 (24) (2000) 6788–6793.
[460] S.M. Elsherbiny, C.S. Shao, A. Acheampong, M.A. Khalifa, C. Liu, Q. Huang, Green synthesis of broccoli-derived carbon quantum dots as effective photosensitizers for the PDT effect testified in the model of mutant Caenorhabditis elegans, Biomater. Sci. 10 (11) (2022) 2857–2864.
[461] Y. Wang, J. Chen, J.K. Tian, G.C. Wang, W.K. Luo, Z.B. Huang, Y. Huang, N. Li, M. M. Guo, X.G. Fan, Tryptophan-sorbitol based carbon quantum dots for theranostics against hepatocellular carcinoma, J. Nanobiotechnol. 20 (1) (2022).
[462] O. Warburg, On respiratory impairment in cancer cells, Science 124 (3215) (1956) 269–270.
[463] O. Warburg, On the origin of cancer cells, Science 123 (3191) (1956) 309–314.
[464] F. Wind, O. Warburg, The Metabolism of Tumors: Investigations from the Kaiser Wilhelm Institute for Biology, Constable & Co. Ltd, Berlin-Dahlem, 1930, p. 282.
[465] S. Yazdanparast, A. Benvidi, S. Abbasi, S.K. Sabbagh, Monitoring the mechanism of anti-cancer agents to inhibit colorectal cancer cell proliferation: enzymatic biosensing of glucose combined with molecular docking, Enzym. Microb. Technol. 148 (2021).
[466] X.D. Lu, Z.D. Zhang, Q. Xia, M.R. Hou, C.G. Yan, Z.L. Chen, Y.K. Xu, R.Y. Liu, Glucose functionalized carbon quantum dot containing organic radical for optical/MR dual-modality bioimaging, Mater. Sci. Eng., C 82 (2018) 190–196.
[467] O. Warburg, Origin of cancer cells, Science 123 (3191) (1956) 309–314.
[468] J.Z. Du, C.Q. Mao, Y.Y. Yuan, X.Z. Yang, J. Wang, Tumor extracellular acidity-activated nanoparticles as drug delivery systems for enhanced cancer therapy, Biotechnol. Adv. 32 (4) (2014) 789–803.
[469] J.F. Shangguan, D.G. He, X.X. He, K.M. Wang, F.Z. Xu, J.Q. Liu, J.L. Tang, X. Yang, J. Huang, Label-free carbon-dots-based ratiometric fluorescence pH nanoprobes for intracellular pH sensing, Anal. Chem. 88 (15) (2016) 7837–7843.
[470] B. Kong, A. Zhu, C. Ding, X. Zhao, B. Li, Y. Tian, Carbon dot-based inorganic-organic nanosystem for two-photon imaging and biosensing of pH variation in living cells and tissues, Adv. Mater. 24 (43) (2012) 5844–5848.
[471] Z.T. Fan, S.X. Zhou, C. Garcia, L.Z. Fan, J.B. Zhou, pH-Responsive fluorescent graphene quantum dots for fluorescence-guided cancer surgery and diagnosis, Nanoscale 9 (15) (2017) 4928–4933.
[472] C. Zhang, Y. Cui, L. Song, X. Liu, Z. Hu, Microwave assisted one-pot synthesis of graphene quantum dots as highly sensitive fluorescent probes for detection of iron ions and pH value, Talanta 150 (2016) 54–60.
[473] F.L. Yuan, L. Ding, Y.C. Li, X.H. Li, L.Z. Fan, S.X. Zhou, D.C. Fang, S.H. Yang, Multicolor fluorescent graphene quantum dots colorimetrically responsive to all-pH and a wide temperature range, Nanoscale 7 (27) (2015) 11727–11733.
[474] M. Zhang, P. Yuan, N. Zhou, Y. Su, M. Shao, C. Chi, pH-Sensitive N-doped carbon dots-heparin and doxorubicin drug delivery system: preparation and anticancer research, RSC Adv. 7 (15) (2017) 9347–9356.
[475] K. Tabatabaeian, M. Simayee, A. Fallah-Shojaie, F. Mashayekhi, N-doped carbon nanodots@UiO-66-NH2 as novel nanoparticles for releasing of the bioactive drug, rosmarinic acid and fluorescence imaging, Daru 27 (1) (2019) 307–315.
[476] M. Ahmadi-Kashani, H. Dehghani, A. Zarrabi, A biocompatible nanoplatform formed by MgAl-layered double hydroxide modified Mn3O4/N-graphene quantum dot conjugated-polyaniline for pH-triggered release of doxorubicin, Mat Sci Eng C-Mater 114 (2020).
[477] C. Atila Dincer, B. Getiren, C. Gokalp, Z. Ciplak, A. Karakecili, N. Yildiz, An anticancer drug loading and release study to ternary GO-Fe3O4-PPy and Fe3O4 @PPy-NGQDs nanocomposites for photothermal chemotherapy, Colloids Surf. A Physicochem. Eng. Asp. 633 (2022).
[478] Z.L. Wu, M.X. Gao, T.T. Wang, X.Y. Wan, L.L. Zheng, C.Z. Huang, A general quantitative pH sensor developed with dicyandiamide N-doped high quantum yield graphene quantum dots, Nanoscale 6 (7) (2014) 3868–3874.
[479] M. Yang, B.Y. Li, K.L. Zhong, Y. Lu, Photoluminescence properties of N-doped carbon dots prepared in different solvents and applications in pH sensing, J. Mater. Sci. 53 (4) (2018) 2424–2433.
[480] Y.Y. Ding, X.J. Gong, Y. Liu, W.J. Lu, Y.F. Gao, M. Xian, S.M. Shuang, C. Dong, Facile preparation of bright orange fluorescent carbon dots and the constructed biosensing platform for the detection of pH in living cells, Talanta 189 (2018) 8–15.
[481] R. Li, Z. Li, X. Sun, J. Ji, L. Liu, Z. Gu, G. Wang, Graphene quantum dot-rare earth upconversion nanocages with extremely high efficiency of upconversion luminescence, stability and drug loading towards controlled delivery and cancer theranostics, Chem. Eng. J. 382 (2020).
[482] M. Pei, X. Jia, P. Liu, Design of Janus-like PMMA-PEG-FA grafted fluorescent carbon dots and their nanoassemblies for leakage-free tumor theranostic application, Mater. Des. 155 (2018) 288–296.
[483] Z. Wang, B. Fu, S. Zou, B. Duan, C. Chang, B. Yang, X. Zhou, L. Zhang, Facile construction of carbon dots via acid catalytic hydrothermal method and their application for target imaging of cancer cells, Nano Res. 9 (1) (2016) 214–223.
[484] Y. Esmaeili, H.S. Ghaheh, F. Ghasemi, L. Shariati, M. Rafienia, E. Bidram, A. Zarrabi, Graphene oxide quantum dot-chitosan nanotheranostic platform as a pH-responsive carrier for improving curcumin uptake internalization: in vitro & in silico study, Biomater. Adv. 139 (2022).
[485] H. Wang, S. Mukherjee, J. Ji, P. Banerjee, Q. Chen, S. Zhou, Biocompatible chitosan-carbon dot hybrid nanogels for NIR-imaging-guided synergistic photothermal-chemo therapy, Acs Appl. Mater. Inter. 9 (22) (2017) 18639–18649.
[486] F.K. Du, Y.H. Ming, F. Zeng, C.M. Yu, S.Z. Wu, A low cytotoxic and ratiometric fluorescent nanosensor based on carbon-dots for intracellular pH sensing and mapping, Nanotechnology 24 (36) (2013).
[487] C.X. Wang, Z.Z. Xu, C. Zhang, Polyethyleneimine-functionalized fluorescent carbon dots: water stability, pH sensing, and cellular imaging, ChemNanoMat 1 (2) (2015) 122–127.
[488] N. Shi, K. Sun, Z. Zhang, J. Zhao, L. Geng, Y. Lei, Amino-modified carbon dots as a functional platform for drug delivery: load-release mechanism and cytotoxicity, J. Ind. Eng. Chem. 101 (2021) 372–378.

[489] Z. Liu, X. Chen, X. Zhang, J.J. Gooding, Y. Zhou, Carbon-quantum-dots-loaded mesoporous silica nanocarriers with pH-switchable zwitterionic surface and enzyme-responsive pore-cap for targeted imaging and drug delivery to tumor, Adv. Healthcare Mater. 5 (12) (2016) 1401–1407.
[490] M.P. Shirani, B. Rezaei, T. Khayamian, M. Dinari, F.H. Shamili, M. Ramezani, M. Alibolandi, Ingenious pH-sensitive etoposide loaded folic acid decorated mesoporous silica-carbon dot with carboxymethyl-beta cyclodextrin gatekeeper for targeted drug delivery and imaging, Mat Sci Eng C-Mater 92 (2018) 892–901.
[491] X. Li, S. Hu, Z. Lin, J. Yi, X. Liu, X. Tang, Q. Wu, G. Zhang, Dual-responsive mesoporous silica nanoparticles coated with carbon dots and polymers for drug encapsulation and delivery, Nanomedicine 15 (25) (2020) 2447–2458.
[492] Z. Chen, T. Liao, L. Wan, Y. Kuang, C. Liu, J. Duan, X. Xu, Z. Xu, B. Jiang, C. Li, Dual-stimuli responsive near-infrared emissive carbon dots/hollow mesoporous silica-based integrated theranostics platform for real-time visualized drug delivery, Nano Res. 14 (11) (2021) 4264–4273.
[493] Y. Wang, W. Shi, S. Wang, C. Li, M. Qian, J. Chen, R. Huang, Facile incorporation of dispersed fluorescent carbon nanodots into mesoporous silica nanosphere for pH-triggered drug delivery and imaging, Carbon 108 (2016) 146–153.
[494] J. Jiao, C. Liu, X. Li, J. Liu, D. Di, Y. Zhang, Q. Zhao, S. Wang, Fluorescent carbon dot modified mesoporous silica nanocarriers for redox-responsive controlled drug delivery and bioimaging, J. Colloid Interface Sci. 483 (2016) 343–352.
[495] M.S. Kang, R.K. Singh, T.-H. Kim, J.-H. Kim, K.D. Patel, H.-W. Kim, Optical imaging and anticancer chemotherapy through carbon dot created hollow mesoporous silica nanoparticles, Acta Biomater. 55 (2017) 466–480.
[496] J. Espina-Casado, T. Fontanil, A. Fernandez-Gonzalez, S. Cal, A.J. Obaya, M. Elena Diaz-Garcia, R. Badia-Laino, Carbon dots as multifunctional platform for intracellular pH sensing and bioimaging. In vitro and in vivo studies, Sensor Actuat. B-Chem. 346 (2021).
[497] A.R. Chowdhuri, T. Singh, S.K. Ghosh, S.K. Sahu, Carbon dots embedded magnetic nanoparticles @chitosan @metal organic framework as a nanoprobe for pH sensitive targeted anticancer drug delivery, Acs Appl. Mater. Inter. 8 (26) (2016) 16573–16583.
[498] S. Zhao, M. Lan, X. Zhu, H. Xue, T.-W. Ng, X. Meng, C.-S. Lee, P. Wang, W. Zhang, Green synthesis of bifunctional fluorescent carbon dots from garlic for cellular imaging and free radical scavenging, Acs Appl. Mater. Inter. 7 (31) (2015) 17054–17060.
[499] Z.Q. Song, F.Y. Quan, Y.H. Xu, M.L. Liu, L. Cui, J.Q. Liu, Multifunctional N,S co-doped carbon quantum dots with pH- and thermo-dependent switchable fluorescent properties and highly selective detection of glutathione, Carbon 104 (2016) 169–178.
[500] J. Ma, C. Ding, J. Zhou, Y. Tian, 2D ratiometric fluorescent pH sensor for tracking of cells proliferation and metabolism, Biosens. Bioelectron. 70 (2015) 202–208.
[501] L. Shi, Y. Li, X. Li, B. Zhao, X. Wen, G. Zhang, C. Dong, S. Shuang, Controllable synthesis of green and blue fluorescent carbon nanodots for pH and Cu2+ sensing in living cells, Biosens. Bioelectron. 77 (2016) 598–602.
[502] W. Shi, X.H. Li, H.M. Ma, A tunable ratiometric pH sensor based on carbon nanodots for the quantitative measurement of the intracellular pH of whole cells, Angew. Chem., Int. Ed. 51 (26) (2012) 6432–6435.
[503] V.J. Sawant, S.R. Bamane, D.G. Kanase, S.B. Patil, J. Ghosh, Encapsulation of curcumin over carbon dot coated TiO2 nanoparticles for pH sensitive enhancement of anticancer and anti-psoriatic potential, RSC Adv. 6 (71) (2016) 66745–66755.
[504] Y. Mao, Y. Bao, L. Yan, G. Li, F.H. Li, D.X. Han, X.B. Zhang, L. Niu, pH-switched luminescence and sensing properties of a carbon dot-polyaniline composite, RSC Adv. 3 (16) (2013) 5475–5482.
[505] L.D. Wang, Y. Chen, Lanthanide doped carbon dots as a fluorescence chromaticity-based pH probe, Microchim. Acta 185 (10) (2018).
[506] S. Zhao, K. Yang, L. Jiang, J. Xiao, B. Wang, L. Zeng, X. Song, M. Lan, Polythiophene-based carbon dots for imaging-guided photodynamic therapy, ACS Appl. Nano Mater. 4 (10) (2021) 10528–10533.
[507] Q. Wang, H. Yang, Q. Zhang, H. Ge, S. Zhang, Z. Wang, X. Ji, Strong acid-assisted preparation of green-emissive carbon dots for fluorometric imaging of pH variation in living cells, Microchim. Acta 186 (7) (2019).
[508] N.K.R. Bogireddy, J. Lara, L. Rodriguez Fragoso, V. Agarwal, One-step hydrothermal preparation of highly stable N doped oxidized carbon dots for toxic organic pollutants sensing and bioimaging, Chem. Eng. J. 401 (2020).
[509] Y.-L. Su, T.-W. Yu, W.-H. Chiang, H.-C. Chiu, C.-H. Chang, C.-S. Chiang, S.-H. Hu, Hierarchically targeted and penetrated delivery of drugs to tumors by size-changeable graphene quantum dot nanoaircrafts for photolytic therapy, Adv. Funct. Mater. 27 (23) (2017).
[510] A. Pyne, S. Layek, A. Patra, N. Sarkar, An easy and smart way to explore the light-emitting responses of carbon dot and doxorubicin hydrochloride assembly: white light generation and pH- dependent reversible photoswitching, J. Mater. Chem. C 7 (21) (2019) 6414–6425.
[511] X. Zhang, Y. Shen, S. Xu, J. Yue, Q. Guo, D. Huang, B. Yang, W. Shi, C. Liang, W. Xu, Intracellular pH-propelled assembly of smart carbon nanodots and selective photothermal therapy for cancer cells, Colloids Surf., B 188 (2020).
[512] X. Sun, M. Chen, Y. Zhang, Y. Yin, L. Zhang, H. Li, J. Hao, Photoluminescent and pH-responsive supramolecular structures from co-assembly of carbon quantum dots and zwitterionic surfactant micelles, J. Mater. Chem. B 6 (43) (2018) 7021–7032.
[513] H. Huang, Z. Guo, C. Zhang, C. Cui, T. Fu, Q. Liu, W. Tan, Logic-gated cell-derived nanovesicles via DNA-based smart recognition module, Acs Appl. Mater. Inter. 13 (26) (2021) 30397–30403.
[514] L. Yang, B. Hu, A.-H. Liu, Y. Zhang, A hollow-structured nanohybrid: intelligent and visible drug delivery and photothermal therapy for cancer, Talanta 215 (2020).
[515] S. Qu, H. Chen, X. Zheng, J. Cao, X. Liu, Ratiometric fluorescent nanosensor based on water soluble carbon nanodots with multiple sensing capacities, Nanoscale 5 (12) (2013) 5514–5518.
[516] Y. Zhao, Y. Xie, Y. Liu, X. Tang, S. Cui, Comprehensive exploration of long-wave emission carbon dots for brain tumor visualization, J. Mater. Chem. B 10 (18) (2022) 3512–3523.
[517] S. Durrani, Z. Yang, J. Zhang, Z. Wang, H. Wang, F. Durrani, F.-G. Wu, F. Lin, Nucleus-targeting pH-Responsive carbon dots for fast nucleus pH detection, Talanta (2023) 252.
[518] C. Jiang, H. Wu, X. Song, X. Ma, J. Wang, M. Tan, Presence of photoluminescent carbon dots in Nescafe (R) original instant coffee: applications to bioimaging, Talanta 127 (2014) 68–74.
[519] H. Yao, L. Su, M. Zeng, L. Cao, W. Zhao, C. Chen, B. Du, J. Zhou, Construction of magnetic-carbon-quantum-dots-probe-labeled apoferritin nanocages for bioimaging and targeted therapy, Int. J. Nanomed. 11 (2016) 4423–4438.
[520] S. Xu, X. He, Y. Huang, X. Liu, L. Zhao, X. Wang, Y. Sun, P. Ma, D. Song, Lysosome-targeted ratiometric fluorescent sensor for monitoring pH in living cells based on one-pot-synthesized carbon dots, Microchim. Acta 187 (8) (2020).
[521] Z. Guo, Y. Jiao, F. Du, Y. Gao, W. Lu, S. Shuang, C. Dong, Y. Wang, Facile synthesis of ratiometric fluorescent carbon dots for pH visual sensing and cellular imaging, Talanta 216 (2020).
[522] Y. Jiao, X. Gong, H. Han, Y. Gao, W. Lu, Y. Liu, M. Xian, S. Shuang, C. Dong, Facile synthesis of orange fluorescence carbon dots with excitation independent emission for pH sensing and cellular imaging, Anal. Chim. Acta 1042 (2018) 125–132.
[523] M.T. Hasan, R. Gonzalez-Rodriguez, C.-W. Lin, E. Campbell, S. Vasireddy, U. Tsedev, A.M. Belcher, A.V. Naumov, Rare-Earth metal ions doped graphene quantum dots for near-IR in vitro/in vivo/ex vivo imaging applications, Adv. Opt. Mater. 8 (21) (2020).
[524] T. Arumugham, M. Alagumuthu, R.G. Amimodu, S. Munusamy, S.K. Iyer, A sustainable synthesis of green carbon quantum dot (CQD) from Catharanthus roseus (white flowering plant) leaves and investigation of its dual fluorescence responsive behavior in multi-ion detection and biological applications, Sustain. Mater. Technol. 23 (2020).
[525] H. Min, Y. Qi, Y. Chen, Y. Zhang, X. Han, Y. Xu, Y. Liu, J. Hu, H. Liu, Y. Li, G. Nie, Synthesis and imaging of biocompatible graphdiyne quantum dots, Acs Appl. Mater. Inter. 11 (36) (2019) 32798–32807.
[526] R. Su, X. Xiong, Y. Li, X. Wei, S. Zheng, J. Zhao, S. Zhou, A pH-triggered fluorescence-switchable extracellular vesicle for tracing drug release and improving drug delivery, Biomater. Sci. 9 (17) (2021) 5812–5823.
[527] Y. Dong, P. Du, P. Liu, Absolutely "off-on" fluorescent CD-based nanotheranostics for tumor intracellular real-time imaging and pH-triggered DOX delivery, J. Mater. Chem. B 8 (35) (2020) 8002–8009.
[528] S. Rainu, S. Parameswaran, S. Krishnakumar, N. Singh, Dual-sensitive fluorescent nanoprobes for detection of matrix metalloproteinases and low pH in a 3D tumor microenvironment, J. Mater. Chem. B 10 (28) (2022) 5388–5401.
[529] P. Karfa, E. Roy, S. Patra, D. Kumar, R. Madhuri, P.K. Sharma, A fluorescent molecularly-imprinted polymer gate with temperature and pH as inputs for detection of alpha-fetoprotein, Biosens. Bioelectron. 78 (2016) 454–463.
[530] X. Chen, Y. Fan, J. Sun, Z. Zhang, Y. Xin, K. Li, K. Tang, P. Du, Y. Liu, G. Wang, M. Yang, Y. Tan, Nanoparticle-me diate d specific elimination of soft cancer stem cells by targeting low cell stiffness, Acta Biomater. 135 (2021) 493–505.
[531] H. Nie, M. Li, Q. Li, S. Liang, Y. Tan, L. Sheng, W. Shi, S.X.-A. Zhang, Carbon dots with continuously tunable full-color emission and their application in ratiometric pH sensing, Chem. Mater. 26 (10) (2014) 3104–3112.
[532] Y. Jiang, K. Pu, Multimodal biophotonics of semiconducting polymer nanoparticles, Accounts Chem. Res. 51 (8) (2018) 1840–1849.
[533] Y. Bai, J. Zhao, S. Wang, T. Lin, F. Ye, S. Zhao, Carbon dots with absorption red-shifting for two-photon fluorescence imaging of tumor tissue pH and synergistic phototherapy, Acs Appl. Mater. Inter. 13 (30) (2021) 35365–35375.
[534] S. E, Q.X. Mao, X.L. Yuan, X.L. Kong, X.W. Chen, J.H. Wang, Targeted imaging of the lysosome and endoplasmic reticulum and their pH monitoring with surface regulated carbon dots, Nanoscale 10 (26) (2018) 12788–12796.
[535] Z. Yang, B. Hou, Y. Yang, L. Jiang, A. Xie, Y. Shen, M. Zhu, A pH-induced charge convertible nanocomposite as novel targeted phototherapy agent and gene carrier, Chem. Eng. J. 353 (2018) 350–360.
[536] C.A. Choi, Z.A.I. Mazrad, J.H. Ryu, I. In, K.D. Lee, S.Y. Park, Membrane and nucleus targeting for highly sensitive cancer cell detection using pyrophosphate and alkaline phosphatase activity-mediated fluorescence switching of functionalized carbon dots, J. Mater. Chem. B 6 (37) (2018) 5992–6001.
[537] T. Feng, X. Ai, G. An, P. Yang, Y. Zhao, Charge-Convertible carbon dots for imaging guided drug delivery with enhanced in vivo cancer therapeutic efficiency, ACS Nano 10 (4) (2016) 4410–4420.
[538] A.I. Robby, S.G. Kim, H.J. Jo, G. Lee, H.S. Lee, K.D. Lee, J.H. Ryu, S.Y. Park, Tumor microenvironment-responsive touch sensor-based pH-triggered controllable conductive hydrogel, Appl. Mater. Today 25 (2021).
[539] S.G. Kim, B. Ryplida, P. Pham Thi My, H.J. Won, G. Lee, S.H. Bhang, S.Y. Park, Reduction-triggered paclitaxel release nano-hybrid system based on core-crosslinked polymer dots with a pH-responsive shell-cleavable colorimetric biosensor, Int. J. Mol. Sci. 20 (21) (2019).
[540] B. Ryplida, G. Lee, I. In, S.Y. Park, Zwitterionic carbon dot-encapsulating pH-responsive mesoporous silica nanoparticles for NIR light-triggered photothermal therapy through pH-controllable release, Biomater. Sci. 7 (6) (2019) 2600–2610.

[541] J. Wan, S. Xu, J. Li, M. Yu, K. Zhang, G. Wei, Z. Su, Facile synthesis of multifunctional pharmaceutical carbon dots for targeted bioimaging and chemotherapy of tumors, Nanoscale 14 (31) (2022) 11359–11368.
[542] S.I. Grivennikov, F.R. Greten, M. Karin, Immunity, Inflammation, and Cancer, Cell 140 (6) (2010) 883–899.
[543] D. DeNardo, P. Andreu, L.M. Coussens, Interactions between lymphocytes and myeloid cells regulate pro- versus anti-tumor immunity, Cancer Metastasis Rev. 29 (2) (2010) 309–316.
[544] B.Z. Qian, J.W. Pollard, Macrophage diversity enhances tumor progression and metastasis, Cell 141 (1) (2010) 39–51.
[545] C.L. Shen, Q. Lou, J.H. Zang, K.K. Liu, S.N. Qu, L. Dong, C.X. Shan, Near-infrared chemiluminescent carbon nanodots and their application in reactive oxygen species bioimaging, Adv. Sci. 7 (8) (2020).
[546] H.J. Won, B. Ryplida, S.G. Kim, G. Lee, J.H. Ryu, S.Y. Park, Diselenide-bridged carbon-dot-mediated self-healing, conductive, and adhesive wireless hydrogel sensors for label-free breast cancer detection, ACS Nano 14 (7) (2020) 8409–8420.
[547] Z. Li, W.D. Liu, P.J. Ni, C.H. Zhang, B. Wang, G.B. Duan, C.X. Chen, Y.Y. Jiang, Y. Z. Lu, Carbon dots confined in N-doped carbon as peroxidase-like nanozyme for detection of gastric cancer relevant D-amino acids, Chem. Eng. J. 428 (2022).
[548] L. Wang, J. Zheng, Y. Li, S. Yang, C. Liu, Y. Xiao, J. Li, Z. Cao, R. Yang, AgNP-DNA@GQDs hybrid: new approach for sensitive detection of H2O2 and glucose via simultaneous AgNP etching and DNA cleavage, Anal. Chem. 86 (24) (2014) 12348–12354.
[549] D. Chakraborty, S. Sarkar, P.K. Dase, Blood dots: hemoglobin-derived carbon dots as hydrogen peroxide sensors and pro-drug activators, ACS Sustain. Chem. Eng. 6 (4) (2018) 4661. -+.
[550] K. Phukan, R.R. Sarma, S. Dash, R. Devi, D. Chowdhury, Carbon dot based nucleus targeted fluorescence imaging and detection of nuclear hydrogen peroxide in living cells, Nanoscale Adv. 4 (1) (2021) 138–149.
[551] S. Bhattacharya, R. Sarkar, S. Nandi, A. Porgador, R. Jelinek, Detection of reactive oxygen species by a carbon-dot-ascorbic acid hydrogel, Anal. Chem. 89 (1) (2017) 830–836.
[552] H. Li, L. Guo, A.X. Huang, H. Xu, X.M. Liu, H.M. Ding, J. Dong, J. Li, C.N. Wang, X.T. Su, X.F. Ge, L.Q. Sun, C.J. Bai, X.L. Shen, T. Fang, Z.H. Li, Y. Zhou, L.S. Zhan, S.H. Li, J.W. Xie, N.S. Shao, Nanoparticle-conjugated aptamer targeting hnRNP A2/B1 can recognize multiple tumor cells and inhibit their proliferation, Biomaterials 63 (2015) 168–176.
[553] J. Xi, C. Xie, Y. Zhang, L. Wang, J. Xiao, X. Duan, J. Ren, F. Xiao, S. Wang, Pd nanoparticles decorated N-doped graphene quantum dots@N-doped carbon hollow nanospheres with high electrochemical sensing performance in cancer detection, ACS Appl. Mater. Interfaces 8 (34) (2016) 22563–22573.
[554] A.L. Xu, P. He, C.C. Ye, Z.D. Liu, B.L. Gu, B. Gao, Y.Q. Li, H. Dong, D. Chen, G. Wang, S.W. Yang, G.Q. Ding, Polarizing graphene quantum dots toward long-acting intracellular reactive oxygen species evaluation and tumor detection, Acs Appl. Mater. Inter. 12 (9) (2020) 10781–10790.
[555] L.L. Shang, X.J. Song, C.B. Niu, Q.Y. Lv, C.L. Li, H.F. Cui, S.T. Zhang, Red fluorescent nanoprobe based on Ag@Au nanoparticles and graphene quantum dots for H2O2 determination and living cell imaging, Microchim. Acta 188 (9) (2021).
[556] S.G. Kim, B. Ryplida, N.N. Giang, G. Lee, K.D. Lee, S.Y. Park, Tuning conductivity and roughness of diselenide polymer dot-coated surface for ROS-mediated selective real-time wireless detection of cancer cells, Chem. Eng. J. 426 (2021).

Hang Wang obtained her BSc degree majoring in Microelectronics Science and Engineering from Ningbo University in 2021. She is currently a PhD student at Shanghai Institute of Microsystem and Information Technology (SIMIT), Chinese Academy of Science. Her research interests include the synthesis and applications of GQDs for tumor diagnosis and therapy, and bio-microelectronics.

Siwei Yang is a professor at Shanghai Institute of Microsystem and Information Technology (SIMIT), Chinese Academy of Science. He received his PhD from SIMIT in 2017. Prof. Yang first prepared a new 2D carbon-based semiconductor C_3N in 2017. His research interests include controllable preparation, applications of 2D carbon-based semiconductors (in nanoelectronics, nano-photonics, and nanomedicine), and GQDs and other graphene derivatives.

Guqiao Ding is a professor at Shanghai Institute of Microsystem and Information Technology (SIMIT), Chinese Academy of Science. He received his BSc and MSc from Suzhou University and PhD from Shanghai Jiao Tong University. Prof Ding joined SIMIT in 2010. Research in his laboratory currently includes the preparation and application of graphene, graphene oxide, GQDs, and new 2D carbon-based materials.